7-26-1995

An experimental study of the effects of double-diffusive convention processes during the solification of binary alloys

Richard Burton
Florida International University

FLORIDA INTERNATIONAL UNIVERSITY

Miami,Florida

AN EXPERIMENTAL STUDY OF THE EFFECTS OF DOUBLE-DIFFUSIVE CONVECTION PROCESSES DURING THE SOLIDIFICATION OF BINARY ALLOYS.

A thesis submitted in partial satisfaction of the

requirements for the degree of

MASTER OF SCIENCE

IN

MECHANICAL ENGINEERING

by

Richard Burton

1995

To: Dean Gordon R. Hopkins

College of Engineering and Design.

This thesis written by Richard Burton, and entitled, AN EXPERIMENTAL STUDY OF THE EFFECTS OF DOUBLE-DIFFUSIVE CONVECTION PROCESSES DURING THE SOLIDIFICATION OF BINARY ALLOYS, having been approved in respect to style and intellectual content, is referred to you for judgement.

We have read this thesis and recommend that it be approved.

Y. Cao

J. Moore

R. Schoephoerster

M. A. Ebadian, Major Professor

Date of defense: July 26, 1995

The thesis of Richard Burton is approved.

Dean Gordon R. Hopkins
College of Engineering and Design

Dr. Richard L. Campbell
Dean of Graduate Studies

Florida International University, 1995

I dedicate this thesis to my wife, Andrea Claire Burton. Without her love, patience and understanding I would not have been able to complete this work.

ACKNOWLEDGMENTS

I wish to thank all the members of my committee for their expertise, patience and care in reviewing this work. For their constant help and attention to this project I thank the team members of this project, past and present: Ferdinand Desir for his help at the projects inception; W. Kinzy- Jones jr. for his assistance in experimentation; Shawn Dezego for his practical and constant help; Dr. Dong and Dr. Yang for their advise and guidance.

My special thanks to my major professor, Dr. Ebadian for his support, guidance, encouragement and for providing me with the opportunity to work on this project .

ABSTRACT OF THE THESIS

An Experimental Study of The Effects of Double - Diffusive Convection Processes During The Solidification of Binary Alloys

by

Richard Burton

Florida International University, 1995

Miami, Florida

Professor M. A. Ebadian, Major Professor

Experiments were conducted to show the effects of thermal and geometric boundary conditions on the liquid pool of a binary alloy system which is undergoing phase change, solidification. Transparent analogue solutions were selected for study and experimental apparatus were designed and built. Thermal distribution and concentration data were collected and analysed for the melt pool of various selected geometries and boundary conditions of the systems under study. The data indicate that characteristic flows develop for both Hypereutectic and Hypoeutectic concentration levels and that the development of macrosegregation and microsegregation defects in continuous casting materials can be minimised by the adjustment of the process variables.

TABLE OF CONTENTS

LIST OF TABLES

LIST OF FIGURES

LIST OF FIGURES, Contd.

LIST OF SYMBOLS

C	Concentration
D	Mass diffusivity
h	Enthalpy
j	Diffusion flux vector
Le	Lewis number
m	Mass
Nu	Nusselt number
Pr	Prandtl number
Ra	Rayleigh number
Re	Reynolds number
Sc	Schmidt number
Sh	Sherwood number
T	Temperature
t	Time (secs)
u,v,w	Cartesian velocity components
V	Velocity
x	Vertical location
y	Horizontal location
α	Angle of sump
β	Thermal expansion coefficient
ρ	Density
ν	Viscosity, kinematic
μ	Viscosity, dynamic

APPENDICES

CHAPTER 1 - INTRODUCTION

1.1 Background

During the casting of metal alloys, molten metal is poured into a mold to solidify, that is, undergo phase change from liquid to solid form by the extraction of heat energy from the liquid alloy. The geometric shape of the mold becomes the constraining limit to the final form of the solid. Deviations from that final shape can occur due to physical phenomena related both to the properties of the materials involved and the dynamics of the process. One significant source of defects in solid cast materials is the effect of double-diffusive convection in the liquid pool within the mold cavity, prior to the completion of solidification. In contrast to the solidification process of a pure substance, the solidification of a binary system can generate both temperature and concentration gradients in the liquid pool. The two buoyant forces, that are created by these gradients, can interact either constructively or destructively in terms of the fluid flow and heat transfer patterns in the liquid pool. Additionally, the phase change process of a multi-component system will take place across a range of temperatures, unlike single substances which have discrete solidification phase change temperatures. Because of the complicated geometry's of the interphase boundaries of these multi-component systems and the variational nature of the relative solubility of the species in solid or liquid phases, the structural growth can be characterized by a mixture of either dendritic or equaxed crystals. This interphase boundary, in hypereutectic and hypoeutectic binary systems, is referred to as the mushy zone. The interplay of the physical effects of the solidification processes, in this mushy

zone, and the disturbances caused by the convective flow field have significant effects upon the morphology of the final structure of the solid product. The solidification of a binary alloy system is governed by the natural convection processes that are a result of the species and temperature gradients present in the liquid pool of the melt. Double-diffusive convection or thermo-haline/ thermo-solutal convection creates a flow field in which the concentration driven density gradients either augment or oppose the thermally driven density gradients. Assuming laminar flow conditions, the underlying mathematical description of these relationships and theoretical influence upon this research show that there is a great deal of correspondence between the heat and mass transfer processes. The heat transfer parameters controlling the development of the thermal boundary layer, Rayleigh number, Nusselt number and Prandtl number have direct analogues in the concentration terms, Concentration Rayleigh number, Sherwood number and Schmidt number. An additional term of importance is the Lewis number which is a ratio of thermal diffusivity to species diffusivity. The buoyant forces that drive the flow field in double-diffusive convection are caused by the changes in density that occur in the fluid by virtue of the thermal and concentration gradients. Therefore;

$$\text{Density} \rightarrow \rho(T,C)$$

Assuming no reaction is occurring between the component species, the concentration of a component species (i) is expressed as;

$$C_i = m_i / V$$

since, density is a property of matter;

$$\rho_i = m_i / V$$

therefore the aggregate density is;

$$\rho = m_i / V.$$

The principle of mass conservation within a control volume, or continuity of flow through it, implies that for a constituent component (i);

$$\frac{\partial \rho_i}{\partial t} \Delta x \Delta y = \rho_i u_i \Delta y - \left[\rho_i u_i + \frac{\partial}{\partial x}\left(\rho_i u_i \right) \Delta x \right] \Delta y + \rho_i v_i \Delta x$$
$$- \left[\rho_i v_i + \frac{\partial}{\partial y}\left(\rho_i v_i \right) \Delta y \right] \Delta x + m''' \Delta x \Delta y$$

where m''' is the constituent i generation term, indicating that the constituent is being produced or consumed within the control volume. This occurs due to chemical reaction or in this case by the production of, or consumption of the species by the phase change boundary. This is analogous to the heat generation term q''' in the heat transfer expression of continuity. In a two component system, where j_i is the diffusion flux vector and $D_{12} = D_{21} = D$ = mass diffusivity, Fick's law shows that;

$$j_i = -D_{12} C_1.$$

which allows the non-dimensional local Sherwood number to be generated as;

$$Sh = \left(\frac{\partial C}{\partial y} \right)_{y=0} \frac{x}{C_\infty - C_0} = \frac{j_0}{C_0 - C_\infty} \frac{x}{D}$$

$$Sh = 0.332\, Sc^{1/3}\, Re_x^{1/2}, \quad Sc > 1$$

$$Sh = 0.564\, Sc^{1/3}\, Re_x^{1/2}, \quad Sc < 1$$

This number corresponds to the Nusselt number for the heat transfer equivalent. Since Nu = hx/k, if we use the term h_m (mass transfer coefficient) then Sh = h_mx/D. This implies that a non dimensional ratio of thermal diffusivity to species diffusivity is possible, the ratio is called the Lewis number, Le.

$$Le = \alpha/D = Sc/Pr.$$

In the case of a vertical wall boundary layer momentum(in y) is described by;

$$u \frac{\partial v}{\partial x} + v \frac{\partial v}{\partial y} = \upsilon \frac{\partial^2 v}{\partial^2 x} + \frac{1}{\rho}(\rho_\infty - \rho) g$$

Applying a Boussinesq type approximation;

$$\rho \cong \rho_\infty + \left(\frac{\partial \rho}{\partial T} \right)_P (T - T_\infty) + \left(\frac{\partial \rho}{\partial C} \right)_P (C - C_\infty) + \ldots\ldots$$

The thermal expansion coefficient;

$$\beta = -\frac{1}{\rho}\left(\frac{\partial \rho}{\partial T} \right)_P$$

has an analogous parameter, the concentration expansion coefficient;

$$\beta_c = -\frac{1}{\rho}\left(\frac{\partial \rho}{\partial C} \right)_P$$

Therefore the boundary layer momentum equation is;

$$u\frac{\partial v}{\partial x} + v\frac{\partial v}{\partial y} = \upsilon\frac{\partial^2 v}{\partial x^2} + g\beta\left(T - T_\infty\right) + g\beta_c\left(C - C_\infty\right)$$

The flow field is coupled to the temperature and concentration fields by solving the boundary layer concentration and energy equations.

$$u\frac{\partial C}{\partial x} + v\frac{\partial C}{\partial y} = D\frac{\partial^2 C}{\partial x^2}$$

$$u\frac{\partial T}{\partial x} + v\frac{\partial T}{\partial y} = \alpha\frac{\partial^2 T}{\partial x^2}$$

A concentration based Rayleigh number can be obtained by extension of the thermal analogy to the mass transfer driven buoyancy;

$$Ra_H = \frac{g\beta\Delta T H^3}{\alpha\upsilon}, \qquad \text{Thermal Rayleigh number.}$$

$$Ra_{m,y} = \frac{g\beta_c\left(C_0 - C_\infty\right)y^3}{\upsilon D}, \qquad \text{Concentration local Rayleigh number.}$$

This analysis is further complicated by the changes in the wall geometry of the sump as it undergoes solidification, the onset of turbulent flow and the effects of the solidification face when hyper or hypoeutectic solutions are being solidified. additionally, the mushy zone is, at its most simple level, considered a porous medium which complicates many of the assumptions previously adopted. It can be seen that, with

the many variability's involved in mathematically modeling these systems simplifications and assumptions regarding the behavior of the actual flow field have to be made. It is imperative to test these assumptions and the consequent validity of the model by applying a controlled set of boundary conditions to an experimental equivalent setup.

1.2 Applications

Phase change, solidification and melting, of both hypereutectic and hypoeutectic binary mixtures is widely encountered in many engineering applications and geophysical processes. For example, the growth of single crystals for the microelectronics industry, weld pool activity in the fusion welding process, thermo-haline systems, such as solar ponds, for energy storage. Additionally in the casting of metal and metal-ceramic alloys, frequently termed M.M.C., (metal matrix composites). In the solar pond, for example, the stratification of a shallow pool of saline liquid is artificially maintained by the opposition of the density driven flows that form due to temperature and salinity gradients. A stable 'stagnation layer' separates the shallow, mixed convection dominated, region at the surface of the pool from a deeper, mixed convection zone at the bottom. The energy transport from the bottom of the pool to the surface layer is inhibited by this 'stagnation layer' which can transfer energy only by conduction. However, significant volumes of heat energy are radiated to the lower layer, during daylight, thereby increasing the enthalpy of the system. The consequent 'hot pool' of saline liquid can be utilized as a source of energy by the application of enclosed, secondary circulation, heat transfer systems. [Gebhart et al.,1988]

The production of binary alloys for aerostructural purposes are of great importance. Aluminum with secondary alloying components or Nickel with secondary alloy components, have significant applications in airframe and turbine engine component parts manufacturing. For instance, directionally solidified single crystal castings are,

increasingly, being used for high operating temperature turbine blades. While 'near net shape' casting techniques are important in the production of high temperature alloys of this kind, due to the requirement that the end product be, as far as possible, free of defects, the greatest volume of cast material is manufactured using the continuous casting process. In this method, molten alloy is poured into a chilled mold cavity which has a 'starter' billet at its base. As the solid crust forms at the mold wall, the starter billet is mechanically lowered at a speed which corresponds to the continuous volumetric flow rate of molten material being poured into the mold cavity. The resultant product is further cooled, on exiting the base of the mold cavity, by direct impingement sprays of water. The hot, malleable billet is then directed through rolls to the cutting station. Much of the driving justification and the experimental equipment design definition is derived from interest in this continuous casting process, as applied to binary systems. The physical form of the experimental test cavities, rectangular, 16 degree and 4 degree V-shaped sumps, is a direct consequence of the known form that the melt pool achieves during solidification. It should be noted that the liquid pool of the continuously cast product billet takes on an angle that is limited by these, aforementioned, angles, this angle being a function of the adjustment of the process variables. The process variables are, the physical properties of the alloy, the degree of superheat, the descent speed of the billet and the cooling jet temperature. Data derived from a full schedule of experimentation in this area may provide optimization information for this type of casting technique.

1.3 Literature review

Mechanical engineering interest in the solidification phenomena of binary solutions has been evident in the literature for about thirty years. Cole and Bolling (1965) presented a study dealing with natural convection in the melt of alloys undergoing solidification. Later, experimental data were collected by other metallurgists who used temperature data and visual inspection techniques to derive information regarding compositional variations of metallic solids. (Backerud and Chalmers, 1969; Streat and Weinberg, 1974) Their conclusions showed that convection in the melt pool was significantly affecting the segregation of species, species redistribution and dendritic growth rates.

Relevant work has been performed by geophysicist who have identified double-diffusive mechanisms in magma chambers, oceanic environments etc.. This work supports the hypothesis that natural convection in the melt has a significant effect upon the solid structure that forms in a system under phase change. (Mendenhall and Mason, 1923; Chen et al.,1971; Chen, 1974) Further work by Turner with Huppert (1980) and with Chen (1980) support the conclusion that, double-diffusive mechanisms cause layering of the melt pool.

Many of the initial studies on double-diffusive convection were performed by oceanographers, where the temperature and concentration gradients exist in a vertical direction (Turner, 1979, Ostrach, 1983). Other studies have been conducted on solidification systems where a horizontal temperature gradient is present to simulate the

casting process (Hu and El-Wakil, 1974, Benard et al., 1989, Kamotani et al., 1985, Lee et al., 1988, Beckermann, 1987, Christenson and Incropera, 1989).

The use of the aqueous ammonium chloride model for binary solidification was validated in experiments by Szekely and Jassal (1978). This study was an experimental and analytical study which used a single set of boundary conditions. Only temperature and velocity data were collected experimentally, the temperature data were taken at six points and the velocity of the flow field was achieved using dye tracing techniques. Since no solute distribution data were collected the results, a comparison of the early stages of solidification, show no double-diffusive phenomena.

Due to the complexity of modeling double-diffusive convection during the solidification process, theoretical study on this topic is still in the developing stage. Therefore, experimental study is still the most powerful means to understand these basic phenomena. The work of Beckermann and Viskanta (1988) extended the use of the ammonium chloride model by the development of sampling techniques. Concentration measurements were facilitated by the use of hypodermic syringes for the extraction of fluid samples. The concentration is derived by correlation to the refractive index of the sample. With a more extensive, more densely distributed, temperature grid these experiments gave information regarding the double-diffusive effects encountered. Visualization techniques in these experiments employed standard shadow graph apparatus.

Later experimentation (Christenson and Incropera, 1989) extended the use of the simulation using ammonium chloride solutions with a more extensive set of boundary conditions and slight refinements to the data collection procedures of the previous work. Further refinements of the experimental techniques and closer scrutiny of the effects of geometric parameters were studied in papers by Burton, Ebadian et. al. (1993,1994,1995).

An extensive survey of the associated literature, mostly numerical studies, indicates that double diffusive flow and heat transfer in a cavity are very sensitive to changes in the boundary conditions, including changes of geometry and cooling conditions at the exterior boundary, i.e. adiabatic, constant temperature or constant flux, and to the time derivatives of these changes. Incropera's work (1989) with Christenson and Bennon, shows extensive development of the numerical model for the solidification of binary systems. Although the cavity size was fairly small an experimental to numerical model comparison was achieved by this publication. Solidification fits, most closely, the general behavior model of a moving boundary problem, its solid/liquid interface being a time dependent geometric characteristic. The nature of this temperospatial problem is well documented in works involving heat conduction with phase change. In a published study of globulitic solidification in a binary alloy system (Beckermann,1993), a numerical model was developed. This model included techniques to model micronucleation, species diffusion (in solid and liquid phases) and accounted for the movement of the interface boundary. Variation in undercooling, cooling rate, thermophysical properties, spatial and impingement parameters were studied for an Al-Cu alloy. Numerical studies have been conducted using

a continuum model for energy, species and momentum transfer in binary alloy solidification, (Incropera et al, 1992) which looked at the effects of recalescence and solid transport in the melt. Applications of knowledge of double-diffusive flows are seen in the numerical simulation of the effects of magnetic damping of these flows, (Prescott et al, 1992).

Multicomponent systems undergoing phase change are, however, of a higher order of complexity. The development of species segregation mechanisms at the liquid/solid interface and the treatment of the complications due to heat and mass transfer over a range of solidification temperatures lend themselves to a variety of numerical solution techniques. Patankar's (1980), SIMPLE algorithm has been successfully employed to model the turbulent mixed convection of steel and the related heat transfer mechanisms, (Khodadadi et al,1992).

More recent studies have described models of the phase change behavior of systems in which double diffusive convection phenomena are incorporated but experimental validation of these models has been sparse,(McNulty et al. 1994; Incropera and Krane, 1994). Dual scale segregation,(Sundarraj and Voller,1994), multiscale segregation, (Beckermann and Wang,1994) have been applied to binary and multicomponent system models. Additionally, recent works on transport phenomena in solidification have focused on the mechanisms in the mushy zone and have looked at techniques to describe the remelting and solidification characteristics of this region in terms of stereological modeling techniques, (Marsh and Banerjee, 1994).

1.4 Objective

The main purpose of this investigation is to experimentally study the effects of boundary conditions, both geometric and thermal, on the double diffusive flow inside the liquid pool, with a view to quantifying the net effects on the flow field. These data and conclusions will be presented with the goal of developing research paths for an ongoing investigation into methods of defect control in continuous casting processes for binary alloys in industrial applications.

Previous researchers have indicated that the major causes of structural defects and inhomogeneity, macrosegregation and microsegregation, during solidification can be attributed to irregularities in the convection flow pattern in the melt pool and at the mushy zone (Flemings, 1974, and Fisher, 1981). Therefore, knowledge of the transport phenomena of thermally and solutally driven convection in a cavity is essential for maintaining satisfactory control over the solidification process. Since, almost all, commercial castings are alloys of two or more component chemical species, the mechanical properties of the finished product are directly related to the homogeneous distribution of the constituent species or conversely, the degree of inhomogeneity that is present in that distribution.

This experimental program consisted of three discrete phases. The first involved the use of a 16° V-shaped sump, in which a phase change was induced upon the contained working fluid. For these experiments, an aqueous solution of ammonium chloride was employed. The tests were run for 5 %, 15 % , hypoeutectic concentration

regions, eutectic concentration and for 25% hypereutectic concentration solutions. Note, throughout this document all concentration references are weight percent values. This phase of experimentation characterizes the flow field as established in the V-shaped sump.

Concentration NH_4Cl	ρ_l / ρ_s (kg/m^3)	c_l / c_s (J/kgK)	k_l / k_s (W /mK)	D_l (m^2 /s)	β_T (1/K)	β_c	μ (kg / ms)	Δh (J /kg)
10 %	1046.0 / 918.0	3390 / 2078	0.468 / 2.19	0.75×10^{-9}	$2.046 \times 10^{-}$	-0.286	1.3×10^{-3}	3.334×10^{5}
30 %	1077.7 / 1102.0	3249 / 1870	0.468 / 0.393	1.8×10^{-9}	$3.832 \times 10^{-}$	- 0.257	1.3×10^{-3}	3.138×10^{5}

Physical properties of NH_4Cl.

Table 1

The second phase employed a rectangular sump, using ammonium chloride aqueous solutions. Experiments were run to establish the flow field characteristics in eutectic, 19.7 %, hypoeutectic, 5 % and hypereutectic, 25 % liquid melt pools.

The final phase, used either a 4°, 16° V-shaped or a rectangular sump. The rectangular sump was alternately operated with and without bottom cooling. The purpose of this phase of the experimentation being to establish the effects on the flow fields of differing thermal and geometric boundary conditions.

For the first phase of experimentation the following boundary and initial conditions were used;

Run No.	Concentration % wt.	$T_o(C^o)$	$T_i(C^o)$
1	5	-10	10
2	5	-10	5
3	5	-10	0
4	5	-20	10
5	5	-20	5
6	5	-20	0
7	5	-25	10
8	5	-25	5
9	5	-25	0
10	15	-20	10
11	15	-20	5
12	15	-20	0
13	15	-25	10
14	15	-25	5
15	15	-25	0
16	19.7	-20	0
17	19.7	-20	-5
18	19.7	-20	-10
19	25	0	20
20	25	0	15
21	25	-10	25
22	25	-10	15
23	25	-20	25
24	25	-20	15

Boundary and initial conditions, Phase 1.

Table 2

In the absence of significant differentiating behaviors for the other cases, later experiments included the following boundary and initial conditions;

Run No.	Concentration % wt.	$T_o(C^o)$	$T_i(C^o)$
1	19.7	5	-20
2	5	5	-20
3	15	5	-20
4	25	25	-20
5	25	25	-10
6	25	25	-30
7	25	15	-20

Boundary and Initial conditions, other Phases

Table 3

Specifically then, these experiments have four objectives;

1. To establish the characteristic heat transfer mechanisms, flow fields and effects of double diffusive convection on the product of solidification in a V-shaped sump.

2. To establish the characteristic heat transfer mechanisms, flow fields and effects of double diffusive convection on the product of solidification in a rectangular sump.

3. To establish the effects of bottom cooling on the flow field, heat transfer mechanism in a rectangular sump.

4. To establish the effect of the V angle on the flow field and heat transfer mechanism in a V-shaped sump.

CHAPTER 2 - EXPERIMENTAL TEST EQUIPMENT

2.1 - Test sumps

For the purposes of this experimental investigation, three test sumps were constructed. The bulk of material manufactured using the continuous casting method of production is of rectangular cross section. A sump, using that geometry, was utilized with the capability provided to enable the alteration of the sump to achieve differing wall thermal boundary conditions. This was achieved by, interchanging the base of the sump between a cooled copper base and an uncooled acrylic base. Additionally, two sumps were designed and built with V-shaped cross sections, in angles of 4 degrees and 16 degrees in order to simulate the melt pool residual angle as empirically established from previous observations, of the continuous casting process.

a. 16 degree sump

The preliminary design for this sump called for a thin walled copper containment that rejected heat by means of the expansion and consequent phase change of chloroflourocarbon (cfc - R12). In view of the environmental and practical difficulties of this mechanism, a more conventional secondary coolant, cold wall, structure was employed. Cooling walls were manufactured from a monolithic plate of aluminum alloy, 6065-T6, by machining on a Bridgeport vertical milling machine. Aluminum was selected as an alternative to thin walled copper since it provided resistance to the

corrosive effects of Ammonium Chloride and still retained an acceptably large coefficient of thermal conductivity.

The outer walls were machined with secondary fluid cooling galleries and were sealed with a cover plate of aluminum. Each wall was independently manufactured with a base angle of 8° to obtain an assembled enclosure angle of 16° and were attached at the base with 9 x M10 stainless steel bolts, fig.[2.1]

The front and rear of the cavity were closed out by two panels of optical quality acrylic sheet and the top of the unit was fabricated from the same acrylic material. Provision was made to evacuate the front and rear cavities and gauges and valves were installed to isolate and record the internal cavity depression. Similar provision was made to the top plate to allow preprocessing of the experimental fluid.

b. 4 degree sump

As seen in figure[2.2] a more self contained apparatus was developed for the 4° sump. In this unit, coolant channels were machined into a 2 cm plate of C-110 copper plate, an outer wall of 1.5 cm acrylic sheet was fabricated for each wall and the wall units were attached at the base with 6 x M10 stainless steel bolts. Again, the total angle was achieved by machining each wall with a half angle cut at the base. The connected plates were mounted in an acrylic support structure which incorporated the vacuum cavity end plates. The end plate cavities were constructed so that they could be

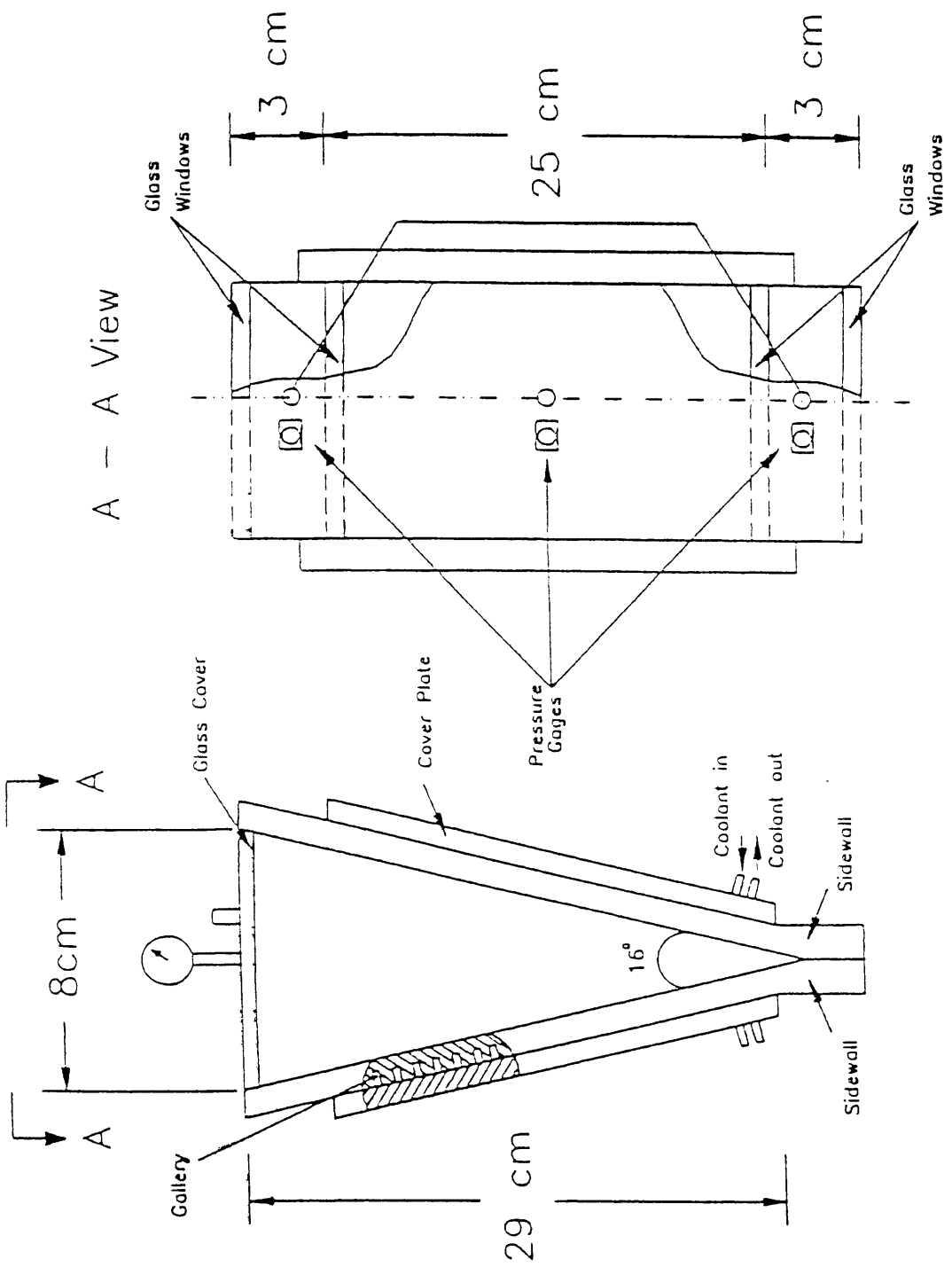

Figure [2.1] 16^0 V-shaped sump, Dimensions.

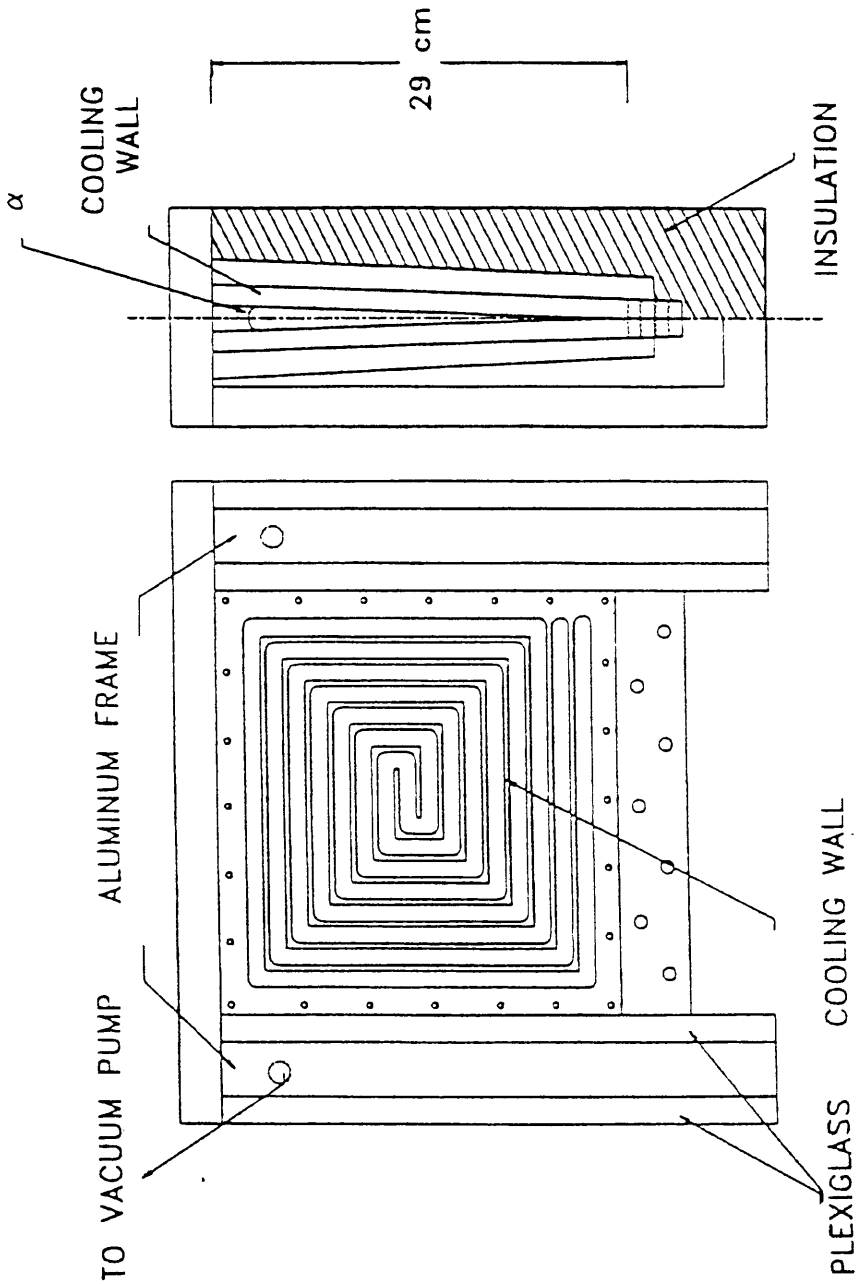

Figure [2.2] 4^0 V-shaped sump, Schematic.

partially filled with an anhydrous desiccating compound to prevent condensation build up during cooling, to aid in visualization.

c. Rectangular sump

The rectangular sump was fabricated in a similar manner to the 4° sump. Two walls, with serpentine galleries were machined from C110 copper plate, the outer panels for these were also machined from C110 copper.

Two bases were fabricated, one from 1.5 cm acrylic sheet and the other from C110 copper plate. Cooling channels were configured in the copper base and by interchanging these base plates two different bottom boundary conditions could be achieved. Either, constant temperature, using the cooled copper base or adiabatic by using the acrylic base. figure[2.3]. End plates, made from acrylic, were manufactured , incorporating access for microsyringe inserts to facilitate fluid sampling.

It should be noted that the thin wall structure and small difference in thermal resistance between the copper and aluminum materials, along with the high heat flow rate achieved by the cooling units virtually negates any differences in the experiments due to this material change

2.2 - Instrumentation and Measurement

a. 16 degree sump

The equipment supplied and utilized for data collection for the 16° sump consisted of a locally fabricated polycarbonate support frame (.25 cm thick) with 17 'E' type thermocouples embedded at locations as specified in figure [2.4] and Table [1]. The

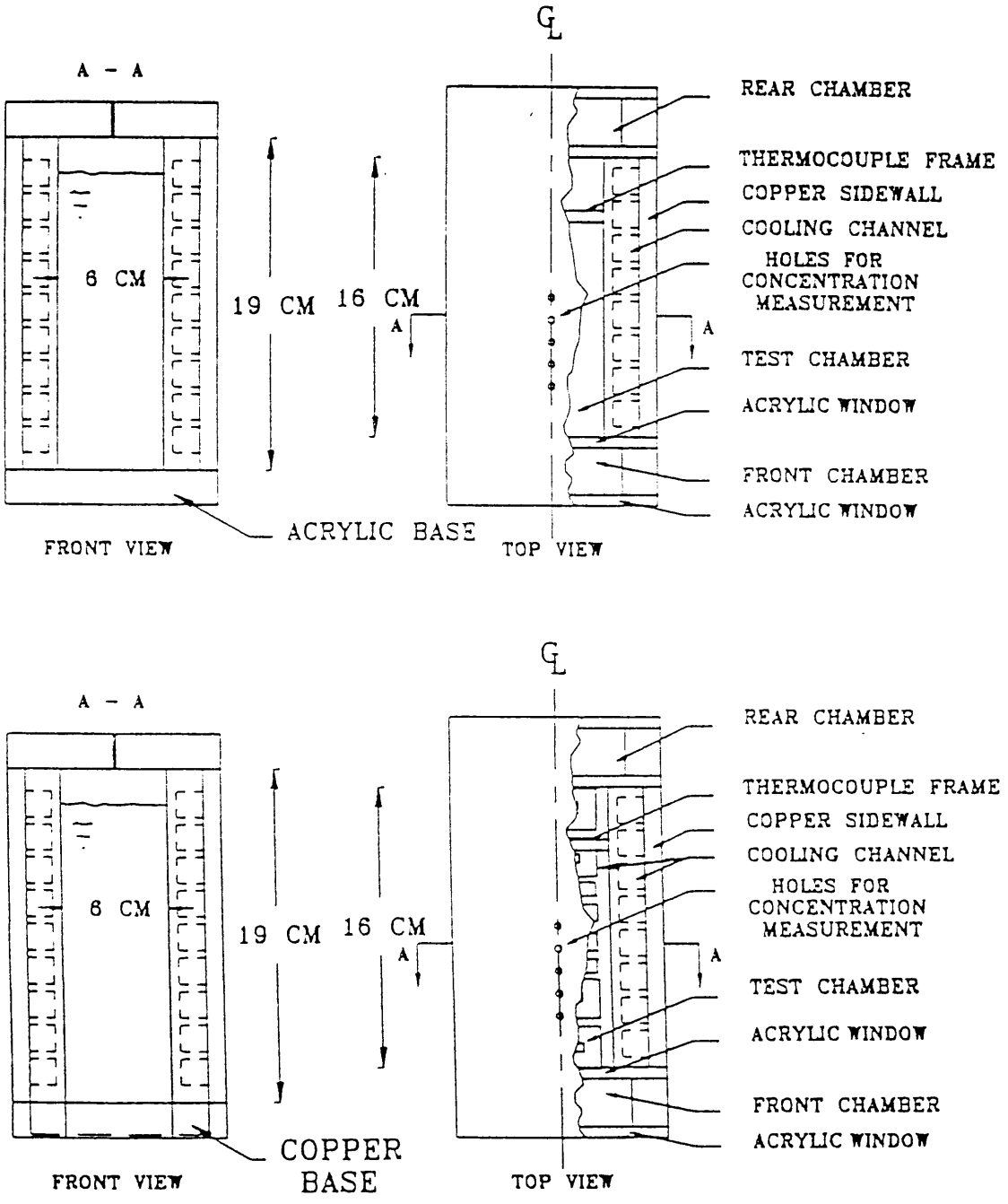

Figure [2.3] Rectangular Sump, configurations a) and b).

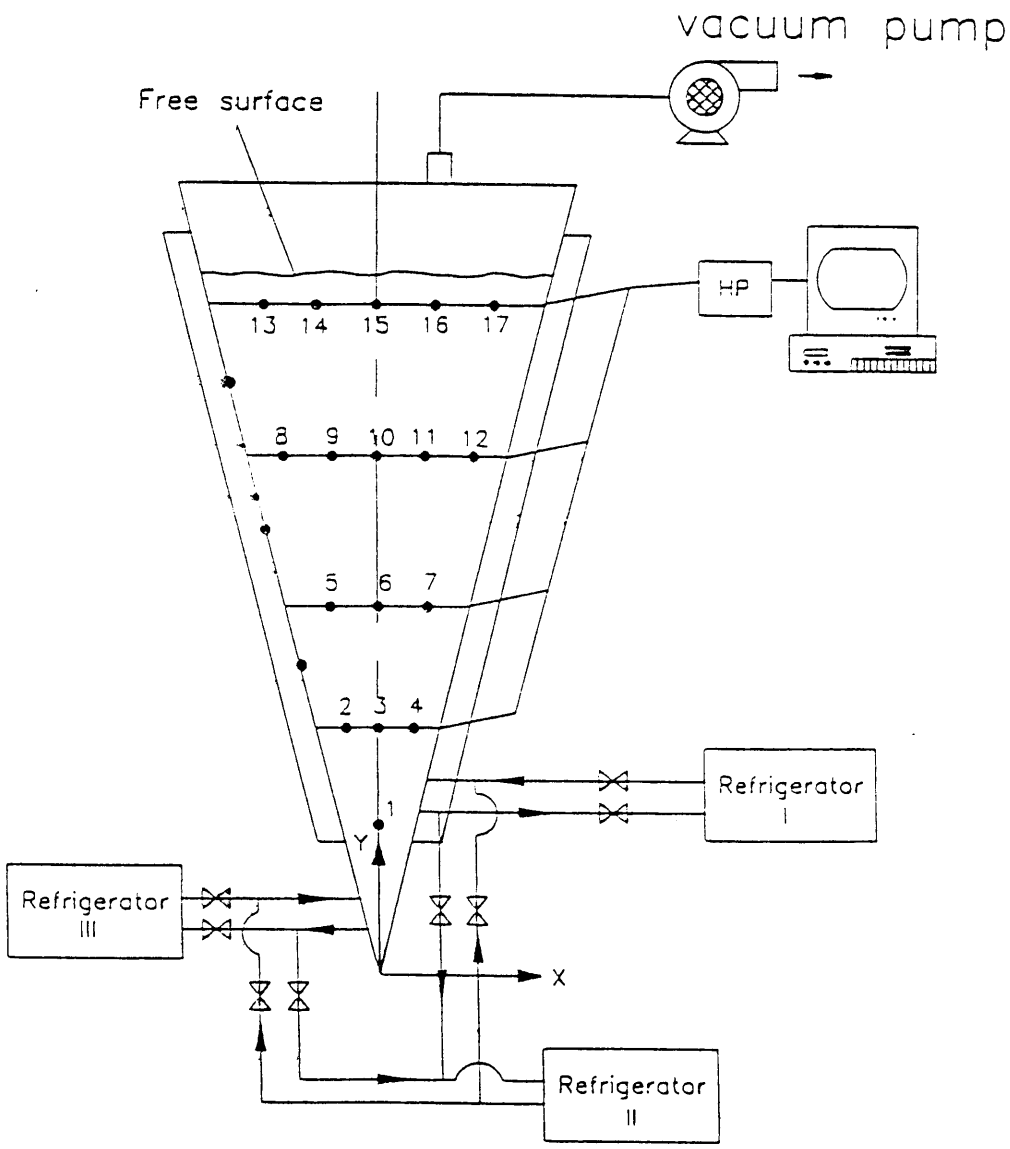

Figure [2.4] Schematic of the cooling system, typical.

thermocouple density was later increased to 40 type 'E' thermocouples as seen in figure[2.5]. These thermocouples were connected to a Hewlett Packard 3852a data acquisition unit, controlled by a model 40826 personal computer utilizing a locally written HP Basic data collection program to store the temperature profile data. The frame was physically located at approximately the mid plane of the sump to ensure minimal environmental end effects.

Provision was made in the top cover to allow the insertion of long microsyringe needles to effect the physical sampling of the fluid in the sump at discrete intervals during the experiments. Since these microsyringes only withdrew approximately .5 - 1.0 ml of fluid the volume of the removed fluid made no significant change to the originating volume of the test fluid. A support frame was used to maintain fixed geometric positioning of the syringes. The fluid samples from different levels in the sump, along the centerline and cross plane to the centerline, were then read in an Abbe refractometer to determine their respective refractive indices. The refractive index of each sample was cross referenced to a locally prepared, refractive index to concentration, correlation, thereby determining the concentration distribution data for the sump.

Videographic recording of the experiment was obtained using a Panasonic model KR 412 CCD camera with specialized lenses and a Sony SVO 160 video recorder. Dye tracing and particle tracing techniques were utilized to qualitatively evaluate the flow patterns seen in the sump. Visual data were captured, as still images, by using Data Translation proprietary hardware and software loaded on a Gateway 2000 40486 personal

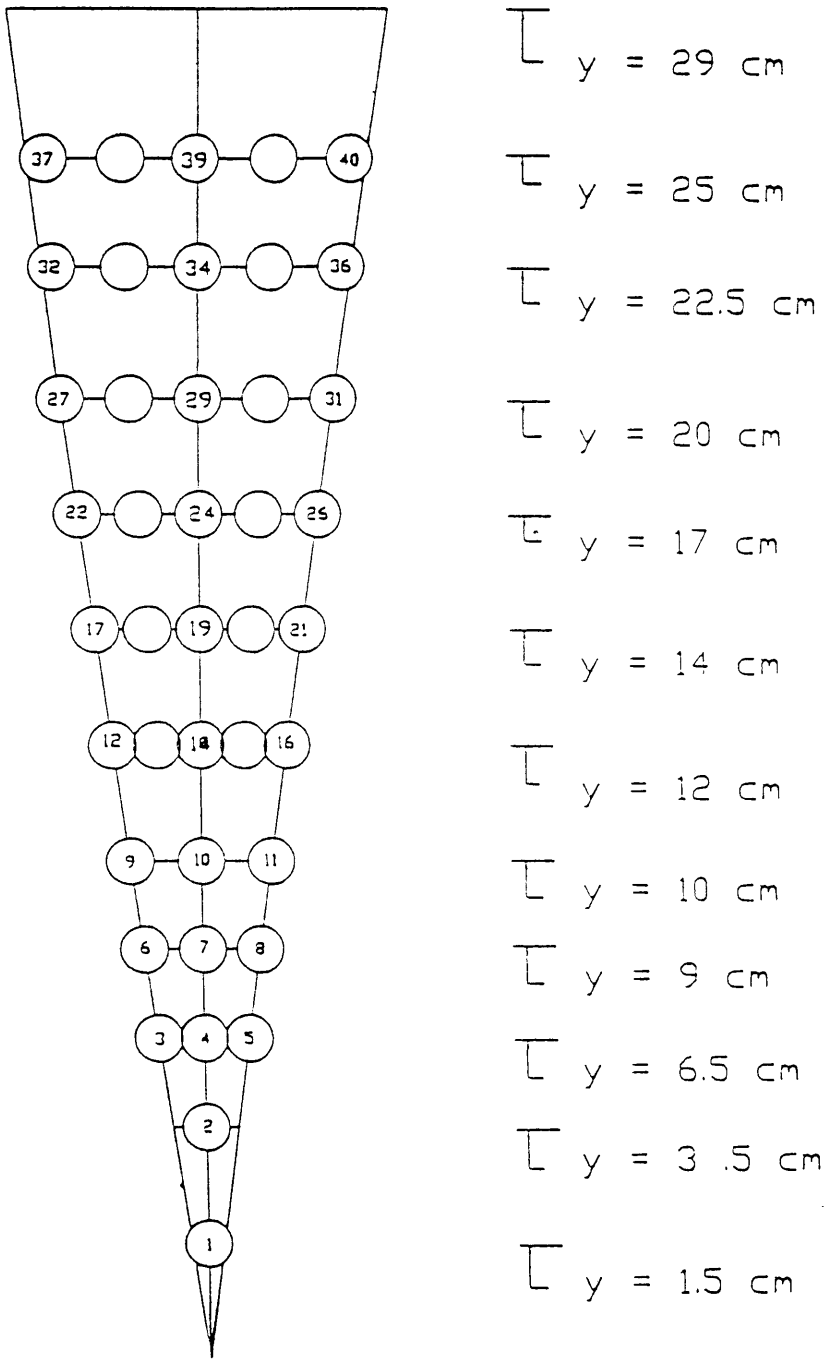

Figure [2.5] Location of Thermocouples, 16^0 V-shaped sump.

computer with video feed from the Videographic data recorder. Additional images were recorded using still photography using a Canon T80 still camera with laser light sheet illumination.

b. 4 degree sump

The 4^{o} sump instrumentation consisted of a modified version of that provided for the 16^{o} sump.

A customized thermocouple grid was manufactured to allow a greater density of temperature data, utilizing 30 type 'E' thermocouples, figure [2.6]. Additional thermocouples were placed for recording the wall temperatures to monitor the boundary accurately. The Hewlett Packard data acquisition system was utilized for temperature data collection. Concentration data were collected, by sampling, through ports machined into the end frame of the sump, microsyringe samples were collected and submitted to the refractive index- concentration correlation procedure previously described. Video recording was performed as in the prior example with still image capture using the Data Translation program.

c. Rectangular sump

The instrumentation of the rectangular sump employed a thermocouple rake using 40 type 'E' thermocouples regularly distributed over a polycarbonate grid, figure [2.7]. Five thermocouples were embedded in each of the walls and, in the case of the C110

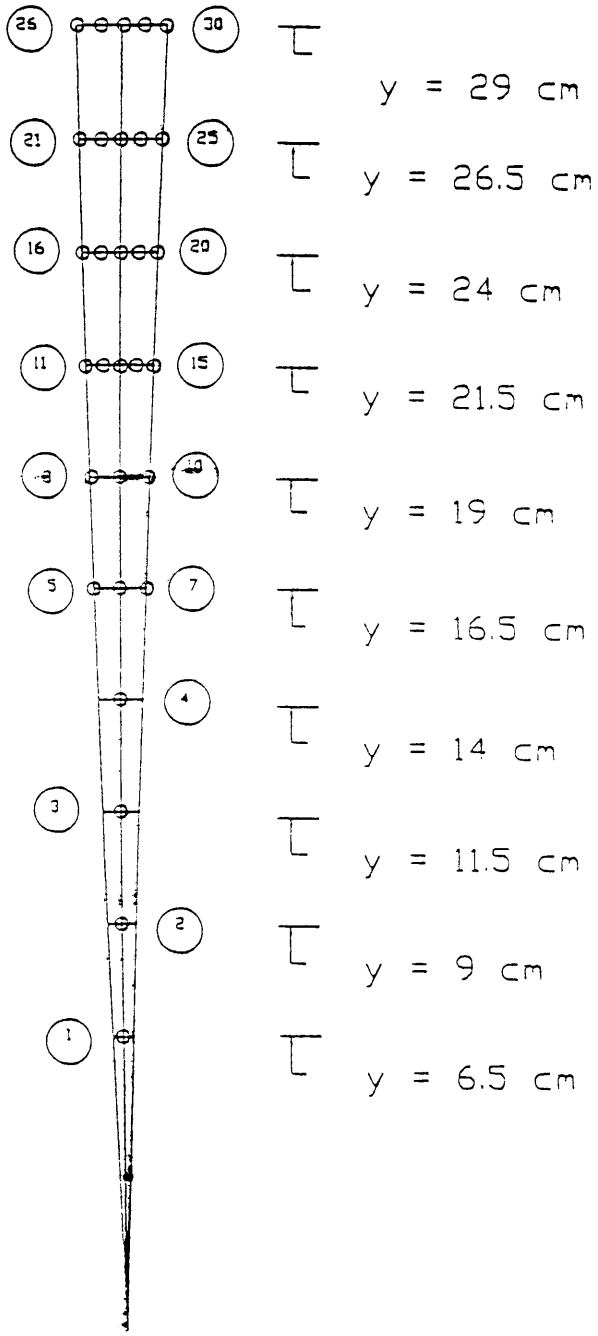

Figure [2.6] Location of Thermocouples, 4^0 V-shaped sump.

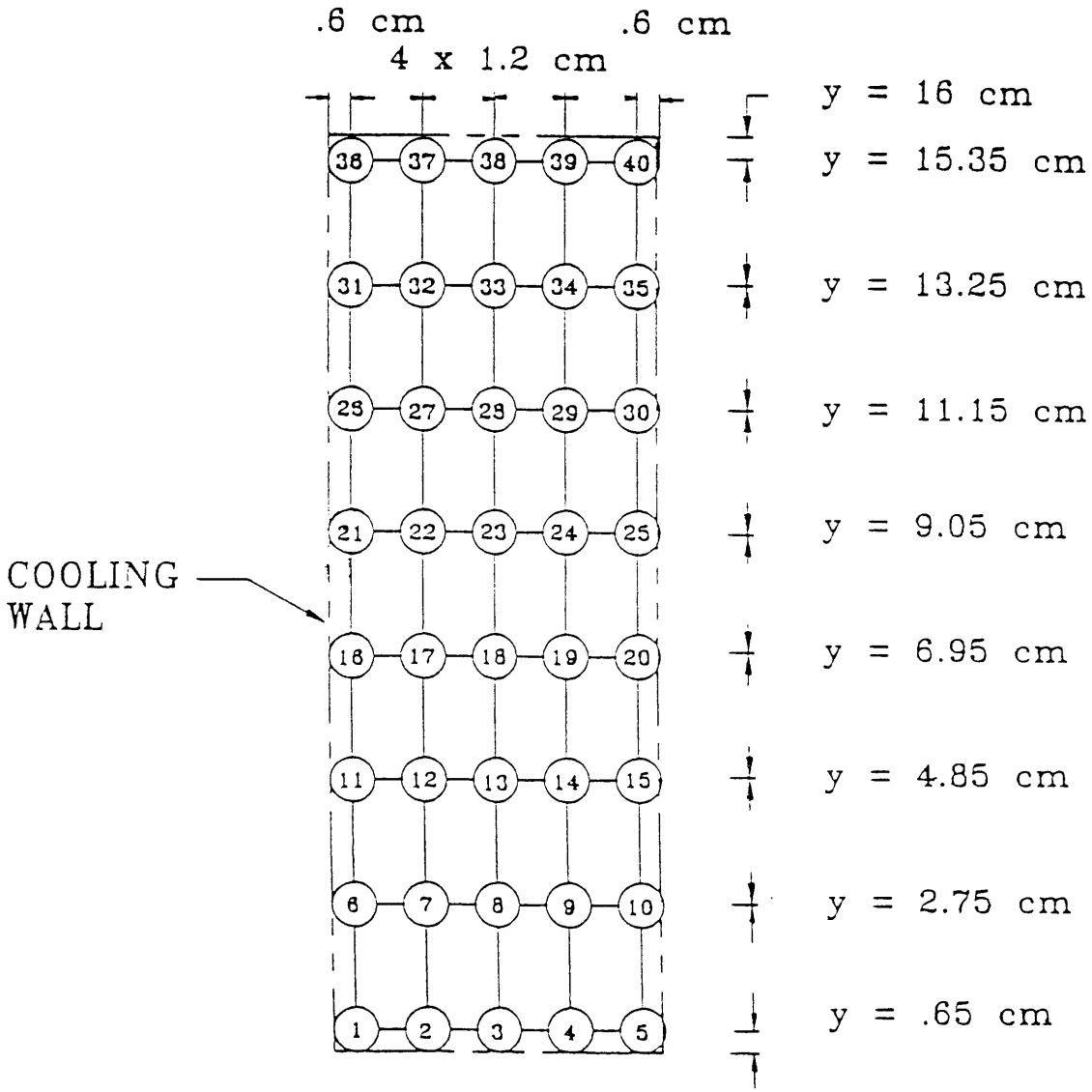

Figure [2.7] Location of Thermocouples, Rectangular sump.

copper base, in the bottom of the lower panel. These were again attached to the Hewlett Packard data acquisition unit to monitor the boundary temperature. End frame access was employed to allow microsyringe sampling and the same Videographic recording of optical data was utilized.

2.3 - Phase change analogue system selection

a. Ammonium chloride, $NH_4Cl.nH_2O$

For the vast majority of experiments in this series the phase change analogue, model, was an aqueous solution of ammonium chloride. Ammonium chloride is an acidic salt produced as a line component from the Solvay process. Commonly referred to as sal ammoniac, it is also a naturally occurring sublimation product of volcanic action. The eutectic concentration for aqueous ammonium chloride is 19.7 weight percent and the eutectic temperature is -15.4 °C. When passing into solution ammonium chloride is mildly endothermic liberating 3.82 kg.cal/g.mole. Since it is an acid salt, with corrosive effects similar to dilute hydrochloric acid, materials selection for the fabrication of the sumps was driven by this consideration. The corrosive effects are complicated by the ammonium ion which can form chemical complexes with both nickel and, importantly for our application, copper cations when in oxidizing conditions.

With regard to materials selection criteria, both aluminum and copper are susceptible to corrosive action when in contact with ammonium chloride solutions. For aluminum, pitting can be observed in solutions of less than 1%, albeit mildly at ambient

temperatures, with greater activity levels when exposed to hotter and more concentrated solutions. Copper is subject to the production of chromophoric products and to stress corrosion cracking by free ammonia, the rates of production of the chromophores being a function of both solution concentration and temperature. These effects are thus reduced in the low temperature range of operation for these experiments.

The principal advantages of ammonium chloride solutions are that they are transparent and that they have phase equilibrium behaviors that are similar to binary metal alloys. Transparency of the analogue system is important for flow visualization and observation of the solidification behavior, additionally the temperature and concentration variation of the refractive index of the liquid is utilized for the monitoring of the concentration distribution in the experimental sump.

b. Sodium carbonate, $Na_2CO_3.nH_2O$

Apart from some mild irritant effects to the skin and eyes, sodium carbonate is a moderately benign chemical compound. With regard to the phase equilibrium behavior of this aqueous system, it has a slightly non-linear liquidus distribution, linearized for analytical purposes in this study, with a eutectic concentration of 5.9 weight percent and a eutectic temperature of - 2.1 ^{o}C. The only significant oxidation hazard from sodium carbonate is in the presence of extremely hot aluminum, where explosive activity can be expected, so for our purposes its relatively neutral corrosive nature was advantageous. However, it is only partially transparent in the range of temperatures around the eutectic temperature, so it is therefore, not as reliable an indicator for concentration-refractive

index correlation purposes in determining the concentration distribution by sampling. In moving into solution sodium carbonate is exothermic producing, 5.57 kg.cal/g.mole.

Figures [2.8, 2.9, 2.10] show a comparison of the phase change equilibrium charts of aqueous ammonium chloride systems , aqueous sodium carbonate systems and that of a binary metallic alloy. It can be seen that the similarities, between the aqueous systems employed and that of the metallic system are evidenced by the nature of the liquidus and solidus geometry's with the existence of the characteristic eutectic point. It should be noted, however, that significant differences between these systems and metallic systems exist in terms of their Prandtl number behaviors. That is, the ratio of the kinematic viscosity to thermal diffusivity, for the respective systems, differ greatly.

2.4 Cooling system

The system employed for cooling the sumps was common to all three experimental setups. Refrigerated cooling equipment was provided for the secondary coolant circuits, this consisted of two Cole Parmer , model 12102-10, Polystat baths each with 750 watts cooling capacity at -20°C and one Fisher scientific refrigerated bath with 450 watts cooling capacity. The smaller capacity unit was connected to the plumbing circuit so that it regulated both walls simultaneously to obtain the prerequisite starting temperature for the experiment. The larger capacity units were connected so that when their reservoir fluid had attained the required boundary condition temperature they could be valved to regulate each wall temperature independently, figure [2.4]

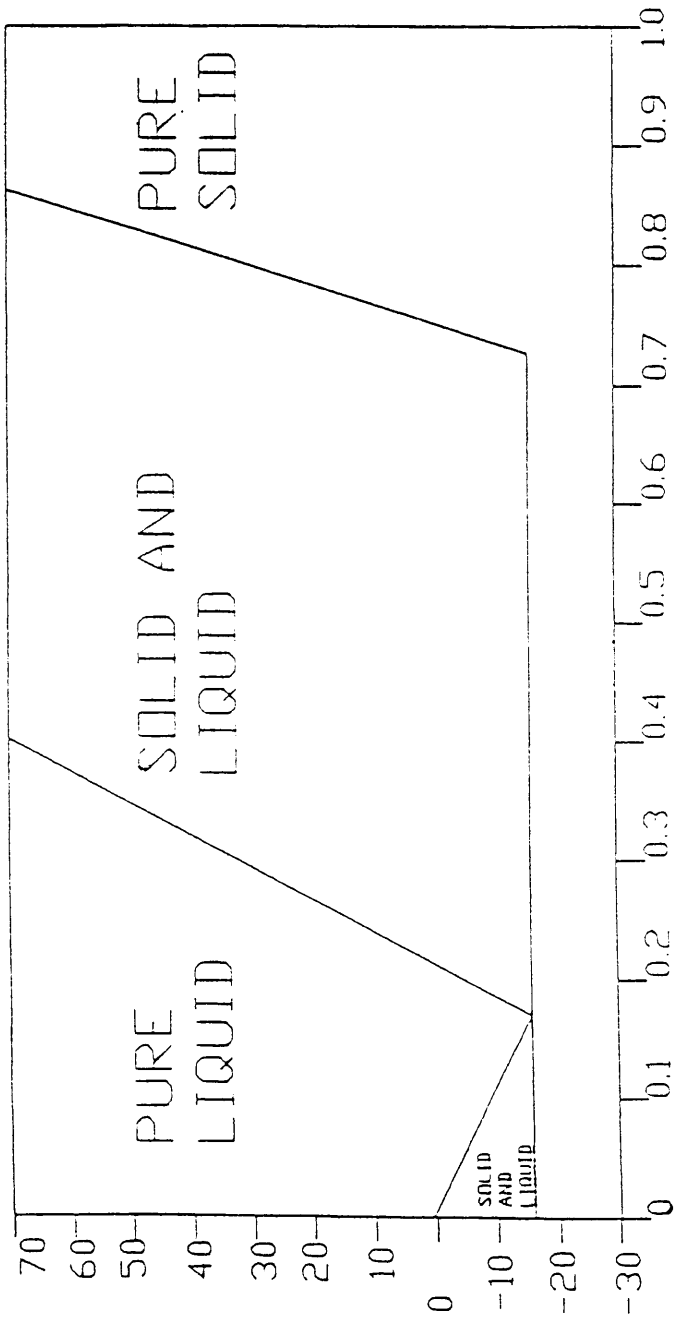

Figure [2.8] Phase Equilibrium diagram - $NH_4Cl.nH_2O$

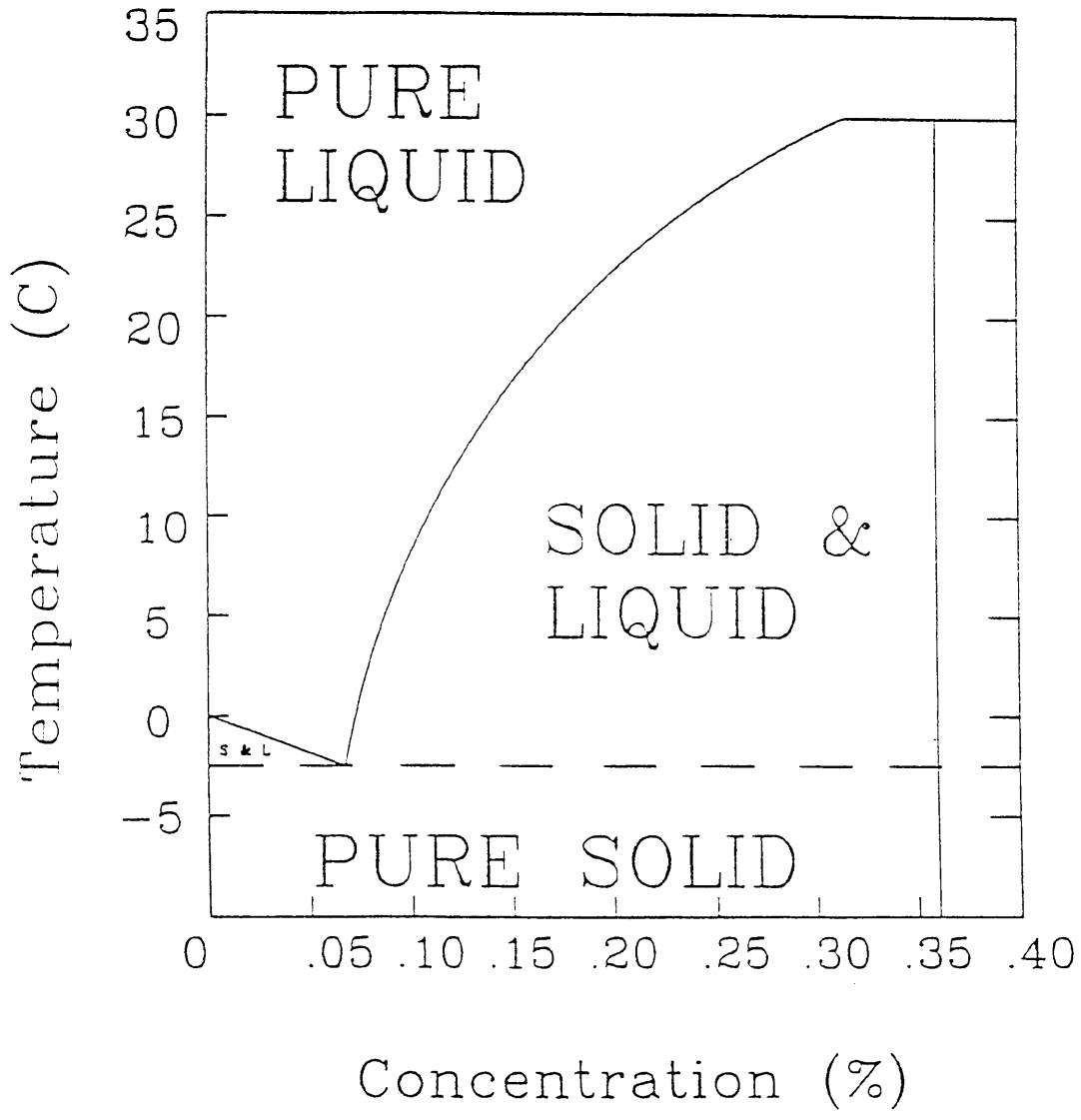

Figure [2.9] Phase Equilibrium diagram -$Na_2CO_3.nH_2O$

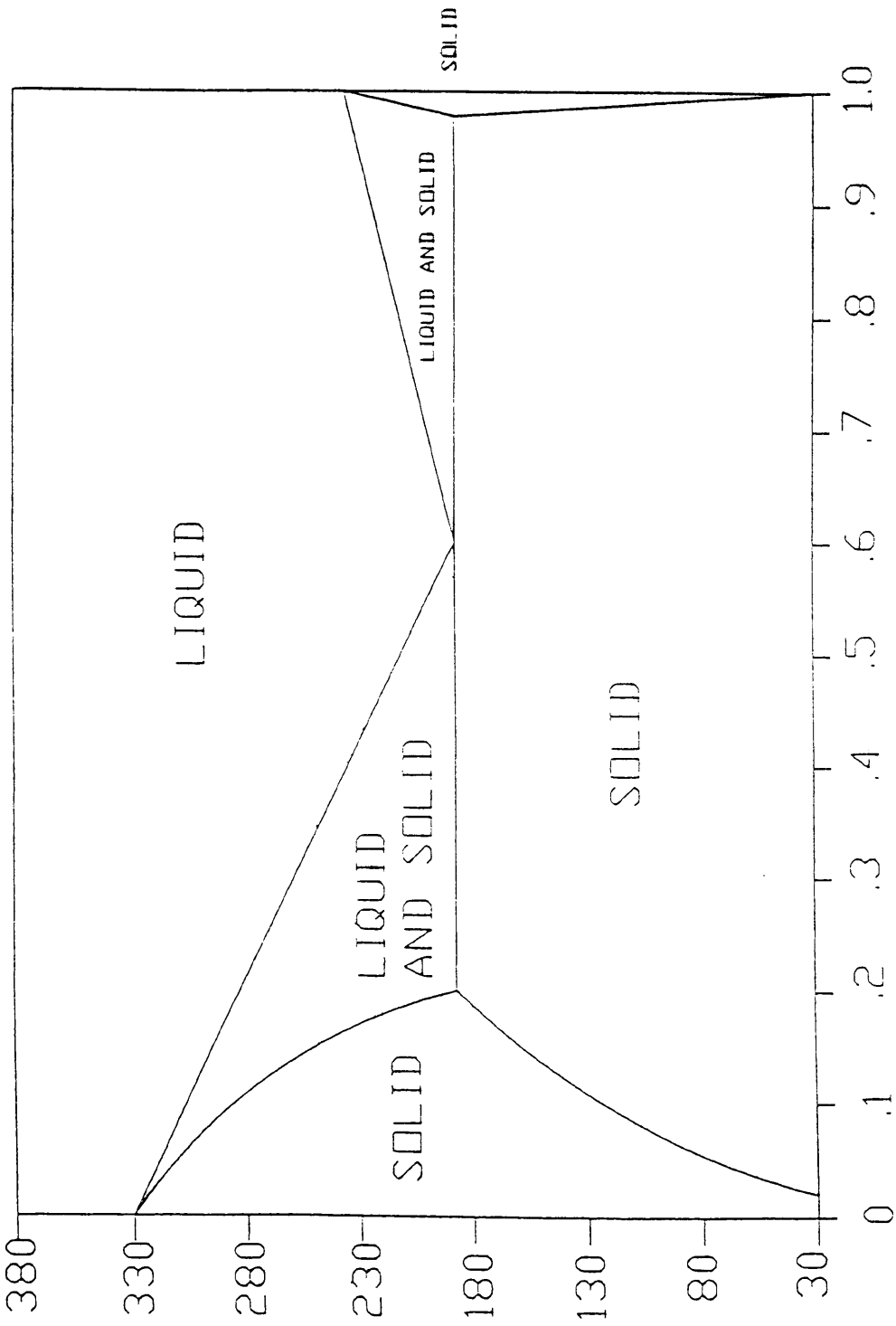

Figure [2.10] Phase Equilibrium diagram - Pb-Sn.

Two inch thick Styrofoam was fitted to provide an insulated containment for the sumps while in operation, thereby minimizing environmental effects upon the experiment.

2.5 Test Procedures

The experimental test procedures for the operation of each of the test sumps was essentially similar. The preliminary setup of the sump consisted of, filling the sump with the analogue fluid and applying vacuum to the front and back cavities and to the air space above the fluid. In order to achieve degassing prior to filling, the analogue fluid was maintained at a temperature close to boiling for a few minutes and then cooled. The test sump was now activated by connecting, through a valving mechanism, the single preheat thermal bath which pumped a water/glycol mixture through both walls, in the cooling passages. The temperature of the walls and the bath as a whole was monitored to attain the experimental preheat required for an individual experiment. When the entire system had attained the preheat temperature, the two chiller baths were activated by valving to feed each wall independently, this valving disconnected the preheat bath from the circuit and this unit was shut down. Constant monitoring was now maintained to acquire a given wall temperature for the experiment using the Hewlett Packard data acquisition system. Temperature monitoring was maintained throughout the duration of each experiment and these data written to a data file. The sampling rate for temperature data was highest at the origination of the test, usually every 60 seconds for the first hour and then every 5 minutes thereafter. Concentration data were collected on a 5 minute sampling basis for

the first hour and subsequently every 15 minutes, typically. Visualization, using the video equipment was constantly acquired and still imagery was acquired at discrete intervals.

The experiment was run until the entire analogue sample had achieved phase change and then the experimental equipment was shut down and cleaned in preparation for future experiments.

Experimental uncertainties occur in the collection of the temperature data and the concentration data. The thermometry calibration of the Hewlett Packard instrumentation achieves a claimed value of 0.05°C. Since, there is a small difference in location of the thermocouple plane and the plane from which concentration samples were taken, these differences have been calculated to cause an potential error of 0.15°C. The cumulative uncertainty for the thermal data is on the order of 0.2°C.

The uncertainties occurring in the measurement of the concentrations in these sumps come from several sources. The positioning of the microsyringe for the sample extraction, the accuracy of the refractometer used for the measurement of the sample's refractive index and the accuracy of the correlation used to determine the concentration from the optical data. The combined effect of the last two conditions has been calculated to be within 0.2 weight percent. Since, great care was taken in fabrication of the microsyringe ports and the microsyringe shaft is a relatively rigid structure, the positional error is neglected.

With regard to the flow field patterns and the data regarding the volumetric growth rates of the solid / mushy interface no evaluation can be presented for the experimental uncertainty. These data are reported in the body of the work as qualitative information. It is important to note that, due to the highly repeatable nature of the reported events and the frequent and careful observation of the experiments performed, reliability of these data is considered to be high. Therefore, the photographic and graphic representations included in this manuscript are highly demonstrative of the typical events in the solidification phase change activity of these experiments.

CHAPTER 3 - EXPERIMENTAL RESULTS AND DISCUSSION

3.1 16° V-Shaped sump experimentation

The simplest case of solidification of a binary mixture is the case of eutectic composition. In eutectic composition, the solution exhibits the phase change behavior of a pure substance, and the convective flow is driven solely by the thermal buoyancy force. Figure [3.1] shows the history of the solid/liquid interfaces in a eutectic concentration solution with initial preheat temperature of 5 °C and a cooling wall temperature of - 20 °C, in diagrammatic form. Thirty minutes after the start of the experiment, Fig. [3.1a] shows that the solid interface developed on the side walls in heterogeneous nucleation. The solid/liquid interfaces appeared very smooth and were distributed evenly across both surfaces. Since the solution temperature in the center of the test chamber was higher than that near the interface, a thermally driven natural convection was generated. The fluid near the cooling interface flowed downward and then rose in the center region to form two, half domain oriented, recirculation loops. As time elapsed, the volume of the solidified region increased, but the liquid region always remained in a V-shape, conforming to the wall geometry, as seen in Figs. [3.1b] through [3.1f.]

For a solution with a hypoeutectic composition, the solute will be ejected during the solidification process and the two-phase interface is characterized as the mushy zone. As a result, there exists a high concentration region in and near the interdendritic zone. Since the

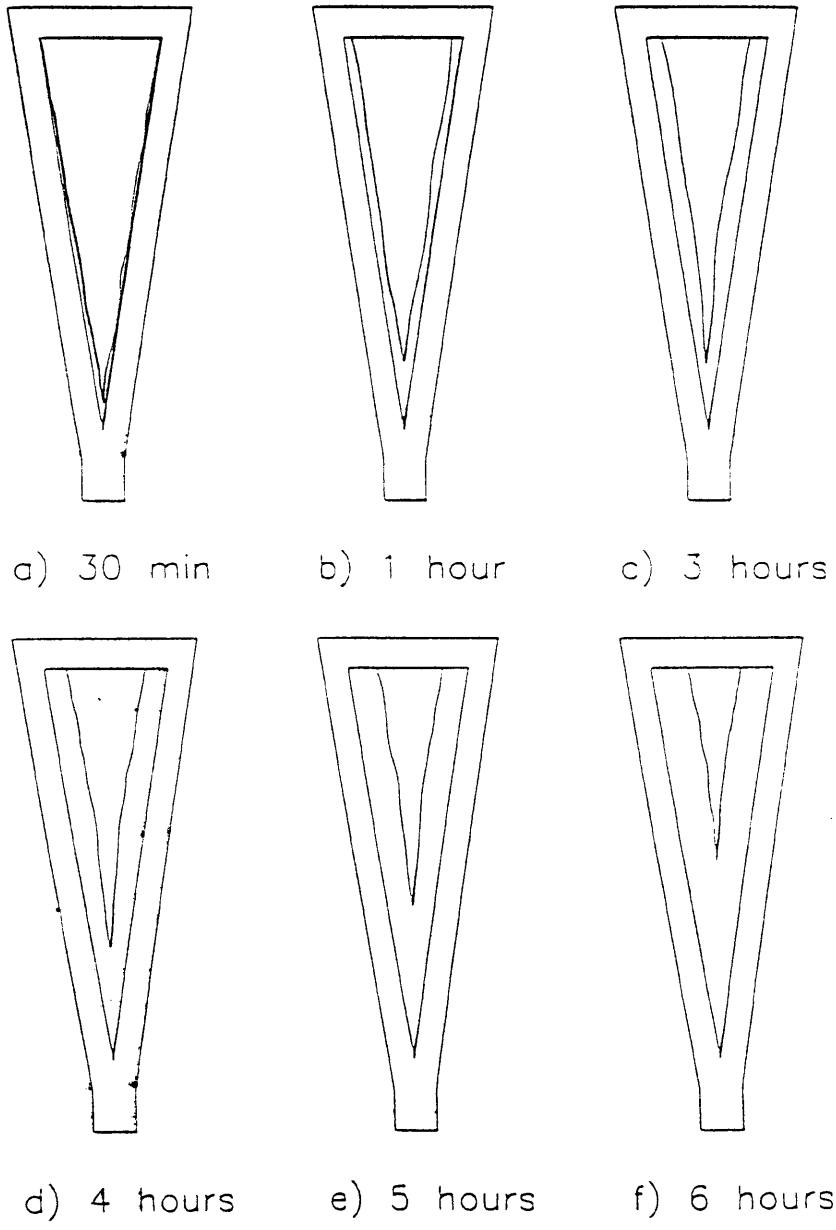

Figure [3.1] Interface growth, 19.7% Concentration.

solute is denser than the solution, a downward flow is generated along the interface by the solute driven natural convection, which acts in the same direction as that of the thermal current. Figures [3.2] and [3.3] show the variation of the temperature contours during the solidification process in a hypoeutectic composition solution (Test Run 2). In this test, a 5% $Na_2CO_3.nH_2O$ composition solution was used with an initial temperature of To = 5° C and a cooling temperature of Tc = - 10°C, respectively. Figure [3.3] shows the temperature variation of thermocouples #8, #9 and #10. These three thermocouples are located about 6.8 cm below the surface of the solution, where thermocouple #8 is 2 mm away from the sidewall and thermocouple # 10 is at the sump centerline position. This figure indicates that the temperatures at the locations of thermocouples #9 and #10 were fairly close to each other and that that of # 8 was always far below the temperature of the other two. It is also interesting to note that instead of continuously decreasing in temperature like locations #9 and #10, the reading of thermocouple #8 displayed a sudden increase in the early stages. In the first 20 minutes, the solution temperature near the side walls (thermocouple #8) steadily dropped to -5.6°C, which is lower than the freezing temperature for this concentration. This overcooling endured a few minutes until the first dendrites appeared. Visual observation indicated that the dendritic region spread very quickly to cover the entire side wall surfaces in less than one minute, while at the same time, the thermocouple reading of #8 jumped to -2.8°C. Figure[3.4] shows the temperature variation along the centerline of the test chamber. The vertical locations of thermocouples, #1, #3, #6, #10, and #15 are 22.5 cm, 17.4 cm, 11.3 cm, 6.8 cm, and 1.7 cm from the bottom, respectively. This figure

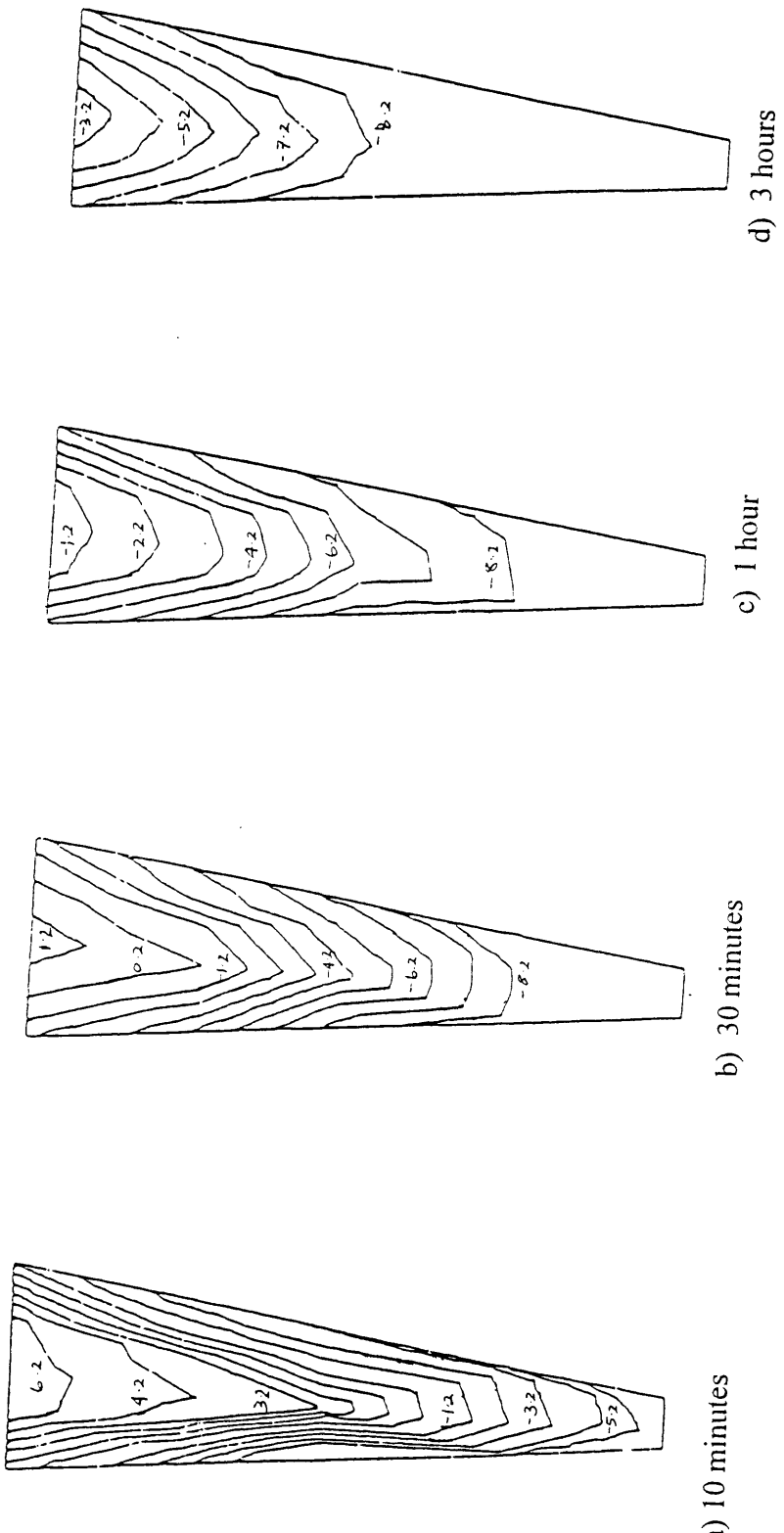

Figure [3.2] Temperature profiles, 5% Concentration.

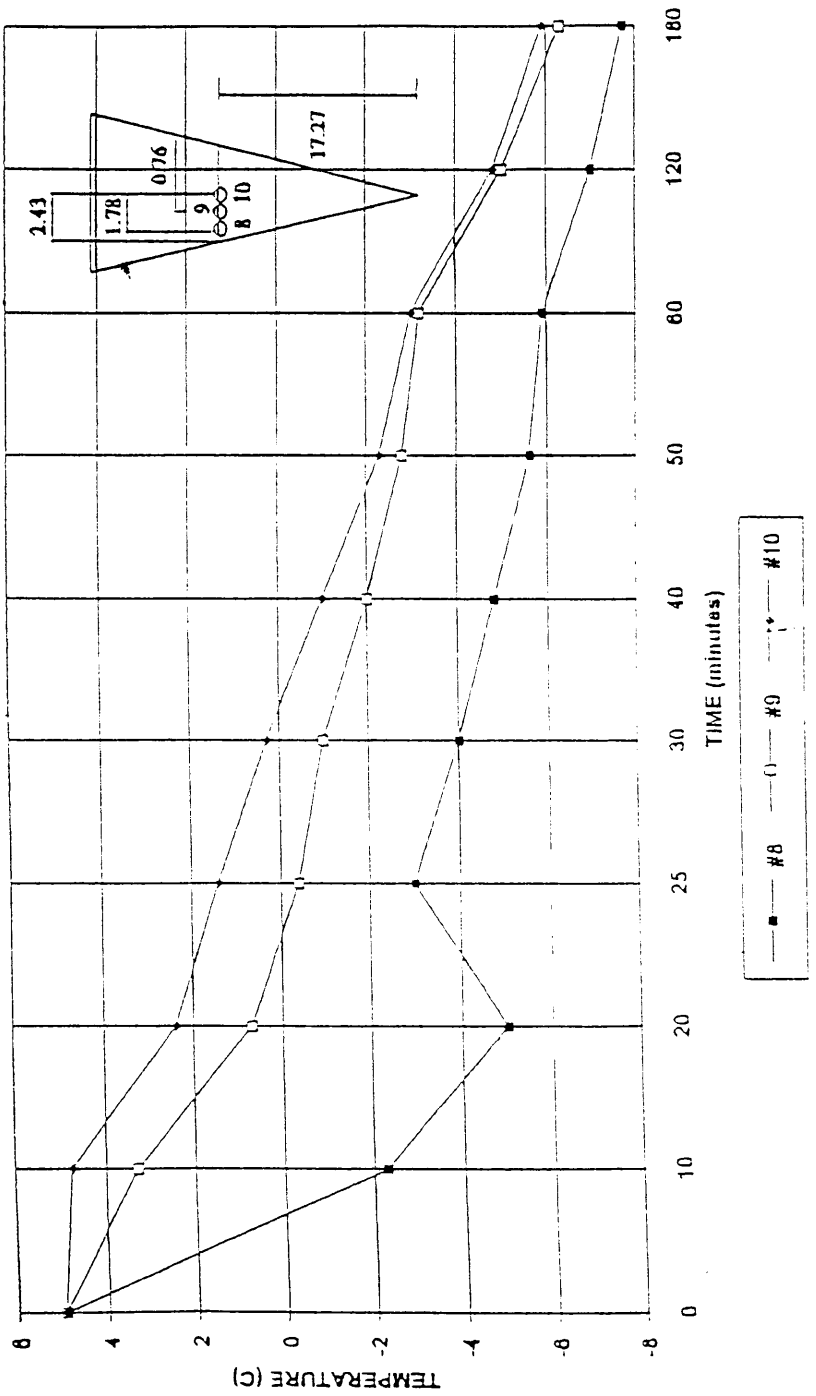

Figure [3.3] Temperature profiles - horizontal, 5% Concentration.
(C_o = 5%, T_c = -10^{0}C, T_i = 5^{0}C)

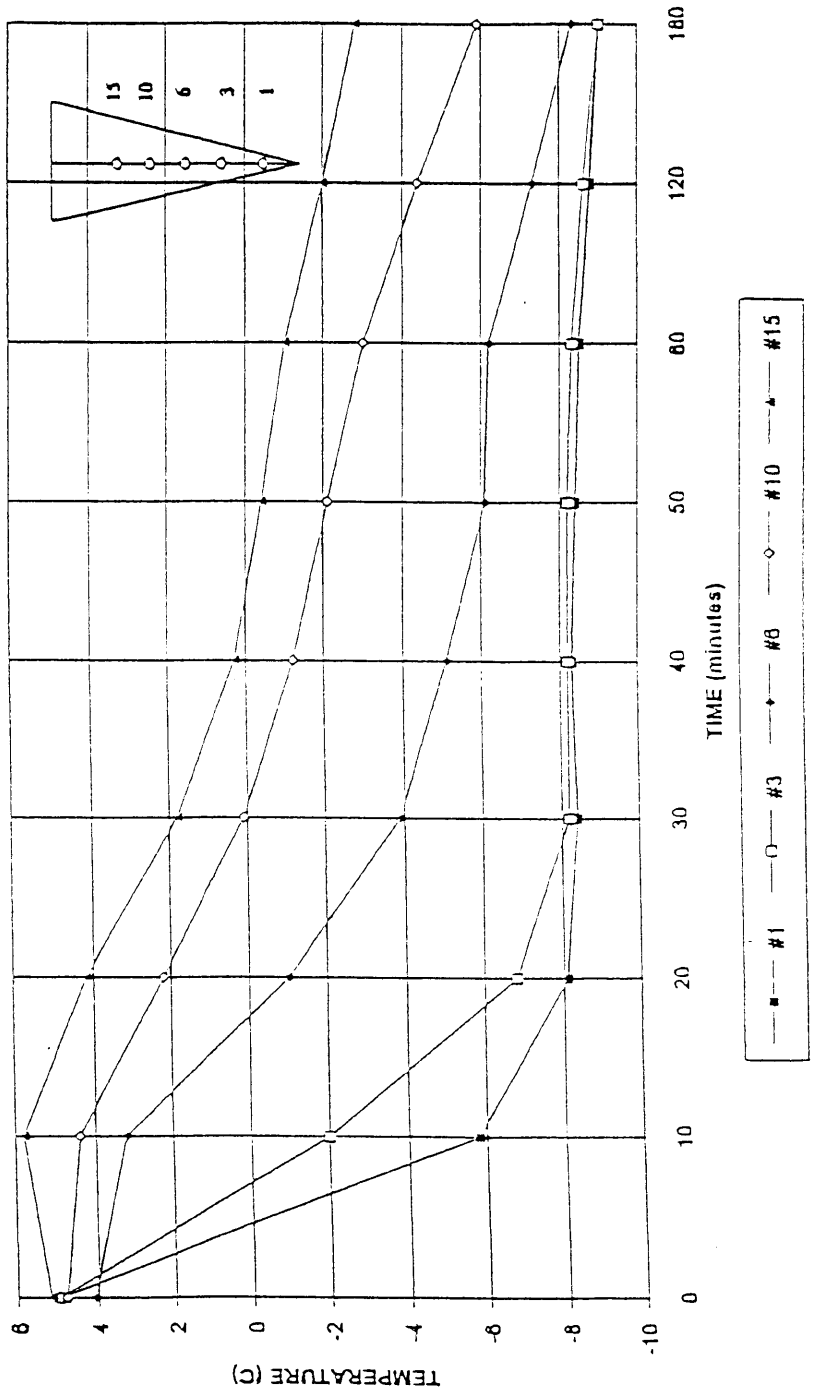

Figure [3.4] Temperature profiles - vertical, 5% Concentration.
(C_o = 5%, T_c = -10^{0}C, T_i = 5^{0}C)

indicates that temperatures in all five locations steadily dropped as time elapsed . The temperature in the upper region of the sump was always greater than that at the lower region.

Figure [3.5] shows the movement of the solid-liquid interface fronts. At t=30 min. Fig. [3.5a], visual observation indicated that the solidified region was composed of mainly long , coarse dendritic structures. As time elapsed, the dendrites became shorter and finer, the solid region appeared as seen in Fig. [3.5b]. Since the solute-rich fluid continuously flowed down along the interface region, the concentration in the bottom region of the test chamber steadily increased, which delayed the solidification process in this region, due to some localized remelting. Figures [3.5c] and [3.5d] show that the interface fronts moved close to each other, and left a long narrow gap between them. Figure [3.6] shows how the concentration changed with time in this case. The probes, C and F, were located 8.9cm below the solution surface, on the centerline of the sump. The figure indicates that the concentration in the liquid pool increased as time elapsed, i.e. after 90 minutes, the concentration at point C had reached almost 10 %.

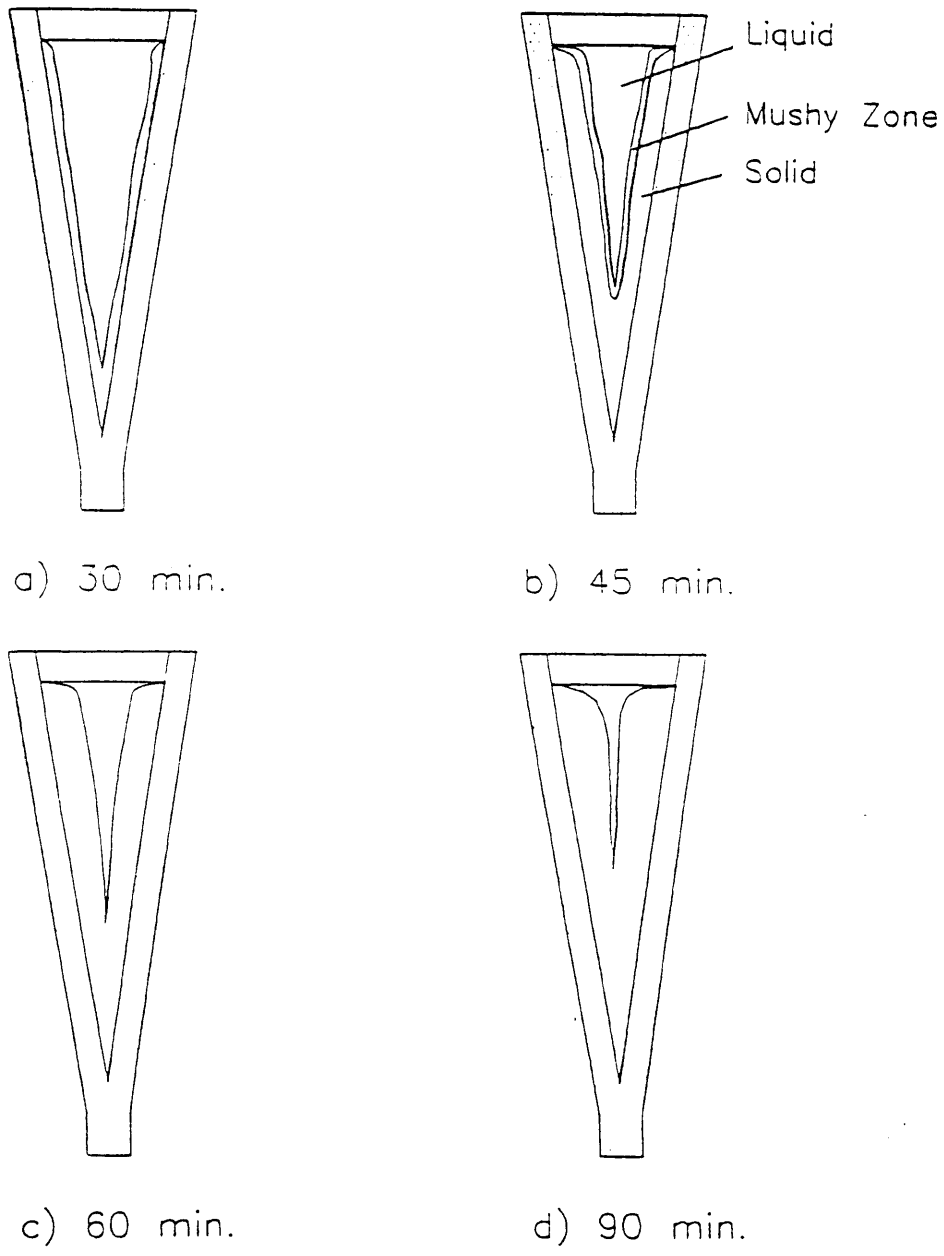

Figure [3.5] Interface growth, 5% Concentration.

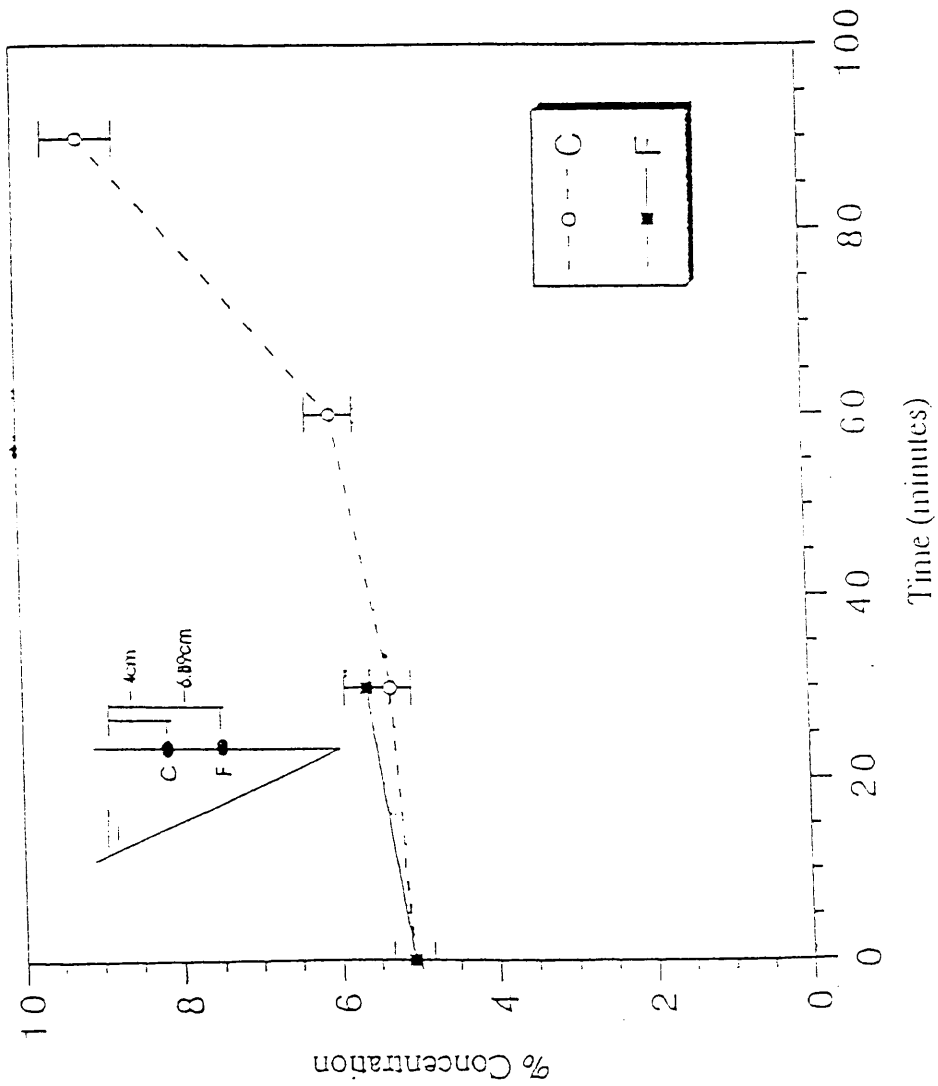

Figure [3.6] Concentration variation - 5% solution.

Figure [3.7] shows solidification in a hypoeutectic composition , in this case 15%, the initial temperature was 5 °C, while the cooling temperature was - 15 °C. The dendrites appeared 15 minutes after the test was initiated. Columnar dendrites occurred on the walls of the top half of the chamber. Some of the loose columnar dendrites were released from the wall and convected into the liquid pool while equiaxed dendrites, apparently homogeneously nucleated, descended to pack into a loose accretion at the bottom apex, forming a mushy zone. Figure [3.7a] illustrates the interfaces of the liquid/mushy/solid front at t = 30 min. It can be seen that a very thin solid built up along the wall, with a thick layer of mushy material between the solid and the solution. Both the mushy and solid regions increased in volume subsequently, as seen in Fig.[3.3] (t = 60 min.). After one hour, the interface between the mushy zone and the solution changed slowly, unlike the solid region's rapid increase in volume (Figs. [3.7c] and [3.7d]). At t = 3 hours, the mushy zone near the bottom apex became solid and at t=4.5 hours, the mushy zone had almost disappeared. Figure[3.8] indicates that the concentration at points C and F continuously increased until reaching eutectic concentration, at around t = 3 hours, then remained constant, which explains why the mushy zone disappeared later on. Figure [3.9a] shows the temperature history for thermocouples #8, #9, and #10. This figure indicates that the horizontal temperature distribution in this situation was much more uniform than was the case for the 5% composition Fig. [3.2]. Also, no overcooling phenomena were observed in this case. Figure [3.9b] shows the vertical temperature distributions along the centerline, it

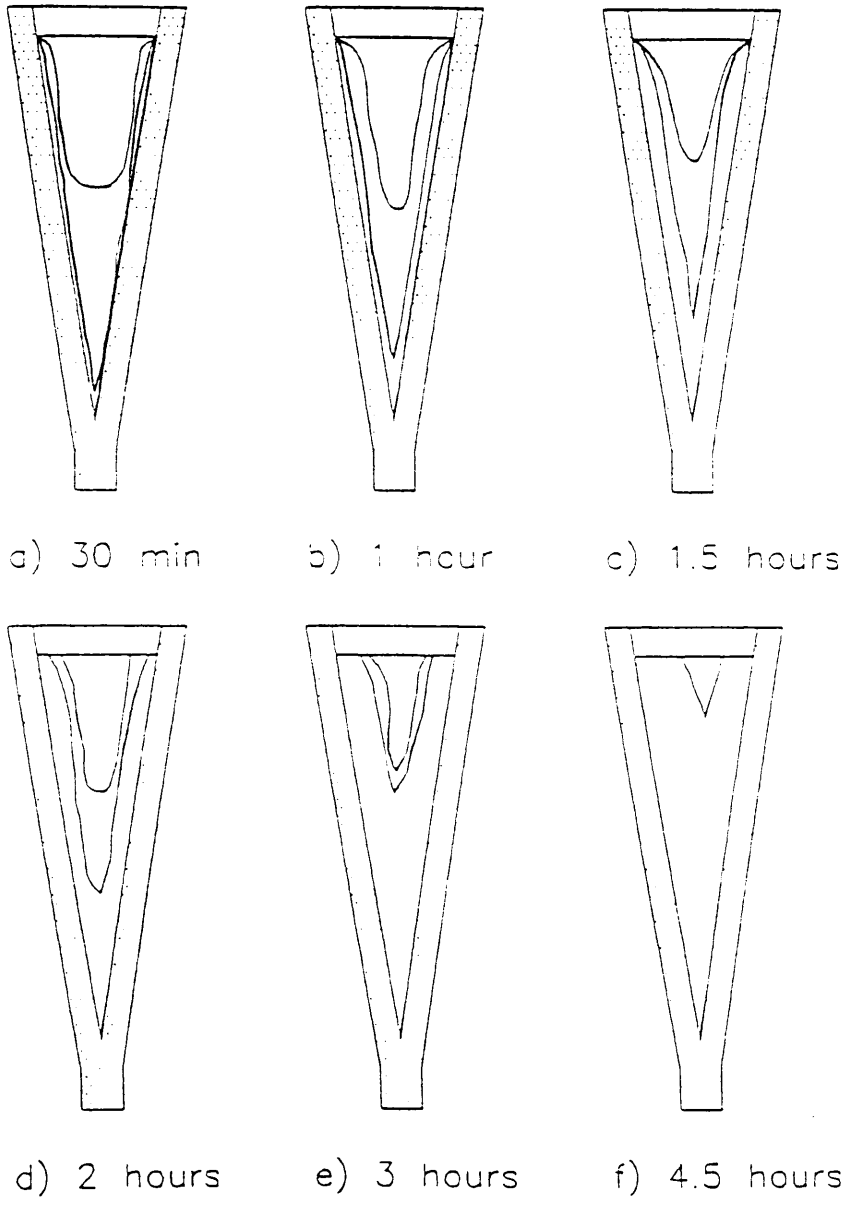

Figure [3.7] Interface growth, 15% Concentration.

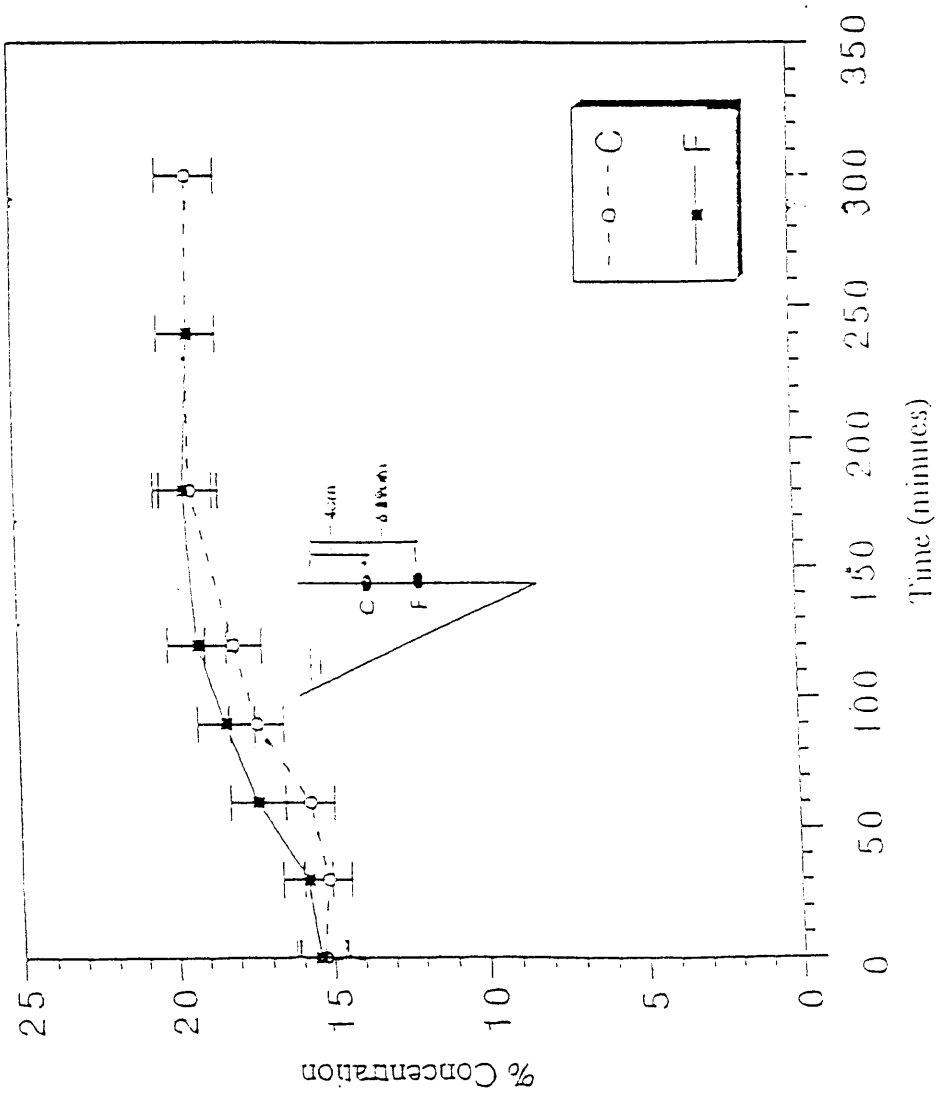

Figure [3.8] Concentration. variation - 15% solution.

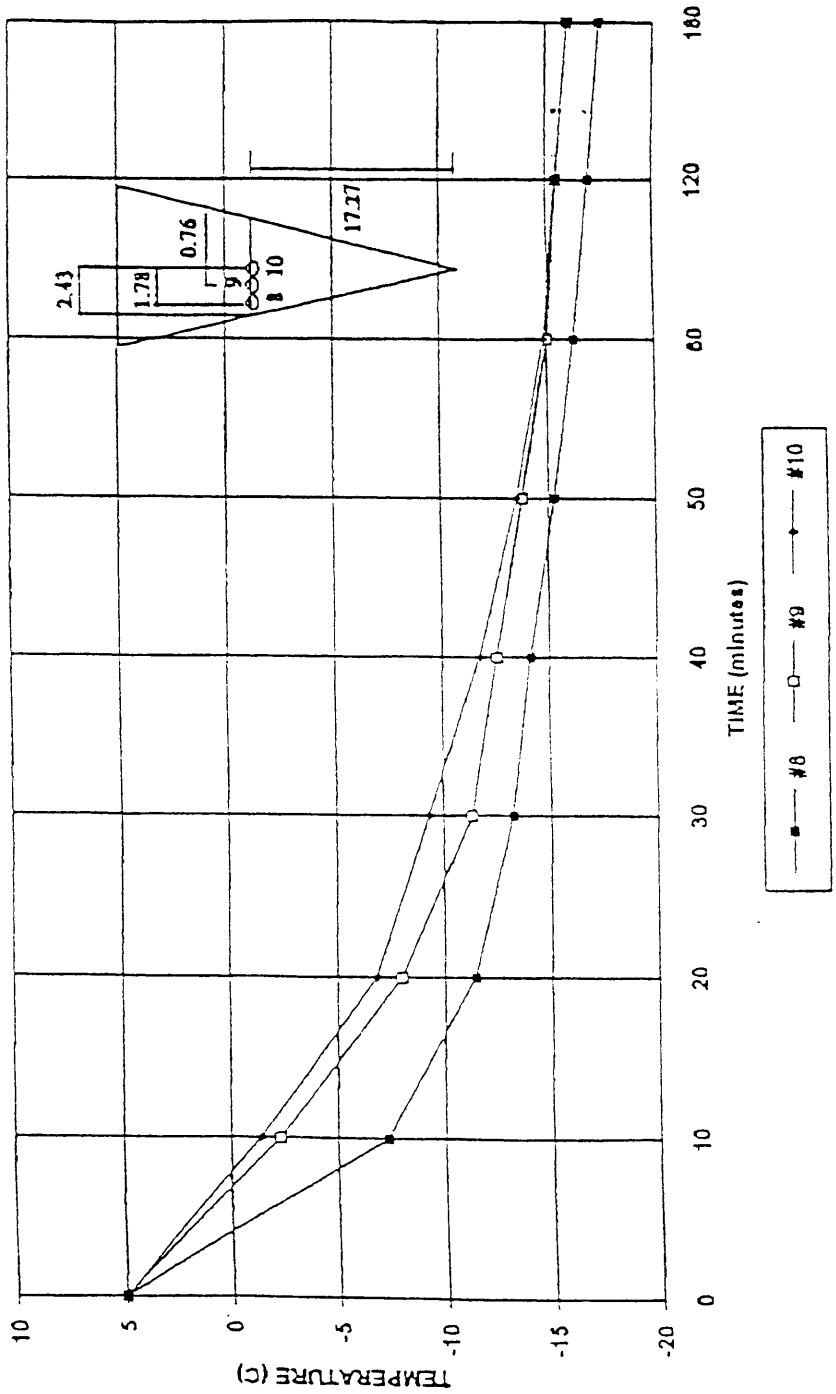

Figure [3.9a] Temperature profiles - horizontal, 15% Concentration.
(C_o = 15%, T_c = -20^{0}C, T_i = 5^{0}C)

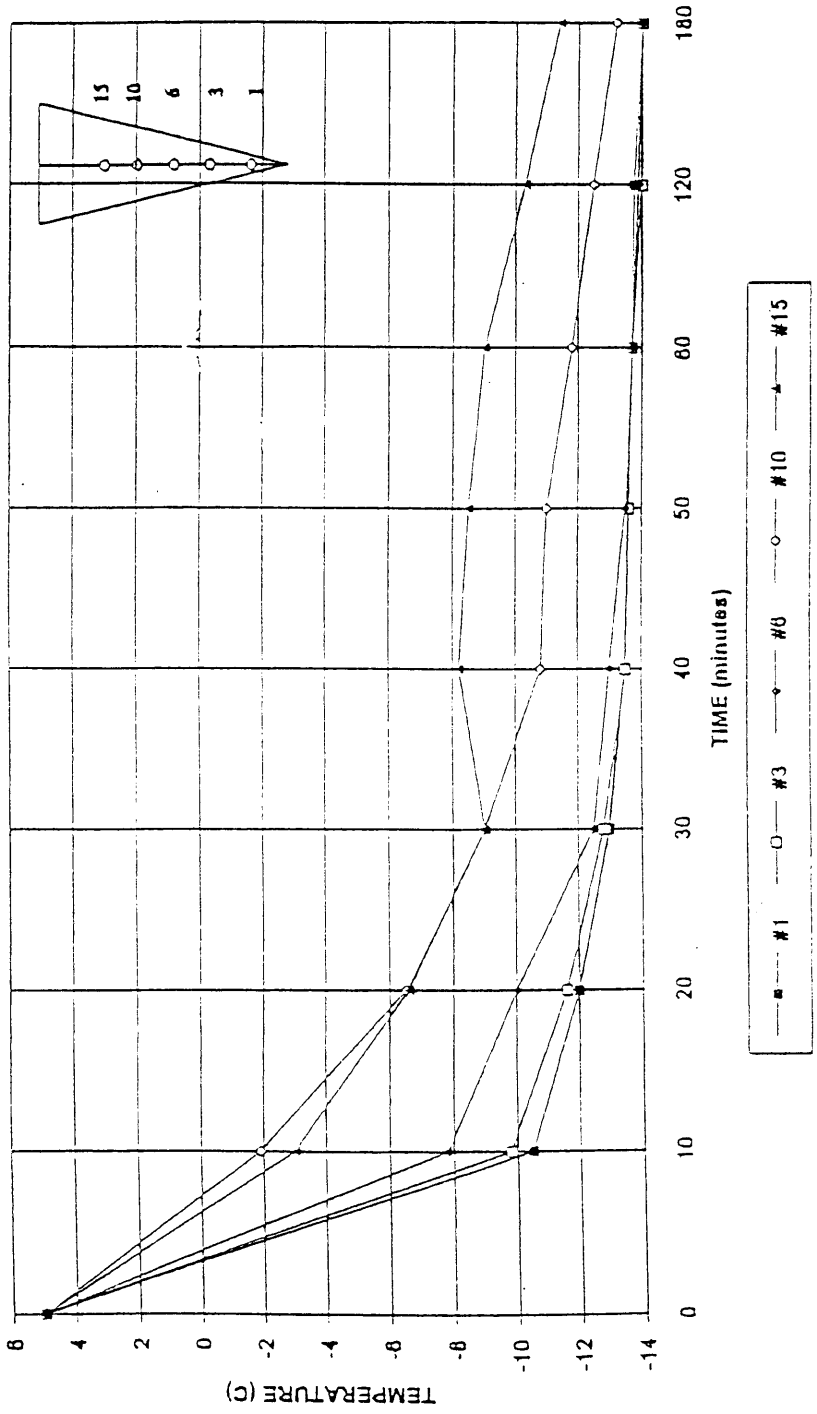

Figure [3.9b] Temperature profiles - vertical, 15% Concentration.
(C_o = 15%, T_c = -20^{0}C, T_i = 5^{0}C)

also indicates that the temperature at this upper point was always higher than that at the lower point, which is consistent with the result for the case of the 5% composition.

In contrast to the hypoeutectic composition, the ejection of water-rich interdendritic fluid will induce an upward flow in the hypereutectic composition solution, which is opposite to the thermally driven flow. Therefore, totally different solidification behavior can be expected in these two cases. Figure [3.10] shows how the interface front moved with time in a hypoeutectic component solution, where the initial concentration is 25%, T_i= 15°C, and T_c= -20°C. Visual observation indicated that a few minutes after starting the test, equiaxed dendrites appeared at the bottom apex first, and then in the entire domain. Many tiny solid particles grew and coalesced as they descended. After about another five minutes, the dendrites settled down to form a mushy zone at the bottom, as seen in Fig. [3.10a.] The mushy zone increased slowly in volume after this, and the solid zone grew beneath the mushy zone, as seen in Figs. [3.10b] through [3.10d]. At t = 1 hour, a narrow solid zone could be seen at the top of the sump. The solid zone appeared to increase at the top of the sump at t = 2 hours, the surface morphology of the solid zone was almost smooth. The solid region continued to grow while the loose mushy zone was reduced in volume. The interface of the solution and the solid at the top of the sump remained smooth. Figure [3.11] shows that the concentration at points, C and F, reached a eutectic value after around two hours and remained that way for the period of experimentation. The results of the horizontal temperature measurements are presented in Fig.[3.12] . This figure indicates that the temperature near the wall at thermocouple #8 was 5- 8 degrees lower than that at the

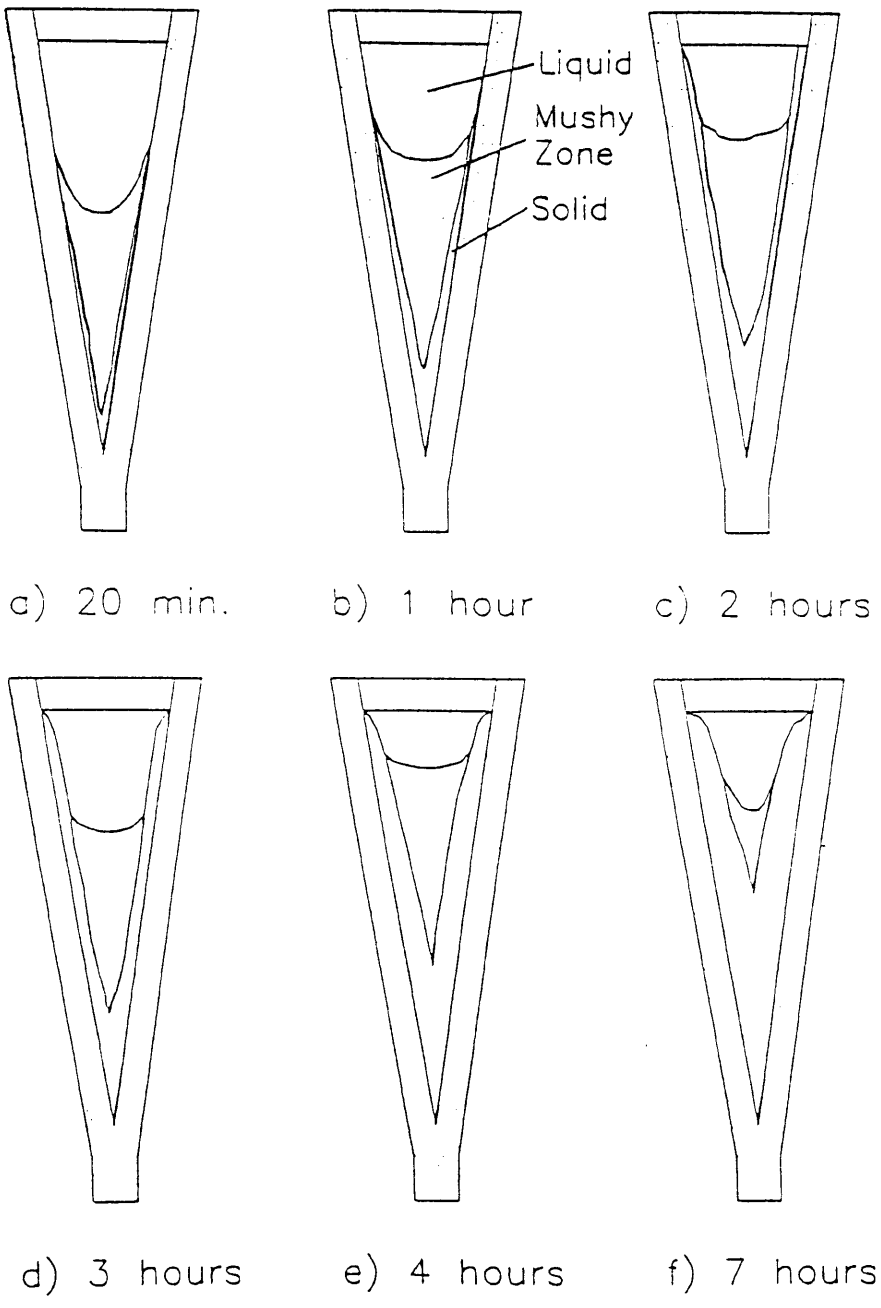

Figure [3.10] Interface growth, 25% Concentration.

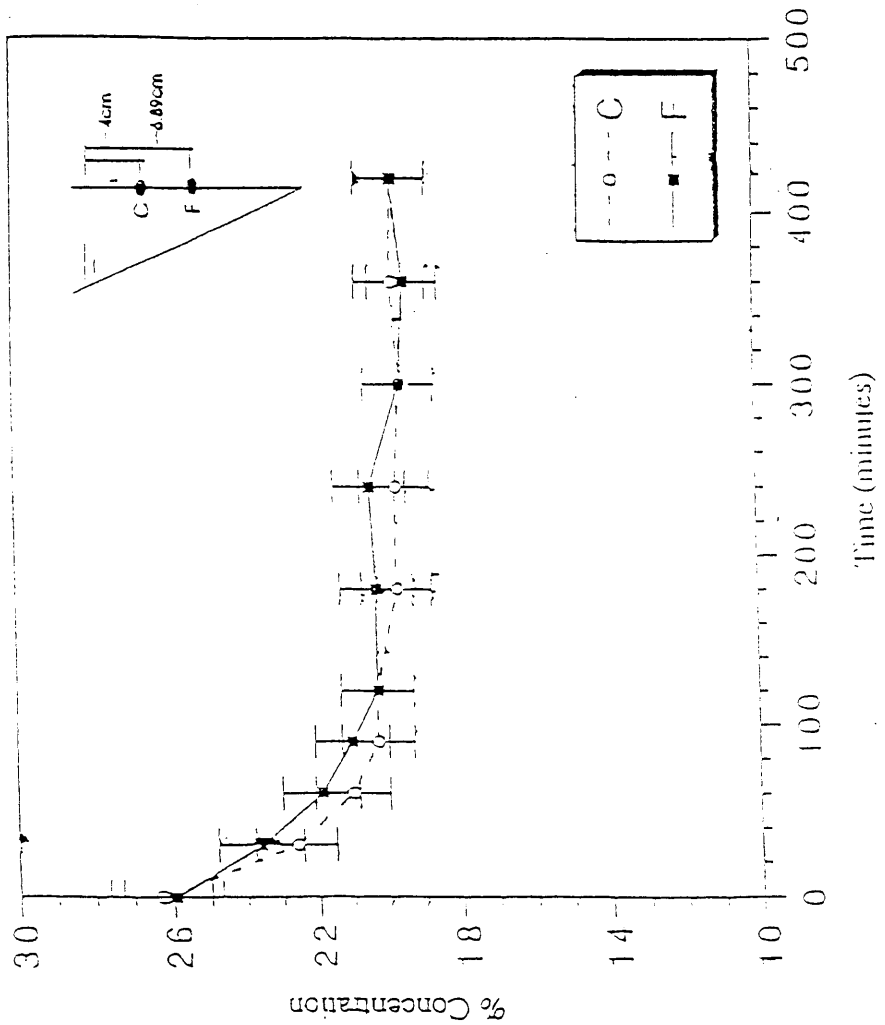

Figure [3.11] Concentration Variation - 25% solution.

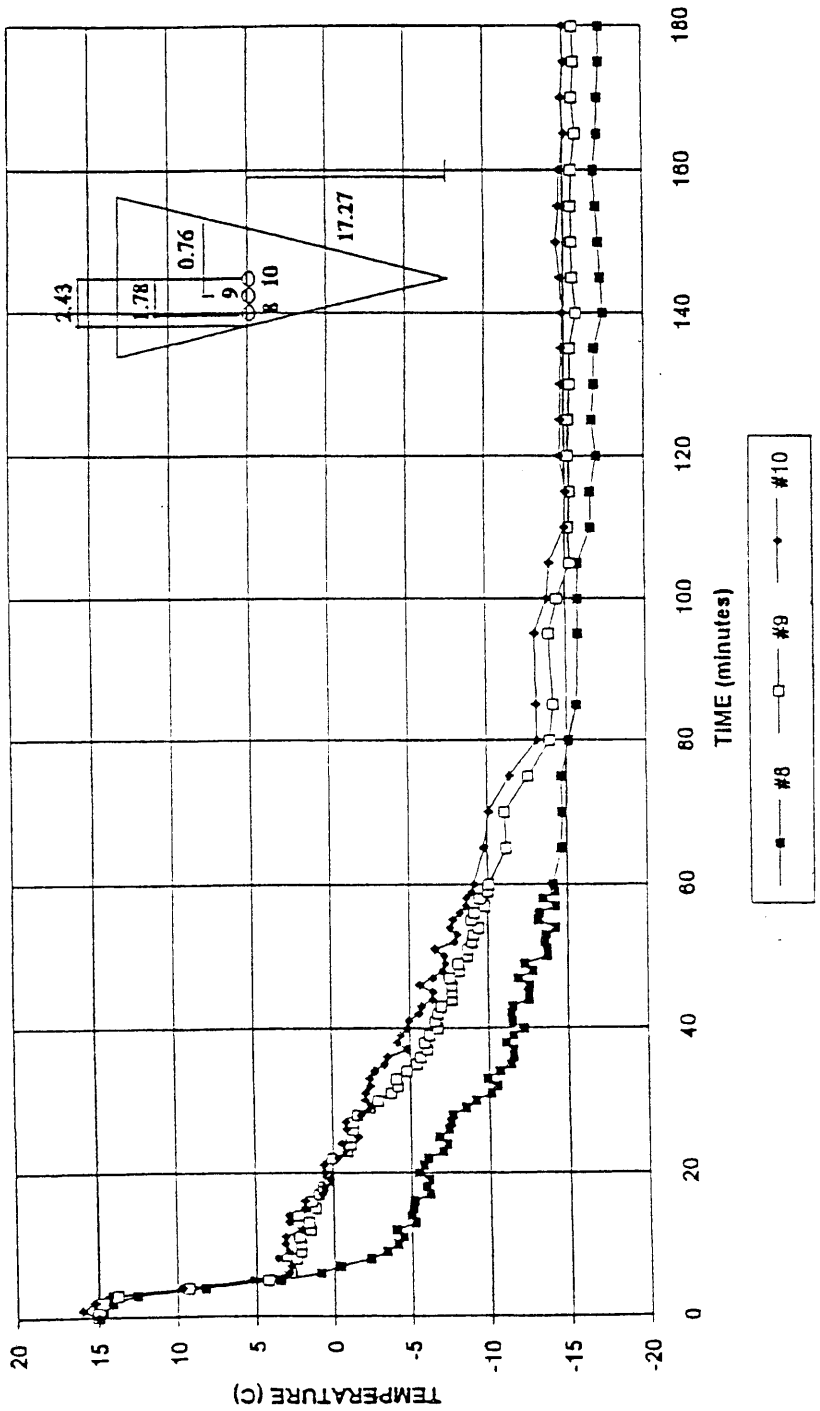

Figure [3.12] Temperature profiles - horizontal, 25% Concentration.
($C_o = 25\%, T_c = -20^0C, T_i = 15^0C$)

thermocouples closer to the centerline (#9 and #10) in the first two hours. Typically, 5^0C for t = 20 min to t = 60 min and then approximately 2^0C difference for the remainder of the experiment. However, the temperature difference between thermocouples #9 and #10 was very minor,approximately 1 degree C throughout. It is interesting to see the difference between Fig.[3.12] and Fig. [3.2], or Fig. [3.9]. Figure [3.13] shows the temperature distribution along the vertical direction. Like that in Fig. [3.12], the temperature fluctuated with time before the solution near this point solidified. It can be seen that the temperature in thermocouple #10 was higher than that in thermocouple #15, between 10 minutes to 120 minutes. That is, the temperature near the top free surface was lower than that in the liquid center. This temperature distribution reflects the effect of the solute-driven flow. As the water-rich fluid was ejected from the dendritic interface, it flowed upward along the interface and then recirculated through the top free surface region. It is interesting to compare the temperature change behaviors of Figs. [3.12] and [3.13] and that of Figs. [3.2], [3.3], [3.9], and [3.10]. In Figs. [3.12] and [3.13], the temperatures at all points fell below 5°C in the first few minutes. The equilibrium phase diagram for NH_4Cl-H_2O Fig.[2.8] indicates that this temperature was below the phase change temperature in the 25% concentration solution, which is why the equiaxed dendrites appeared in the entire solution. In the 5% and 15% initial concentration solutions, a considerable temperature difference existed, which is why the solidification mainly occurred on the side walls with the consequence that dendritic structures formed.

3.2 Rectangular sump experimentation

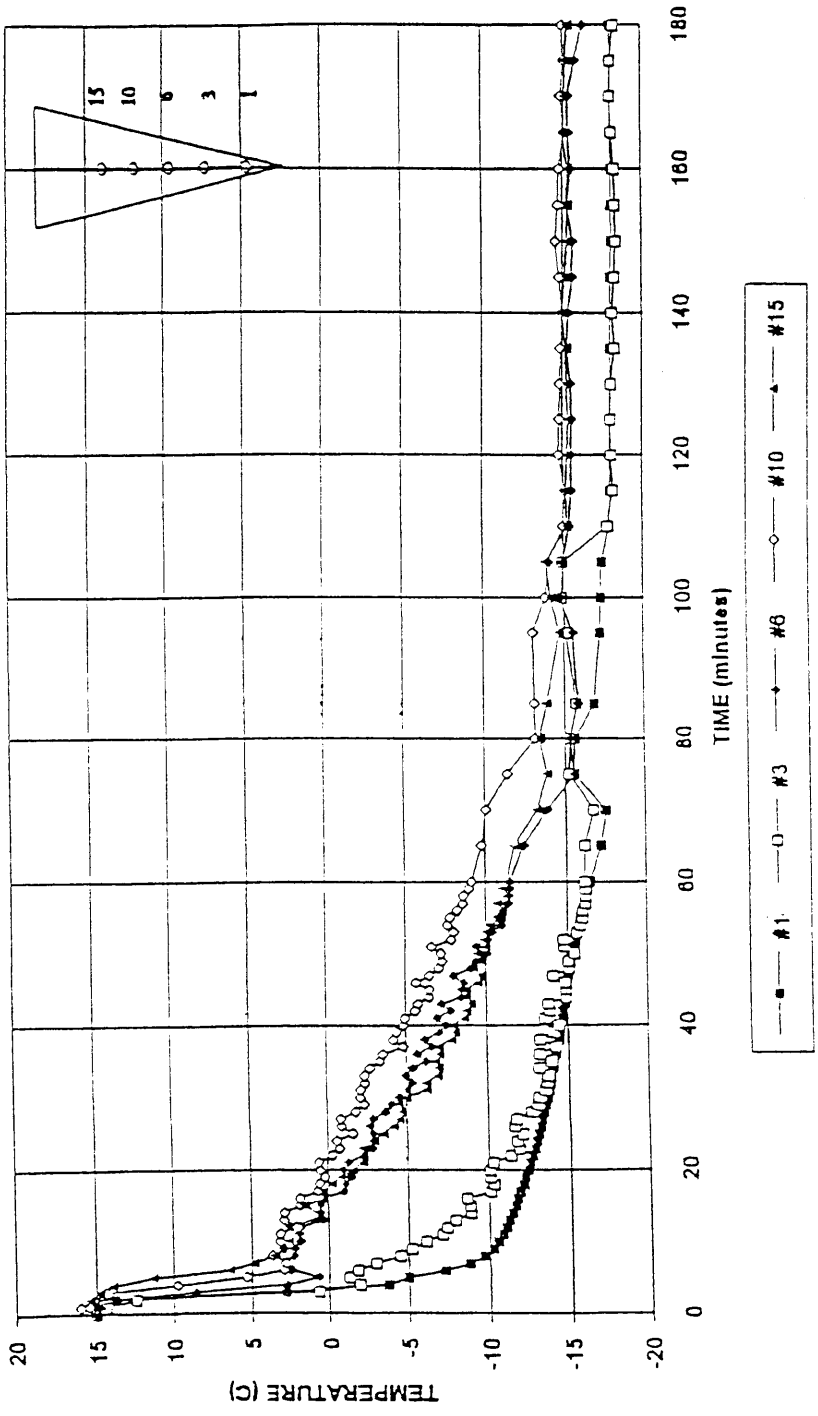

Figure [3.13] Temperature profiles - vertical, 25% Concentration.
(C_o = 25%,T_c = -20^{0}C, T_i = 15^{0}C)

The results of three test runs were selected to be presented in this paper. Table 2 provides the information regarding the initial temperature of the solution , the initial concentration, C_o, and the cooling temperature (wall temperature) in each test run. Test Run I represents the case of the eutectic solidification process. Test Run II indicates the case of hypoeutectic solidification, while Test Run III is hypereutectic solidification. Christenson and Incropera (1989) reported their test data on solidification in a rectangular cavity with one cold and insulated wall. The geometry of their test chamber was 144 mm height, 36 mm wide, and 200 mm deep, which is more similar to the half-domain of our test chamber (our test chamber is 190 mm x 60 mm x 160 mm). Therefore, their results should be a good comparison for this study since the volumes under study are similar.

Test Run	C_o (%)	T_o (°C)	T_c (°C)
I	19.7	5	-20
II	5.0	5	-10
III	25%	15	-20

Summary of experimental conditions.

Table 4

a. Eutectic Solidification (Test Run I)

Figure [3.14] indicates the test data for the temperature distributions inside the test chamber during eutectic solidification. The locations of each thermocouple can be seen

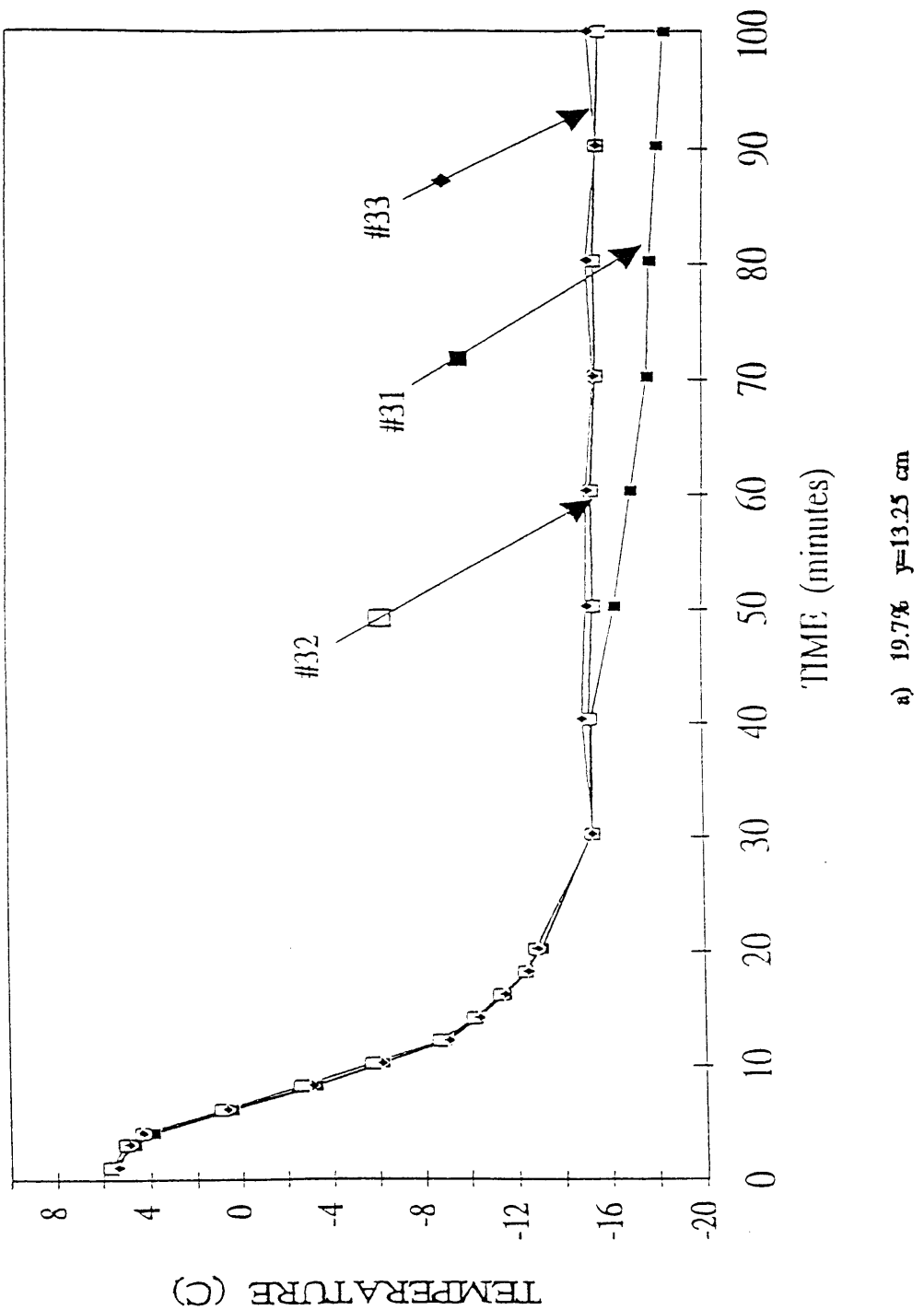

Figure [3.14a] Temperature profiles ,19.7% Concentration.
(C_o = 19.7%,T_c = -20^{0}C, T_i = 5^{0}C)

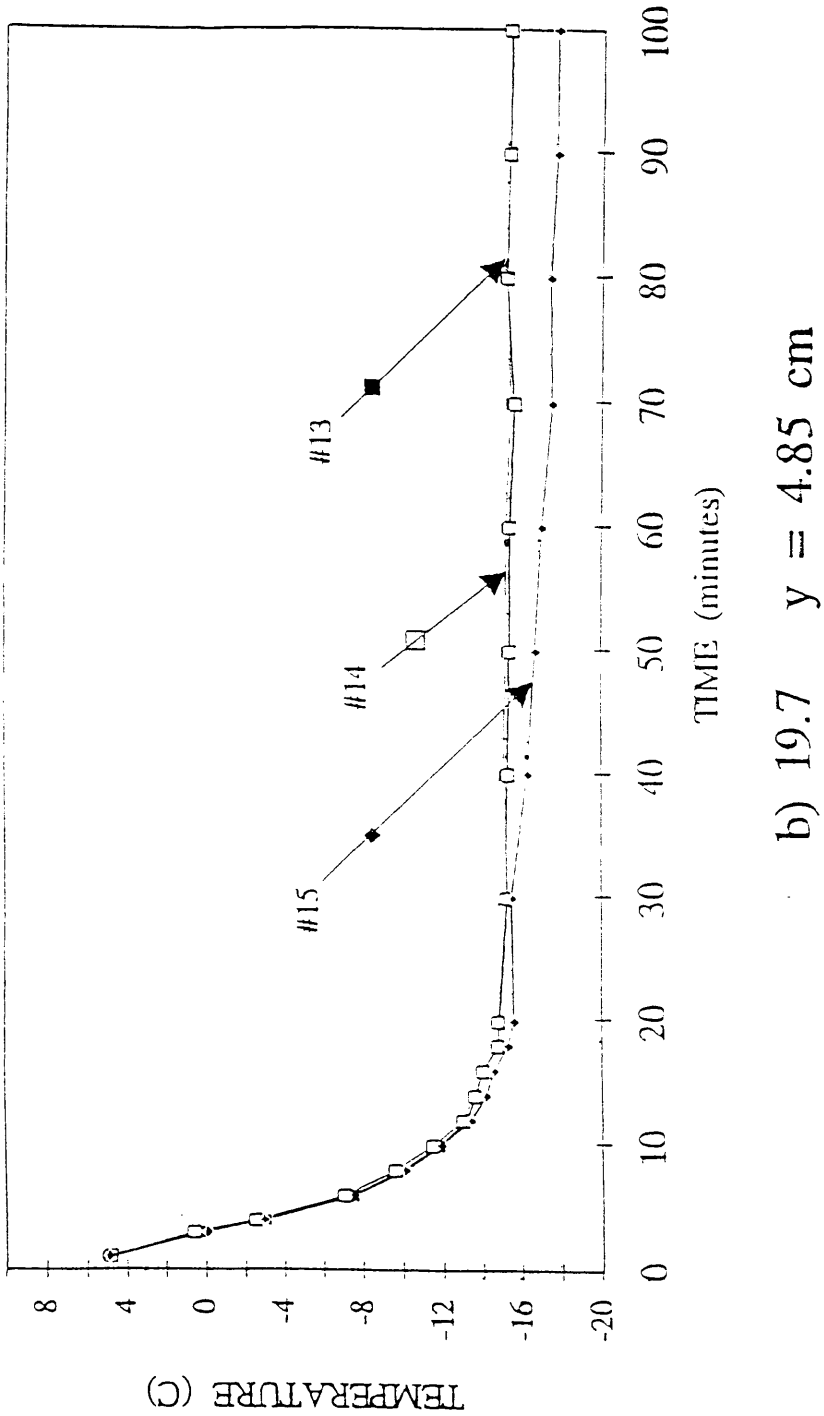

Figure [3.14b] Temperature profiles ,19.7% Concentration.
(C_o = 19.7%,T_c = -20^{0}C, T_i = 5^{0}C)

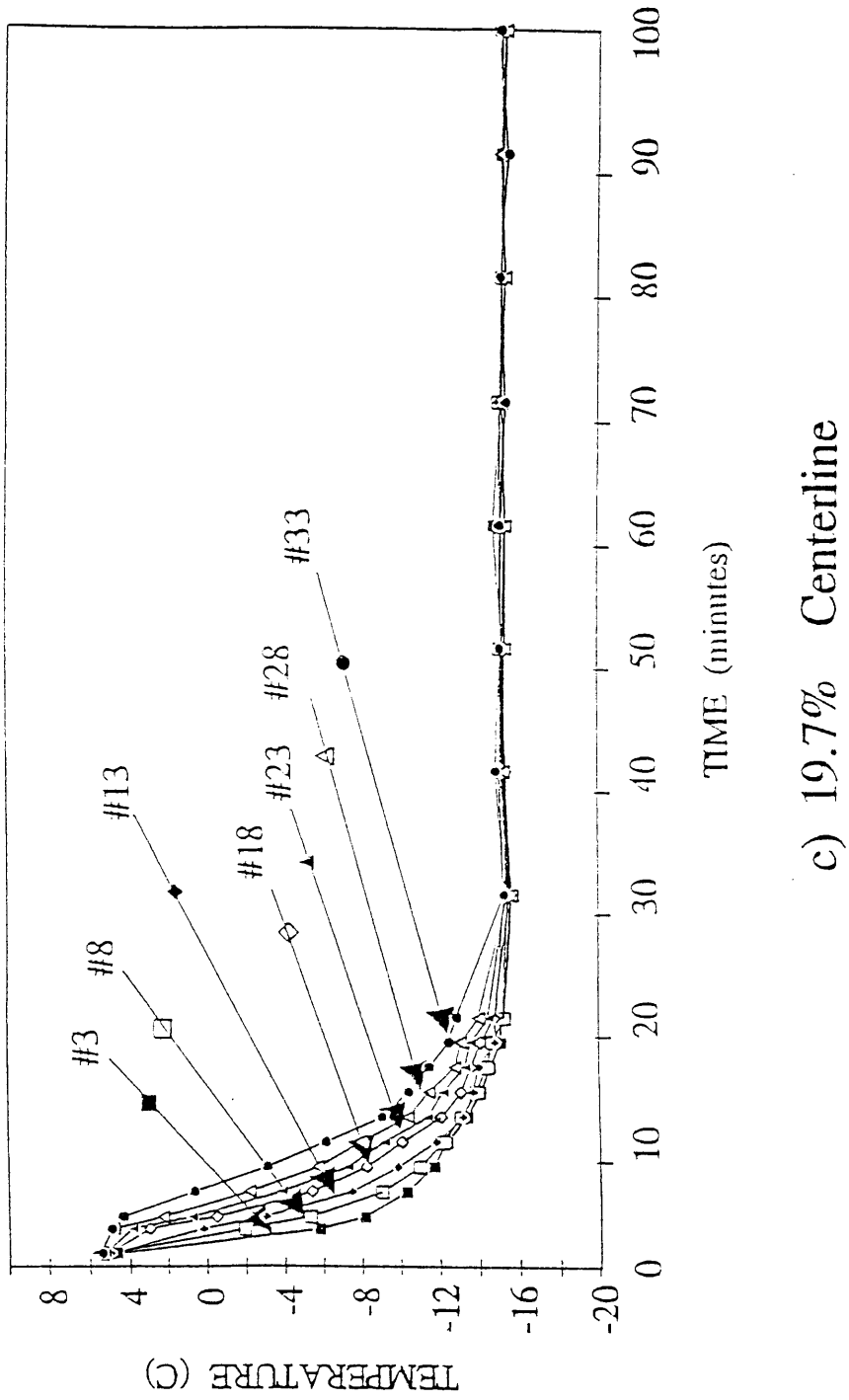

Figure [3.14c] Temperature profiles ,19.7% Concentration.
(C_o = 19.7%,T_c = -20^{0}C, T_i = 5^{0}C)

in Fig. [2.7]. Figure [3.14a] shows the temperature change with time at y = 13.25 cm. Three thermocouples were located about 13.25 cm above the bottom of the test chamber. Thermocouple #31 was 0.6 cm away from the sidewall, and thermocouple #33 was in the center of chamber. It can be seen that during the first 30 minutes, these three thermocouples had almost identical readings until they reached the eutectic phase change temperature, -15.4°C. The temperature of thermocouple #31 began to drop gradually because it had been surrounded by the solidified region. The further temperature decrease of thermocouple #31 was governed by thermal conduction inside the solid. In the liquid pool, thermocouples #32 and #33, show a very uniform temperature horizontally. Figure [3.14b] shows the horizontal temperature history at the y = 4.85 cm level. Very similar to that in Fig. [3.14a], the temperature was very uniform horizontally in the liquid pool. Figure [3.14c] shows the temperature history in the vertical centerline of the test chamber. During the first 30 minutes, a considerable temperature difference existed along the vertical direction. However, since the temperature was higher at the top and lower in the bottom, the liquid was thermally stable. After thirty minutes, all readings reached the same value; that is, the temperature in the entire domain of the liquid pool was equal to the eutectic temperature.

Figure [3.15] shows the history of the solid/liquid interface associated with Test Run I. A half-hour after starting the test, the solid/liquid interface appeared on the sidewalls, Fig. [3.15a]. The solid/liquid interface looked very smooth and had the same thickness along both surfaces. Due to the uniform temperature in the liquid pool, thermal

a) 30 min. b) 60 min. c) 90 min.

d) 180 min.

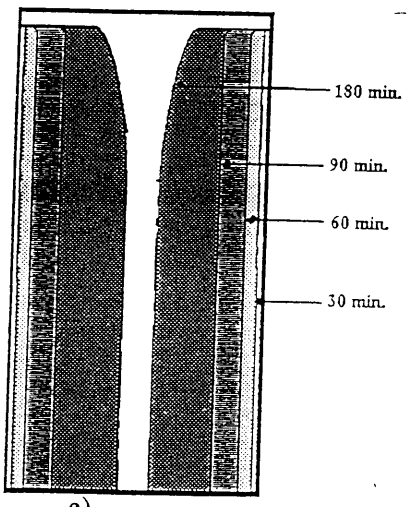

e)

Figure [3.15] Evolution of the Interface Front- 19.7% Solution.

convective heat transfer vanished, which caused the solid/liquid interface to grow parallel to the horizontal direction, Figs.[3.15b] through [3.15d]. A clearer view, diagrammatically represented, of the evolution of the solid front is presented in Fig.[3.15e].

b. Hypoeutectic Solidification (Test Run II)

For a solution with a hypoeutectic composition, the solute will be ejected during the solidification process and the two-phase interface is characterized as a mushy zone. As a result, there exists a high concentration region in and near the interdendritic zone. Since the solute is denser than the solution, a downward flow may be generated along the interface by the solute-driven natural convection. Figure [3.16] shows the temperature distribution in a 5% NH_4Cl-H_2O composition solution. Figure [3.16a] indicates the measured results at the y = 13.25 cm level. This figure reveals that during the first 10 minutes, all three thermocouples had the same readings. Then the readings on thermocouples #32 and #33 got closer to each other, while that of #31 always remained far below that of the other two thermocouples, which indicated the downward solute-rich flow in this region. Figures [3.16b] and [3.16c] show the horizontal temperature distributions in another two levels, y = 9.05 cm and y = 4.85 cm. Unlike that in Fig. [3.16a], these two figures indicate that even at the beginning of the test, a temperature difference existed between the thermocouples near the cooling walls and the thermocouples in the center region. As time elapsed, the temperatures in all thermocouples in these three cross sections continued to decrease. It is interesting to note that instead of continuously reducing the temperature in thermocouple locations #12 and #13 in Fig. [3.16c], the reading of thermocouple #11 displayed a sudden increase in the early stage. After five minutes, the solution temperature near the sidewalls (thermocouple #11) steadily dropped

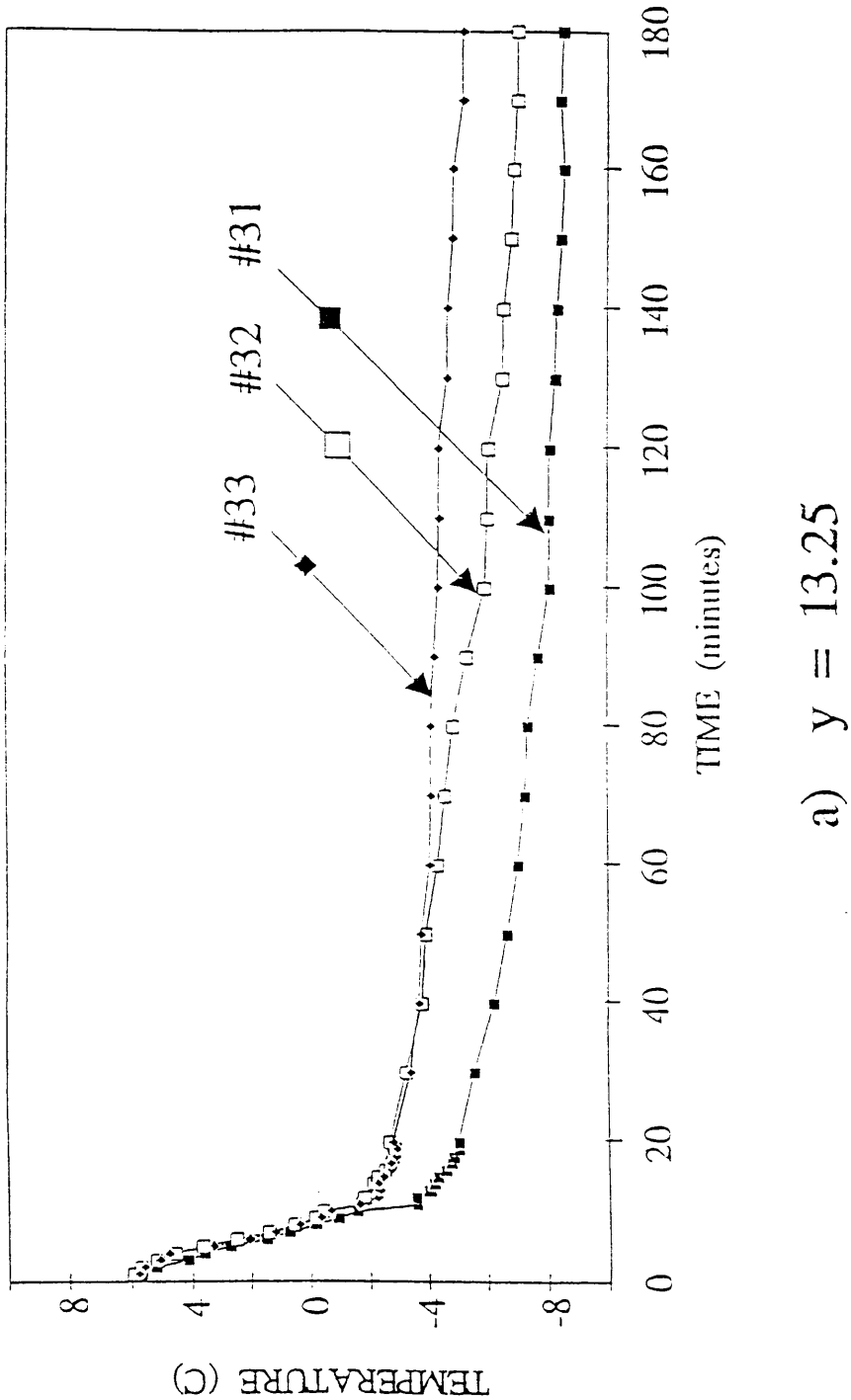

Figure [3.16a] Temperature profiles, 5 % Concentration.
(C_o = 5%,T_c = -10^{0}C, T_i = 5^{0}C)

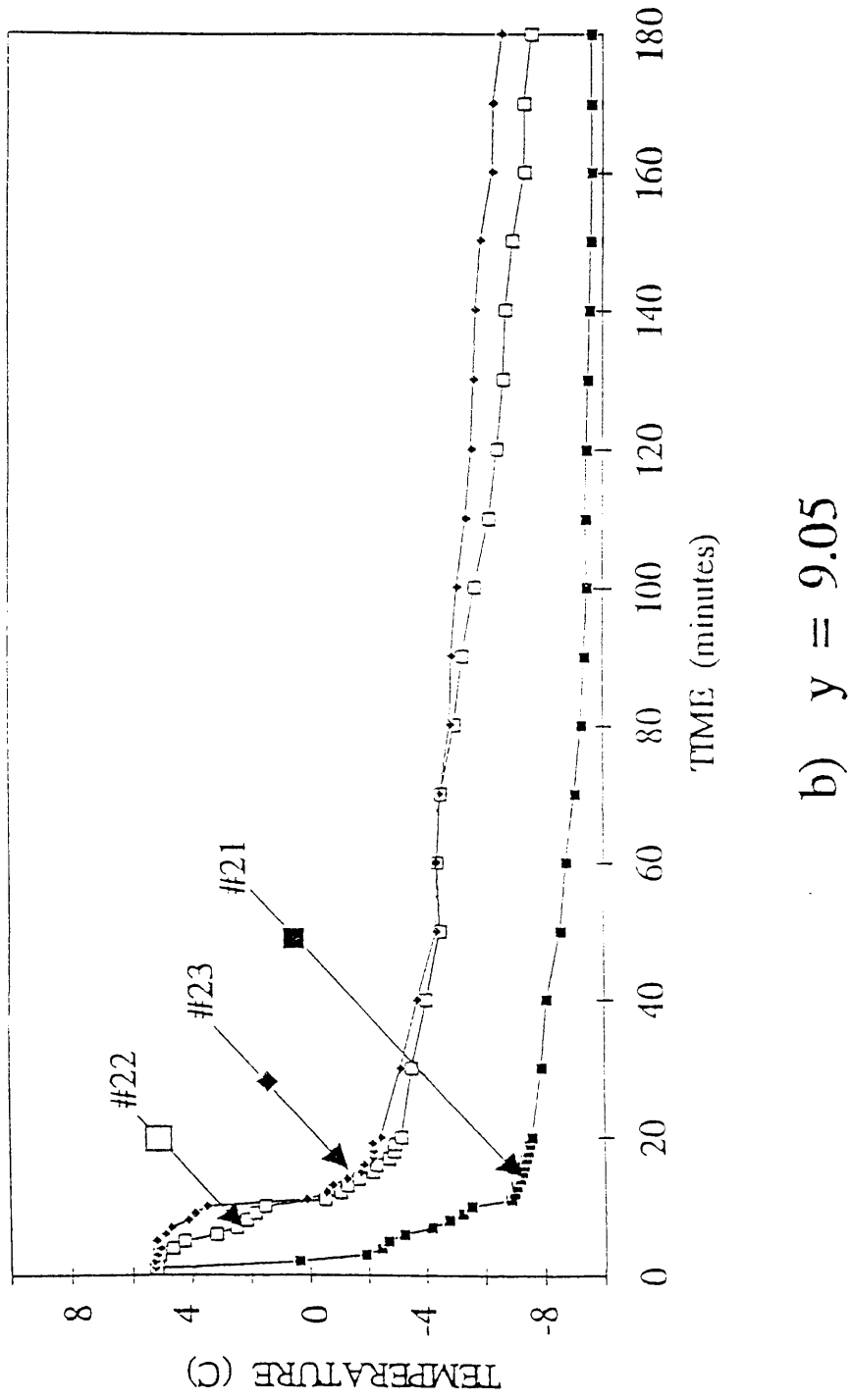

Figure [3.16b] Temperature profiles, 5 % Concentration.
(C_o = 5%,T_c = -10^{0}C, T_i = 5^{0}C)

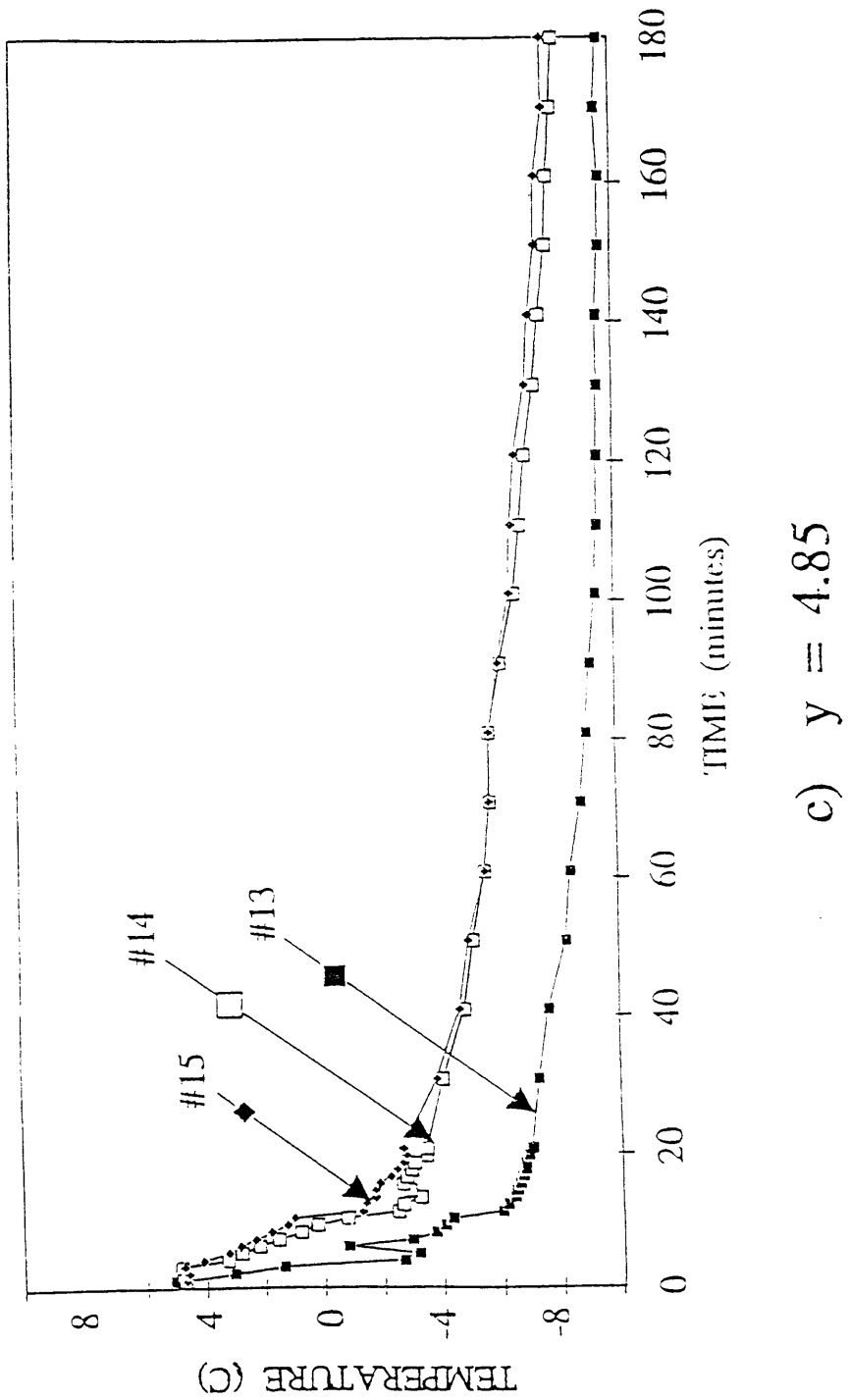

Figure [3.16c] Temperature profiles, 5 % Concentration.
(C_o = 5%, T_c = -10^{0}C, T_i = 5^{0}C)

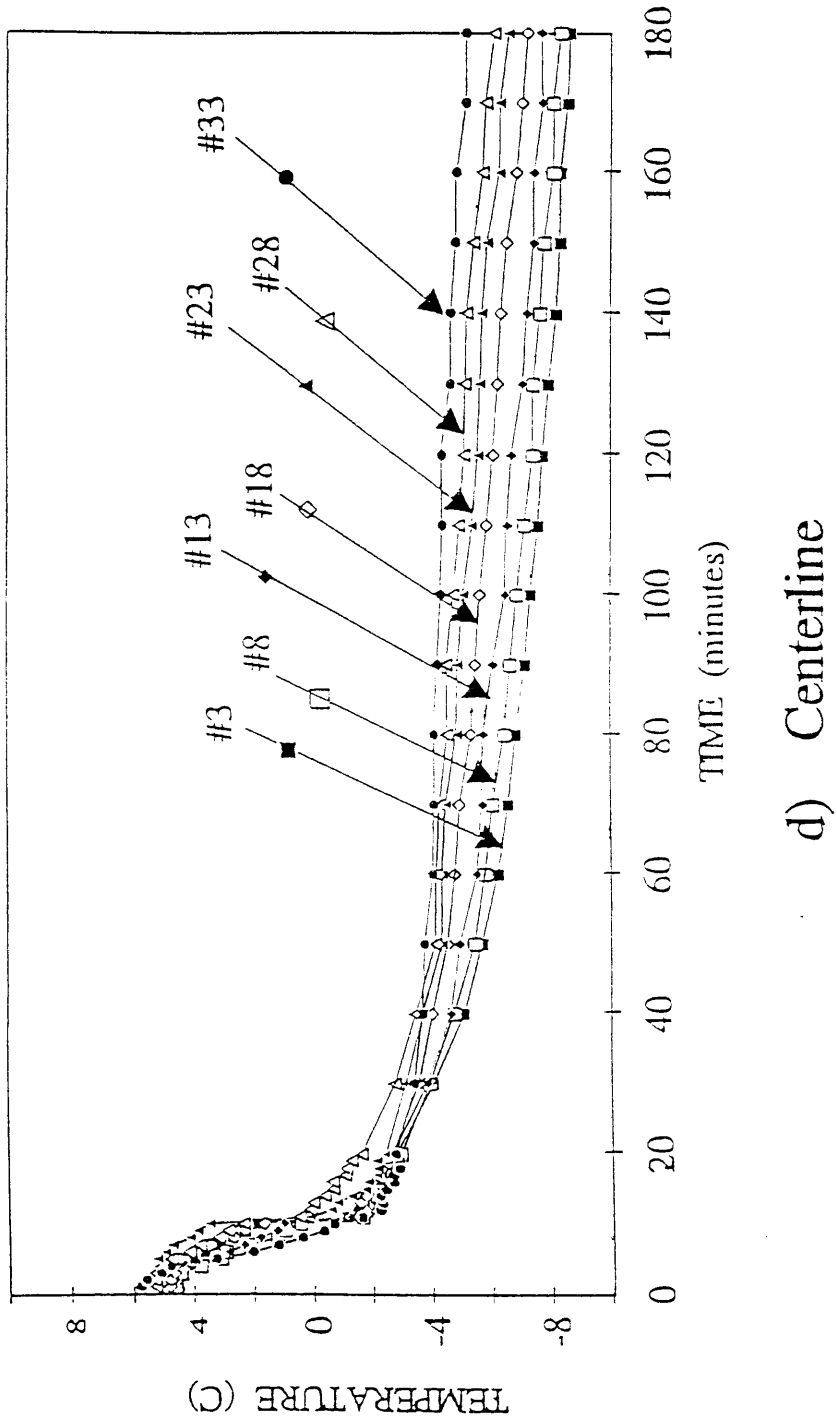

Figure [3.16d] Temperature profiles, 5 % Concentration.
(C_o = 5%, T_c = -10°C, T_i = 5°C)

to around -3°C, which is lower than the phase change temperature for this concentration. However, no dendrites formed at this stage. This overcooling endured for a few minutes until the first dendrite appeared. Visual observation indicated that the dendritic region spread very fast to cover the entire sidewall surfaces in less than one minute. At the same time, the thermocouple reading of #11 jumped to about 2°C, which corresponds to the phase change temperature at this concentration. Figure [3.16d] illustrates the temperature history along the vertical centerline of the test chamber. The temperatures at all seven levels dropped very rapidly in the first 10 minutes; then the rate of temperature reduction slowed down, but the vertical temperature gradient increased. Overall, the temperature was lower at the bottom and was higher at the top, which is unfavorable to natural thermal convection along the centerline.

Figure [3.17] shows the solute concentration history along the vertical center line. The locations of the four probe tips were 2 cm, 6 cm, 9 cm, and 11 cm above the bottom of the test chamber. Initially, the concentrations in all four locations were equal to 5%. The concentrations continuously increased with time due to ejection of the solute during the solidification process, since the concentration was higher at the bottom and lower near the top, which is also unfavorable for solute driven natural convection.

Figure [3.18] illustrates the evolution of the mushy zone and the solid region in the 5% initial concentration solution. At t=15 min. Fig. [3.18a], observation indicated that the solidified region was composed of mainly long and coarse dendrites. As time elapsed, the dendrites became shorter and finer, and the solid region appeared, Figs.

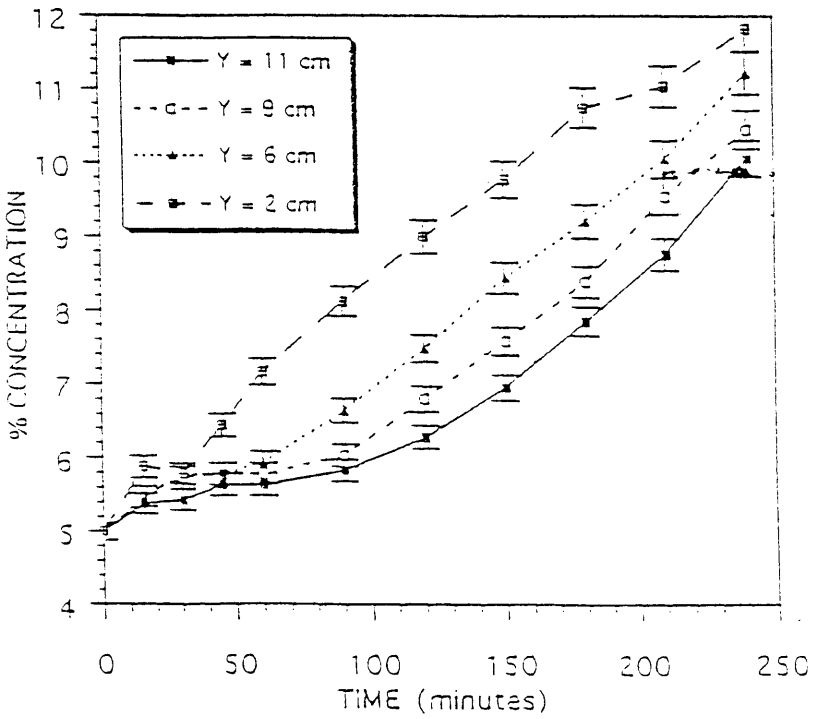

Figure [3.17] Concentration variation - 5% solution.

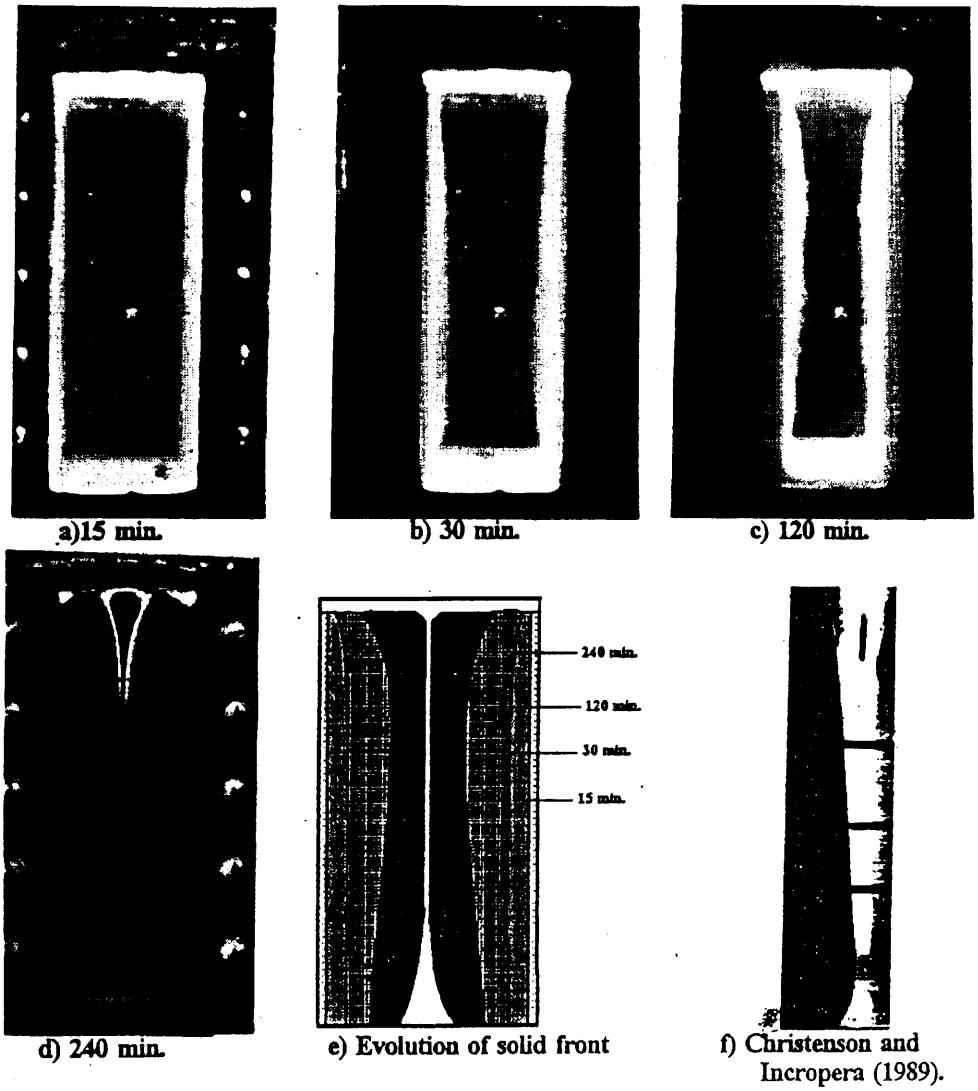

Figure [3.18] Evolution of the Interface Front- 5% Solution.

[3.18b] and [3.18c] beneath the dendritic region. Since the solute-rich fluid continuously flowed down along the interface region, the solidification in the region near the bottom was retarded. Figure [3.18d]shows that the interface fronts moved closer to each other near the top and left a large gap at the bottom. Figure [3.18e]shows the evolution of the solid region during the test process. This figure shows a different solidification behavior with the test conducted by Christenson and Incropera (1989) for the rectangular cavity with one cold wall and one insulated wall (C_0=10%), Fig. [3.18f]. This difference in the observed behavior may be attributable to the fact that while these experiments were full geometric domain(two cold walls), those performed by Christenson and Incropera were half domain (one cold wall, one insulated wall).

c. Hypereutectic Solidification (Test Run III)

In contrast to the hypoeutectic composition, the ejection of water-rich interdendritic fluid will induce an upward flow in the hypereutectic composition solution. Figure [3.19] illustrates the concentration change with time in the five probes located at 2 cm, 6 cm, 9 cm, 11 cm, and 13 cm above the bottom. Concentrations in these five positions continuously diminished. The concentration near the top of the chamber diminished much faster than at the locations near the bottom, and the concentration gradient along the centerline continuously increased. In 30 minutes, the concentration difference between the top and the bottom reached 3%. After that, the concentration gradient along the center decreased, and eventually the concentrations in all positions reached a eutectic value.

Figure [3.20] illustrates the evolution of the mushy zone and the solid front with a 25% initial concentration solution. Observation indicated that a few minutes after starting the test, dendrites appeared on the cooling walls. At the same time, many equiaxed dendrites appeared in the liquid pool. These tiny solid particles grew and coalesced as they descended. After about 10 minutes, the dendrites covered all the cooling walls and the bottom plate, as seen in Fig.[3.20a]. The mushy zone increased slowly after that, and the solid zone grew under the mushy zone, as seen in Fig. [3.20b], t=30 minutes. In this figure, the bright region indicates the mushy zone, where the dark region under the mushy zone indicates the solid ice. At t=120 minutes, the solid and the mushy zone grew mainly

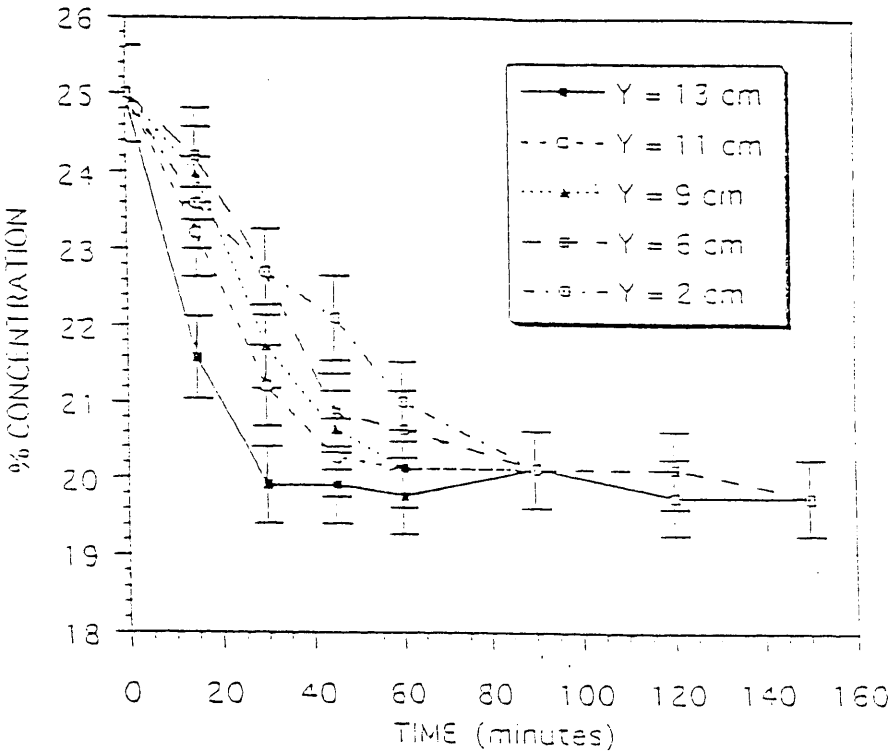

Figure [3.19] Concentration variation - 25% solution.

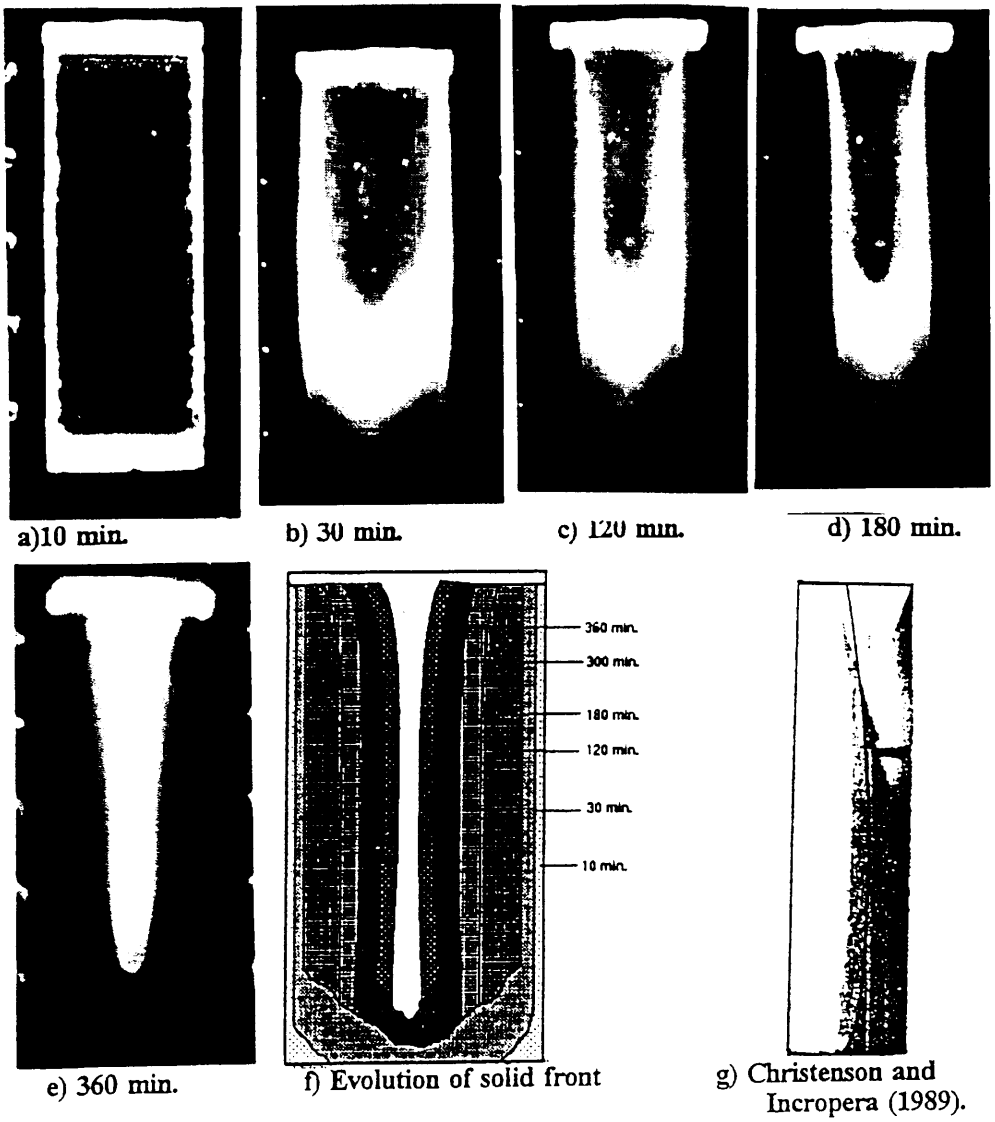

Figure [3.20] Evolution of the Interface Front- 25% Solution.

near the bottom, Fig.[3.20c]. The mushy and solid zones grew continuously, but their growth was at a much slower pace compared to the beginning of the test. Figure [3.20d] shows the mushy/solid fronts after three hours. As the solidification process continued, the solid region grew farther from the cooling wall. The thickness of the loose mushy zone was further reduced as the solidification continued, as seen in Fig. [3.20e]. Figure [3.20f] illustrates the solidification process in detail. For the hypereutectic concentration solution, 30% initial solute concentration, Christenson and Incropera (1988) found that a set of double-diffusive interfaces (two to four, depending on the initial concentration and cooling temperature) formed just a few minutes after the start of the solidification process. In their study, the double-diffusive recirculation region was mainly near the top of the solution surface, and a double-diffusive interface grew in the downward direction. As a result, the solidification near the top was significantly retarded, Fig. [3.20g]. However, in our experimental test, the double-diffusive interface did not form. As seen in Fig. [3.20f], the solidified region along the side cooling walls grew equally in the horizontal direction in our test.

Figure [3.21] shows the temperature history in Test Run III. Figure [3.21a] illustrates the temperature distribution along the vertical centerline. It is interesting to see that the temperature had a higher value near the top and a lower value near the bottom of the test chamber at the beginning of the test. As time elapsed, the temperature near the top decreased much faster than that near the bottom, and eventually the temperature distribution inverted after 6 minutes; that is, the temperature was higher at the bottom and

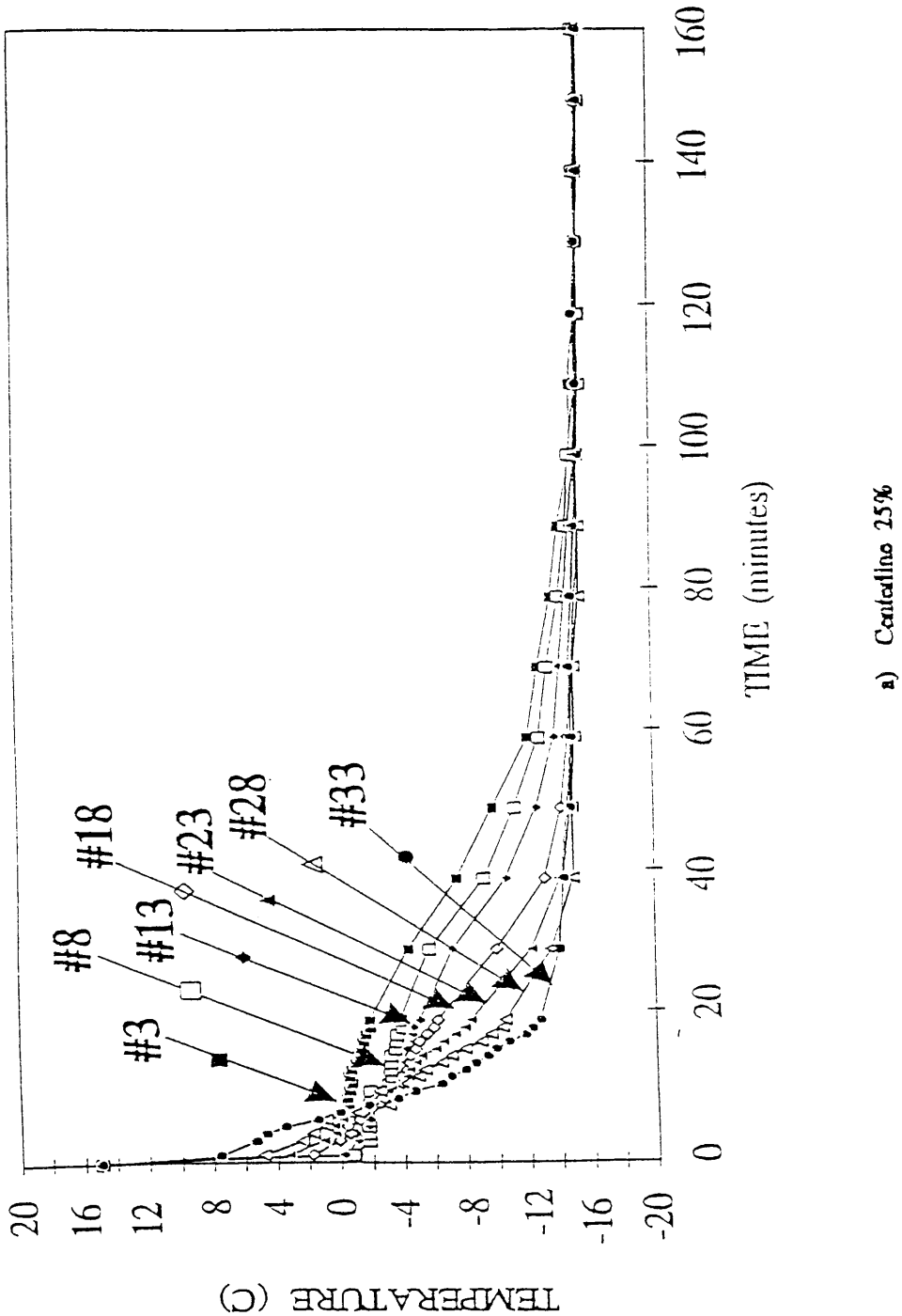

Figure [3.21a] Temperature profiles, 25% Concentration.
(C_o = 25%, T_c = -20^{0}C, T_i = 15^{0}C)

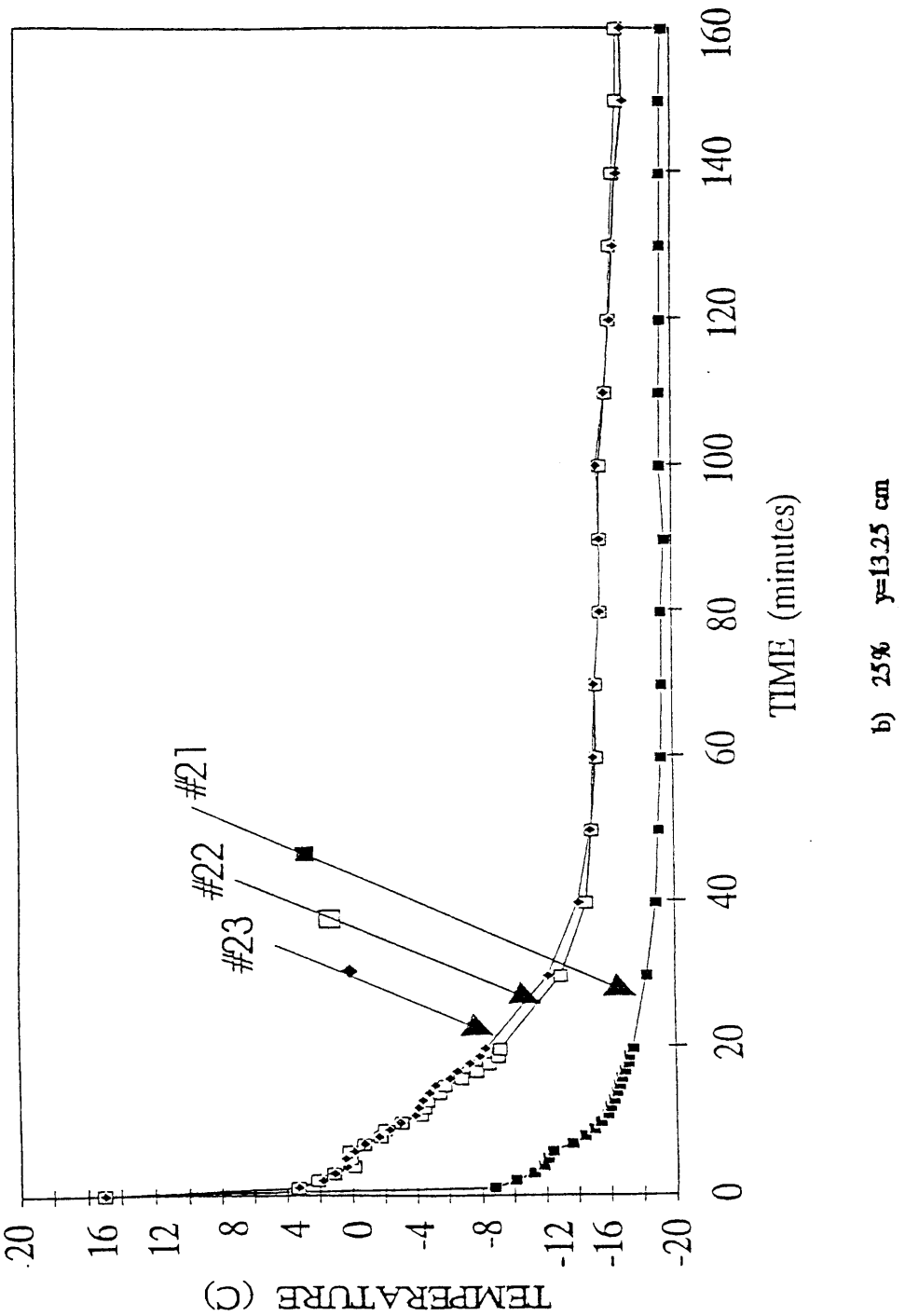

Figure [3.21b] Temperature profiles, 25% Concentration.
(C_o = 25%, T_c = -20^{0}C, T_i = 15^{0}C)

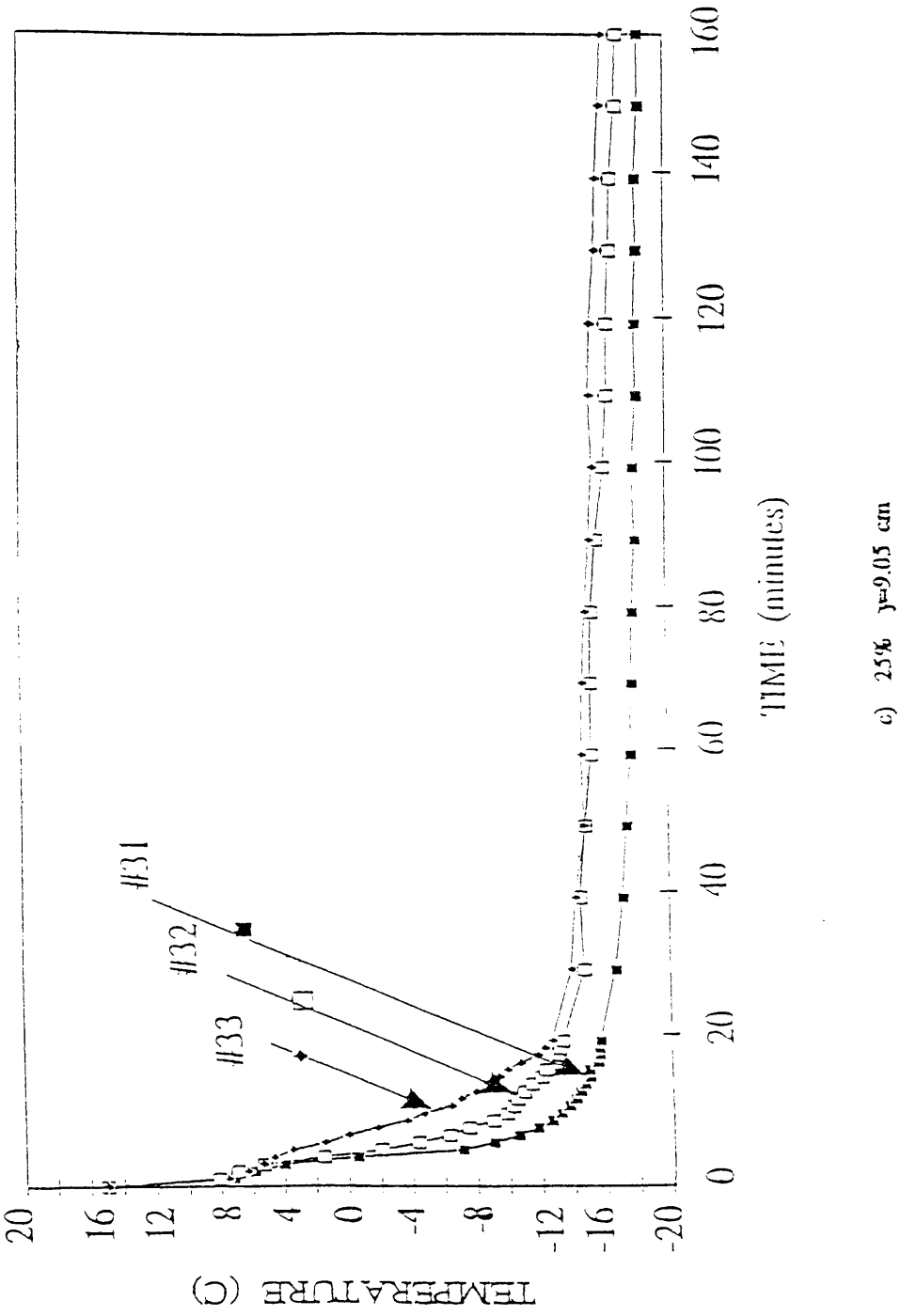

Figure [3.21c] Temperature profiles, 25% Concentration.
(C_o = 25%, T_c = -20^{0}C, T_i = 15^{0}C)

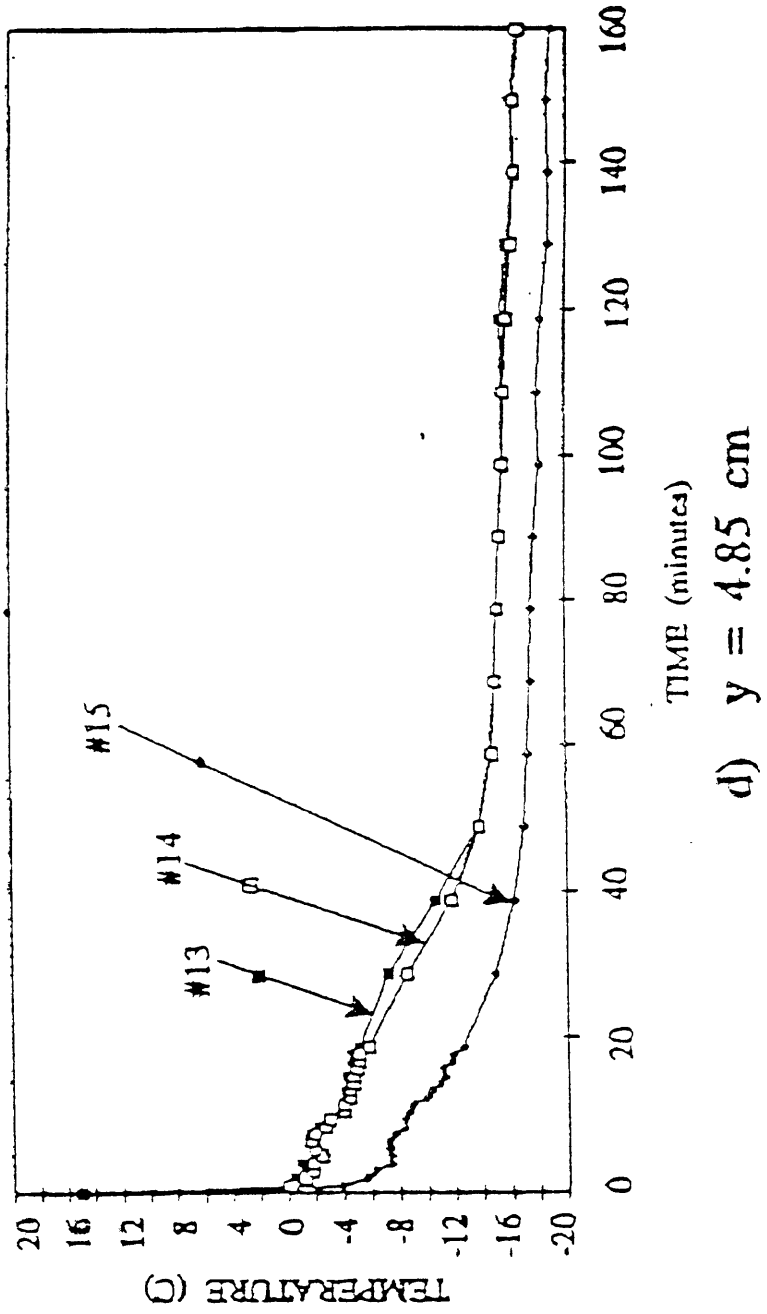

Figure [3.21d] Temperature profiles, 25% Concentration.
(C_o = 25%, T_c = -20^{0}C, T_i = 15^{0}C)

gradually decreased with height. This phenomenon indicates that the temperature distributions before and after 6 minutes were controlled by different mechanisms. Before the dendrites appeared, the flow in the liquid pool was controlled by thermally driven natural convection, in which the liquid rose along the centerline and flowed downward near the solid cooling walls. After dendrites appeared, the cold water-rich liquid was ejected from the dendritic region. Since this cold liquid was lighter than the solution in the liquid pool, it flowed upward near the wall region. When the solute driven force surpassed the thermal driven force, the flow direction was reversed, which resulted in the temperature distribution inversion in Fig.[3.21a]. The temperature gradient reached its highest value at around t = 20 minutes, and then slightly decreased. After t = 90 minutes, all temperatures in the vertical centerline achieved eutectic temperature. Unlike the cases of the eutectic and hypoeutectic solutions, a temperature difference existed along the horizontal direction. From the very beginning, the temperatures of the thermocouples near the cooling wall were far below the temperatures in the center region. This can easily be explained, since thick dendrites covered these thermocouple locations during the earlier time in the solidification process. It is interesting to compare the temperature along the symmetric centerline in our test and the temperature along the insulated wall in the case of Christenson and Incropera (1989). Christenson and Incropera (1989) showed that the wall temperatures at three different levels (45 mm, 65 mm, and 90 mm above the bottom) were within 1^0C of each other at the same instant. Figure [3.21a] indicates the

temperature was rapidly changed along the vertical centerline, and the temperature gradient even changed direction during the solidification process.

3.3 Effects of Boundary conditions

a. Effect of Bottom Cooling

Aqueous sodium carbonate, Na_2CO_3, was chosen as the test solution for this study. This solution was selected because it also possesses a phase change behavior similar to a binary alloy system. The phase change temperature is relatively warmer than ammonium chloride solutions and is therefore easier to solidify . This made for more rapid experimentation without significantly reducing the facility of the model. To simulate the metal casting process, a hypereutectic concentration of 10% was utilized with initial temperature of 15 °C and a cooling temperature of - 15 °C. Experimental tests were conducted on two rectangular test sumps, both having the same geometry and dimensions Fig. [2.3], 19cm x 6cm x 16cm (height x width x depth). Both sumps have two copper sidewalls, front and back plexiglas windows, and a plexiglas top cover. The bottom wall of sump A, Fig. [2.3a] is constructed of a plexiglas plate to simulate an adiabatic boundary condition. The bottom wall of sump B Fig. [2.3b], is made of a copper plate. Channels 12mm wide by 12mm deep were machined into the back surfaces of the copper sidewalls and bottom wall to serve as gutters for the coolant. Five thermocouples were installed inside each cooling wall to measure the wall temperature. The cooling wall was assumed to have a uniform temperature since the temperature difference between these thermocouples is less than 1°C for the cooling walls. The test sump was then covered with a siphon box to insulate it from the ambient. The front and rear chambers were kept in a vacuum during the

test, and the front of the siphon box was kept open for recording by the video camera. Due to its length, the test section was assumed to be a two-dimensional chamber. Figure [2.7] shows that forty thermocouples were equally distributed in eight horizontal lines, where y indicates the vertical location in relation to the bottom surface of the test sump. The distance between the two thermocouples is 1.2 cm in a horizontal direction and 2.1 cm in the vertical direction. The thermocouples near the wall are 0.6cm away from the solid wall.

Figure [3.22a]shows the temperature distribution along the centerline of test sump A. Thermocouple # 3 (only numbers will be used to present thermocouple locations in this section) is 0.65 cm from the bottom wall, and #38 is 15.35 cm from the bottom. For the first four minutes, the temperatures of all thermocouples continuously decreased. Between 4 to 10 minutes, the majority of the thermocouples increased in temperature and then decreased again. The large volumes of dendrites that appeared were associated with this rise in temperature. Since different mechanisms for controlling the flow patterns in the liquid pool before and after solidification are involved, separate discussions are given for the period before and after the 4 minutes. In the first four minutes, the temperature of #13 (4.85 cm above the bottom) reduced by almost 16°C. At higher levels, the temperature reduction was less, for example, the temperature of #33 reduced only 4°C during this time period.

Figure [3.22b] shows the horizontal temperature distributions at two heights. This figure indicates that at y=4.85 cm, the three thermocouples (#11 through #13) had the same temperature in the first four minutes, which indicates a strong horizontal direction flow

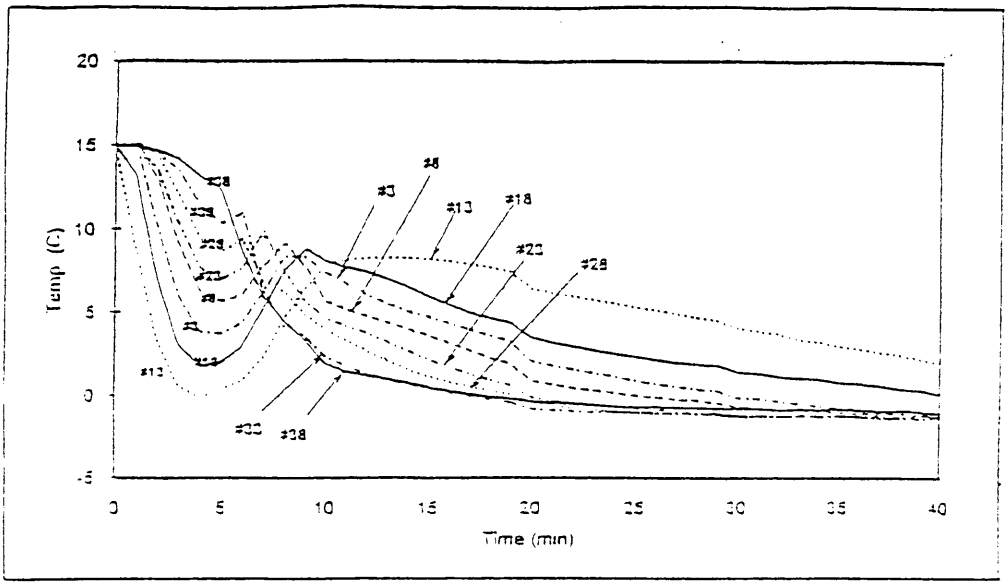

a) Vertical temperature history.

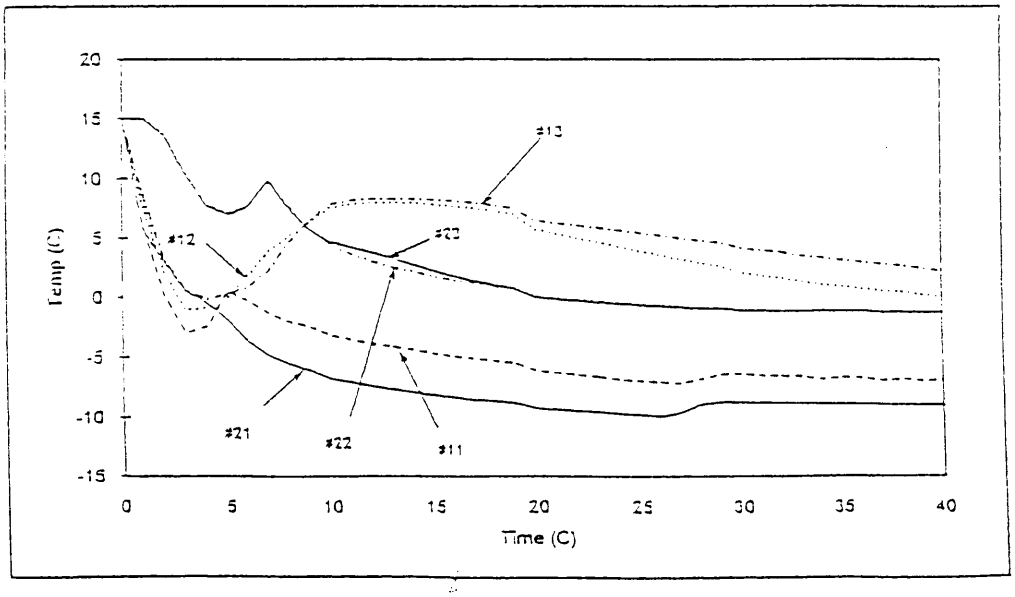

b) Horizontal temperature history.

Figure [3.22] Temperature profiles, 10% Concentration, Na_2CO_3.

around this area. At y=9.05 cm, the horizontal temperature distribution was much different from that of y=4.85 cm. The temperature of a thermocouple near the cooling wall, #21, was far below the temperatures of the thermocouples in the center region (#22 and #23) during the same time period. Since the solution was well mixed before the test, the cooling walls were parallel to the centerline, and no phase change occurred, the only possibility for obtaining the temperature distribution like in Fig. [3.22] was from the thermally driven convective flow as shown in Fig. [3.23a]. Figure [3.23a] shows that the fluid flowed down along the cooling wall, then flowed from the wall region to the center of the sump around 5cm from the bottom. After that, it flowed upward as it warmed. A small flow loop also existed in the bottom region below this large flow loop, as seen in Fig. [3.23a].

After 4 minutes, Fig. [3.22a], shows that the temperatures of all the thermocouples along the centerline increased, except for #38. Figure [3.22b] shows that at y=9.05cm, the temperatures of thermocouples #22 and #23 increased around 3°C and then dropped after that, while the temperature of the thermocouples near the wall continuously decreased with time. At y=4.85 cm, the temperature increased even the thermocouple near the wall, #11. The temperature changes in Figs. [3.22a] and [3.22b] indicate that the fluid flow changed its direction during this period of time, that is, the fluid flowed downward along the centerline and upward near the solid wall region. This downward flow brought the warm fluid from the top region to warm the thermocouples below it. This inverse flow loop was driven by the concentration gradients generated by solidification. During solidification of a hypereutectic solution, the solute will be solidified first, while the water will be ejected

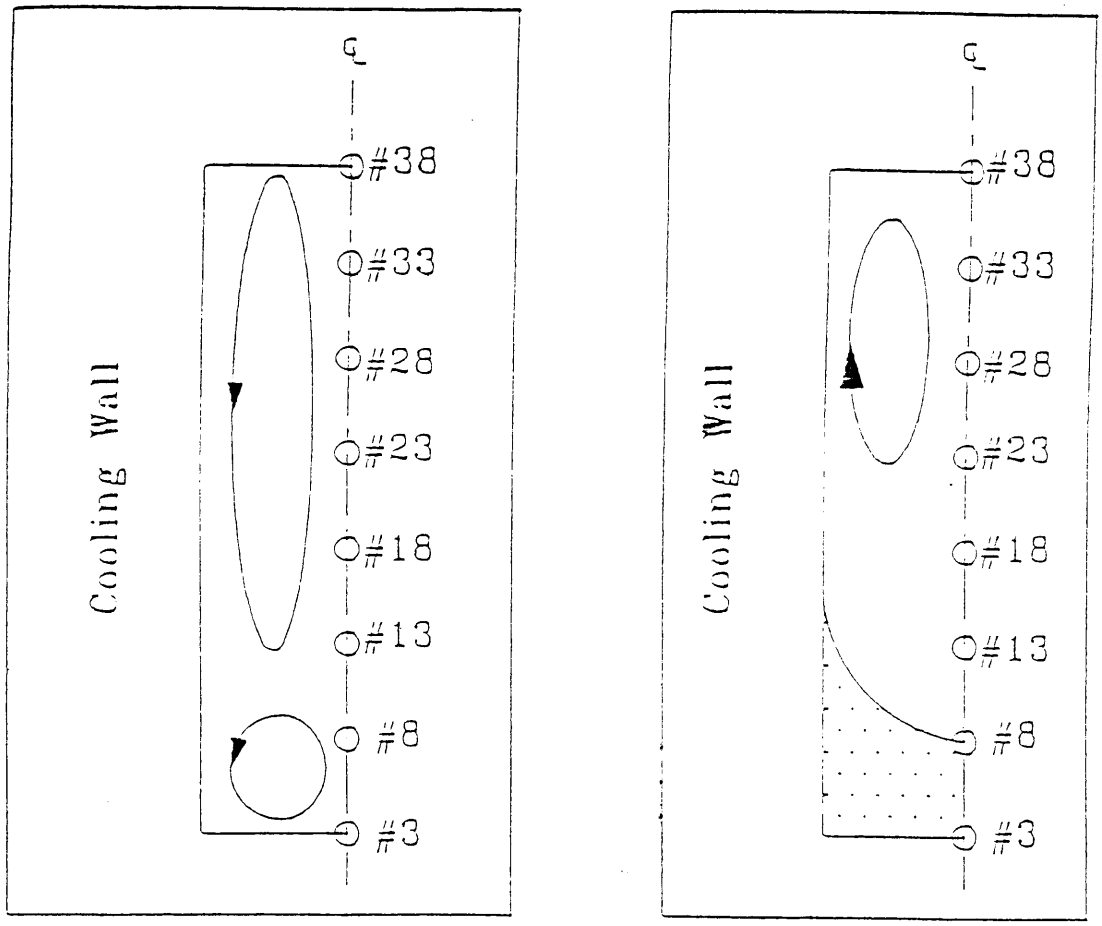

a) b)

Figure [3.23] Flow patterns in the Rectangular sump.

from the dendritic region. Since the water was lighter than the solution, it generated an upward buoyancy force near the wall region.. It is interesting to see that the temperature of #13 reduced much slower than that at other locations. It had a negative temperature gradient in all directions after 10 minutes, as seen in Figs. [3.22a] and [3.22b]. This suggests that the fluid heat transfer around thermocouple #13 was mainly controlled by conduction. The fluid flow inside the liquid pool can be illustrated as in Fig. [3.23b], which shows that the bottom region is covered by loose equiaxed dendrites, only one flow loop is formed during this period of time, as observed in the previously described visualization experiments.

Figure [3.24] illustrates the temperature distributions along the centerline in test sump B. Before the dendrites appeared, a negative temperature gradient existed from the top to the bottom along the centerline, which indicates only one thermally driven flow loop in each half-domain. The thermal convective flow in sump B was not as strong as in sump A due to the small temperature gradient between the center and wall region. After dendrites appeared at around the fourth minute, the bottom region was rapidly covered with dendrites, which is evidenced by the fact that the temperature of thermocouple #3 dropped rapidly below the eutectic temperature. The concentration driven convective flow overcame the thermally driven flow after 10 minutes. Unlike what occurred in sump A, no significant temperature increase was observed in sump B. Comparatively, the temperatures of the liquid pool in sump B reached uniformity much faster than that in sump A.

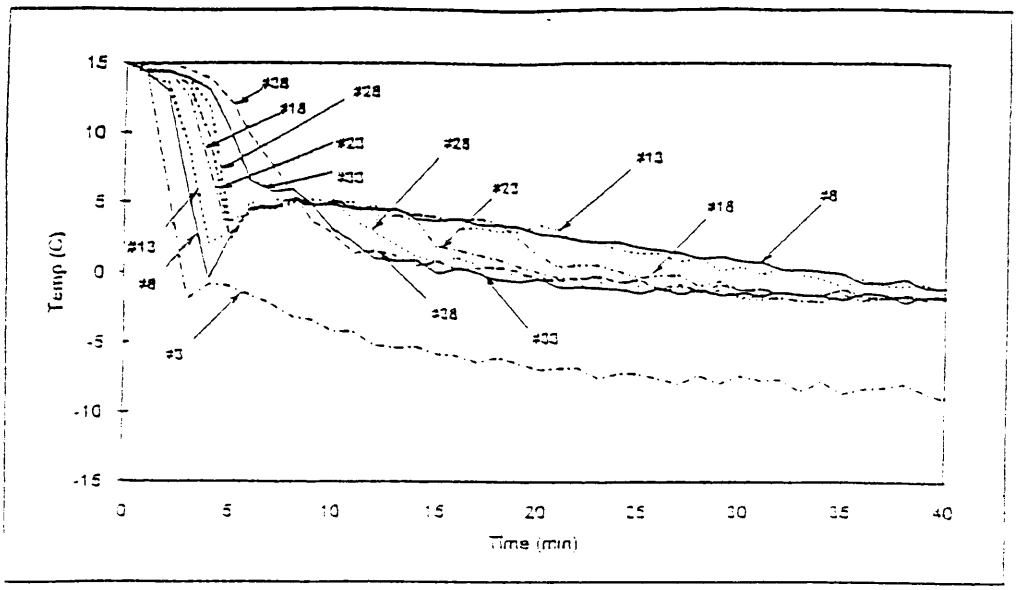

a) Vertical temperature history.

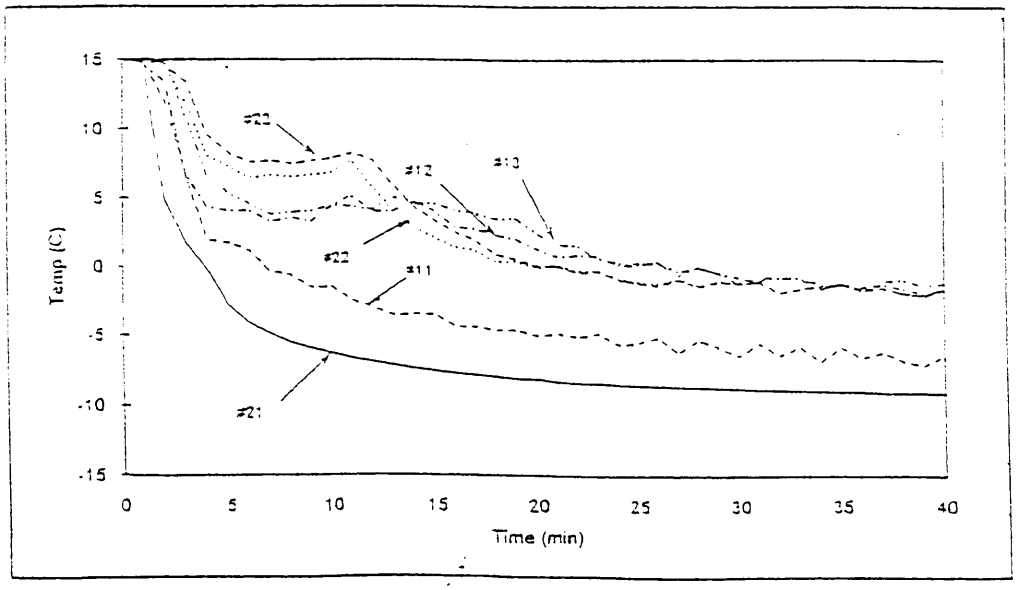

b) Horizontal temperature history.

Figure [3.24] Temperature profiles, 10% Concentration, Na_2CO_3.

b. Effect of the Angle of the Sump

During the continuous casting process, the melted material is poured into a water-cooled mold and exits the mold from the bottom. The material near the cooled mold is solidified first and forms a V-shaped liquid crust. The angle of the V-shape is about 4 to 16 degrees, which depends on the crust movement speed, the temperature difference between the liquid and the cooling wall, and the thermal properties of the casting material. The purpose of this study is to determine the effect of the sump (crust) angle on the double-diffusive flow pattern.

Two test sumps were built to study the effect of the angle on the flow patterns. Both sumps have a dimension of 29 cm in height and 25 cm in height. Figure [2.2] is a schematic view of the V-shaped test sump. The test sump consists of two cooling sidewalls, front and back vacuum chambers and a plexiglas cover. The angle, a , of sumps C and D was 16 degrees and 4 degrees, respectively. Five E-type thermocouples were installed inside each sidewall to measure the wall temperature. The front and rear vacuum chambers were made with plexiglas so that the solidification process could be observed and recorded by a video camera. The two cooling walls were attached on the front and rear vacuum chambers to form a V-shaped sump. The sidewalls were insulated by using polystyrene expanded foam . Forty-one thermocouples were installed inside the liquid pool of sumps C and thirty in D to monitor the temperature changes during the test. Details of the location of each thermocouple are given in Figs. [2.5] and [2.6].

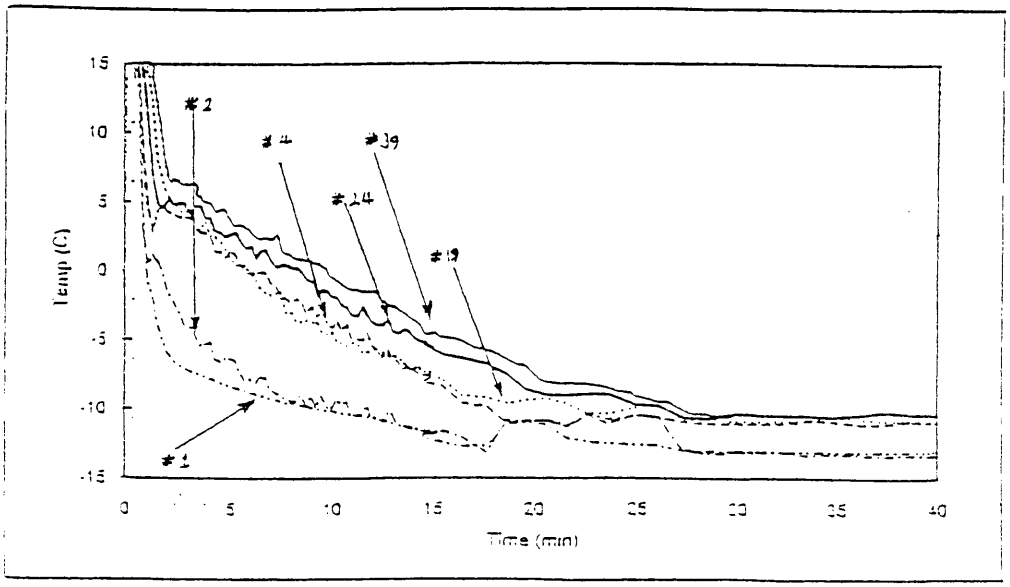

a) Vertical temperature history of 16° v-shape.

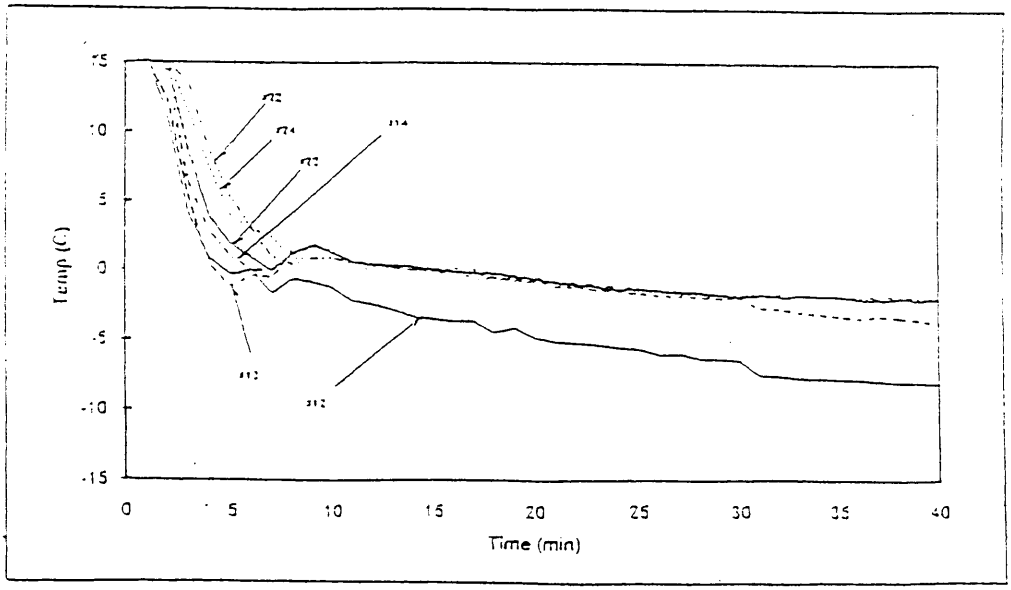

b) Horizontal temperature history of 16° v-shape.

Figure [3.25] Temperature profiles, 16^0 V shaped sump.

Figure [3.25a] depicts the temperature distribution in sump C along the centerline. This figure indicates that before the dendrites appeared, which happened around 5 minutes after the test started, the heat transfer in the liquid pool was controlled by thermal convective flow. According to the temperature distribution along the centerline, two flow loops existed in the liquid pool. One was between thermocouples #24 to #39, and another one was in the region between thermocouples #4 to #19. In the region below thermocouple #2, the dominant heat transfer mechanism was conduction. Figure [3.25b] shows the temperature distribution along two horizontal lines. At y=12 cm, Fig.[3.25b] shows that the fluid temperature increased from the wall to the centerline (thermocouples #12, #13, and #14) in the first four minutes. However, at y=17 cm, the temperature of thermocouple #24 (at the centerline) was lower then the temperature of #22 and #23 at the same height, which indicates a strong upward convective flow near the center region.

Figure [3.26a] shows the vertical temperature distribution along the centerline in sump D. This test sump has a very large height/width ratio, which is around 13 based on the maximum width of the sump (the maximum distance between the two cooling walls is less than 2 cm). Solidification started around t=8 minutes. Unlike the behavior in the sump with the 16° angle, this figure indicates that the temperature increased smoothly as the height increased before the dendrites appeared. It should be emphasized that the distance between the cooling wall and the centerline increased as the height increased. Figure [3.26b] illustrates the temperature distributions along two horizontal locations, y=21.5 cm and y=26.5 cm. This figure indicates that the temperature increased smoothly from the cooling wall to the centerline. The temperature distribution presented in Figs. [3.26a] and

[3.26b] reflects that conductive heat transfer was the dominate heat transfer mechanism during this period. After solidification occurred, Figs. [3.26a] and [3.26b] illustrate that the temperatures at different thermocouples were close to each other, but the temperature still increased smoothly from the cooling wall to the centerline and from the bottom to top e.g. conduction was still the dominant mechanism for heat transfer inside the liquid pool.

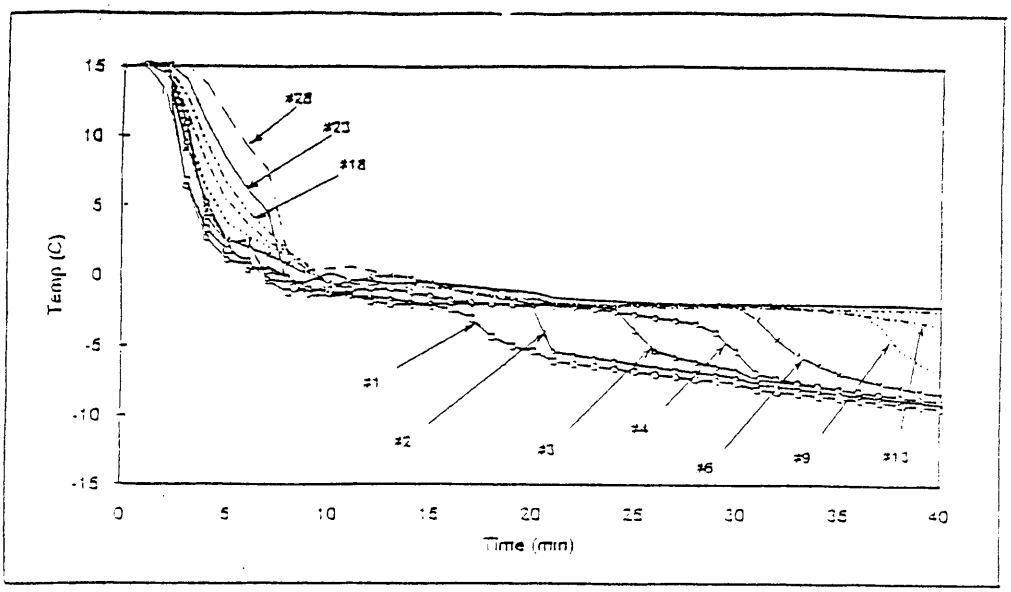

a) Vertical temperature history of 4° v-shape.

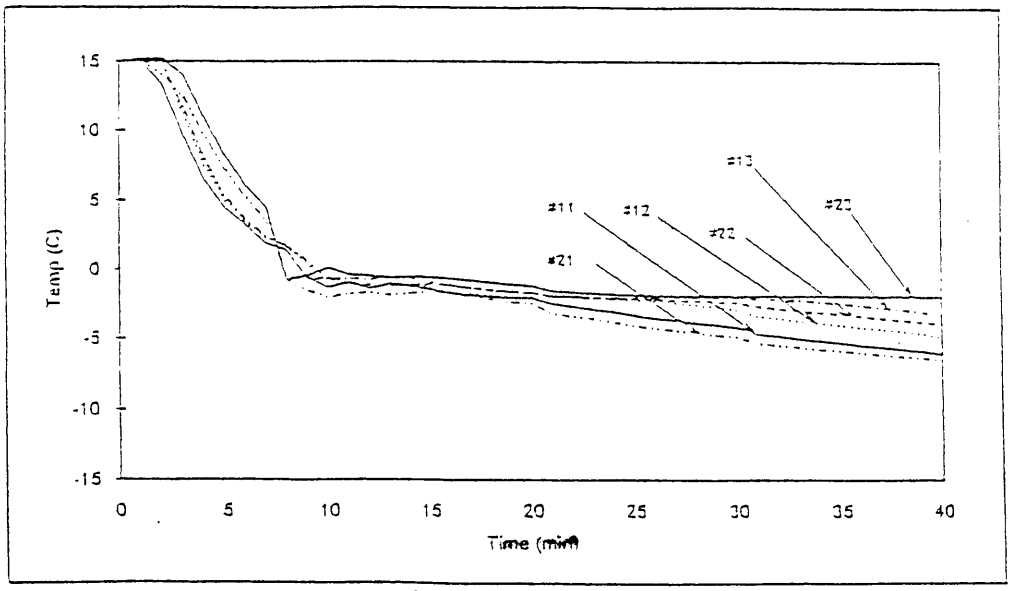

b) Horizontal temperature history of 4° v-shape.

Figure [3.26] Temperature profiles, 4^0 V shaped sump.

CHAPTER 4 - CONCLUSIONS AND RECOMMENDATIONS

4.1 Conclusions

a. 16 degree V- shaped sump

It is significant that in the case of the 16 degree V-shaped sump, using eutectic concentration, while two flow loops occurred in half domain ,vertically separated, orientation, no stratification was observed despite a large difference in the preheat to cooling temperatures. In the case of the 5% hypoeutectic test, the phase change boundary, mushy zone, acts as a species source for the melt pool. The concentration driven flow assists the thermally driven flow. In the absence of a nucleation mechanism overcooling phenomena were observed. When crystal structures do form, heterogeneously at the walls, a rapid formation of dendritic structures is accompanied by a local rise in temperature, suggesting that a short term increase in cooling rate at this time may help in the formation of finer structures. Initial crystal structures are coarse and later formations are shorter and finer, this change of structure is accompanied by a concentration increase in the melt pool which tracks, fairly closely, the liquidus profile. Since there was an increase in the concentration at the base of the melt pool, remelting and consequent suppression of the solid formation occurred. These crystals were primarily either short dendritic types or equiaxed, eutectic forms. In the 15% solution, columnar dendrites quickly formed at the walls and particles were convected into the melt where they acted as nucleation cells for equiaxed growth. Since the initial concentration in this case is closer to the eutectic, the mushy zone is thinner and the melt pool concentration stabilized quickly at a, close to,

eutectic value because of the species rejection from the mushy interface. No overcooling phenomena were observed. For the hypereutectic case, solute ejection from the solid/liquid interface brought the melt pool to a concentration value approaching the eutectic. This rapid change of concentration, therefore, caused the formation of greater volumes of eutectic structures.

b. Rectangular sump.

In the rectangular sump, with eutectic solution, the entire domain quickly reached the eutectic temperature. Since, the expectation is that a eutectic melt pool will be driven solely by thermal convection, this rapid temperature homogenenisation leads to flow field stagnation, no gradient, of any consequence, exists. Crystal growth is essentially parallel to the walls and of eutectic form. The 5% hypoeutectic case, in this sump, again demonstrated the overcooling effect, with the associated rapid dendritic early growth. Also, the solidification at the base of the sump was again retarded by the accumulation of more concentrated fluid. The comparison to the hot wall, cold wall experimentation suggests that the proximity of the other wall, aspect ratio, is critical to the flow pattern. Coupling of the flow fields changes the solidification behavior, since it increases the remelting and therefore the amount of eutectic formed. For hypereutectic concentrations, the concentration gradient at the centerline is increased. A, volumetrically, more limited amount of the eutectic precipitate was incorporated into the dendritic solid, as time progressed. Absence of the previously reported double diffusive interface can be attributed to the coupling of the wall effects on the flow field. The early flow was dominated by thermally driven

mechanisms, since no double diffusive interfaces were formed, with a consequent reduction in circulation strength, the suppression of solid formation evident in the hot wall/ cold wall model of Incropera did not occur, again attributable to the coupling of the wall steams in this model. As evidenced by the temperature inversion, flow driving mechanisms change from thermal to concentration driven. From an experimentally interesting viewpoint, the difference in the temperature distribution will significantly change the flow pattern as well as the solidification behavior. Therefore, the test results suggest that, a test with one cold wall and one insulated wall cannot adequately simulate the situation of solidification with a symmetric cooling wall.

In the case of hypereutectic solutions in the rectangular sump where the bottom cooling is investigated, the data suggest that the thermal convectively maintained warm cell, found in the sump A experiments, is suppressed by the application of bottom cooling. This is due to the more homogeneous temperature distribution achieved in the B cell.

During static ingot solidification, this hot spot in sump A may result in local structural defects and inhomogeneity, bottom cooling can effectively improve this drawback.

c. Effects of boundary conditions.

The experiments into the effect of the v angle, which in casting processes is a function of the descent speed of the ingot and the pour rate, suggest that, prior to solidification at the walls, double diffusive mechanisms create strong convective flows in

the center region of the 16 degree sump. After solidification occurred, the concentration driven buoyancy force balanced the thermal convection, and the temperature changed smoothly in all directions that is, the heat transfer during this period was dominated by thermal conduction. In the 4 degree sump, however, the double diffusive mechanisms are suppressed by the lack of a thermal gradient, of any significant driving force, from the outset. Since, the geometry of the liquid pool depends on the ingot movement speed and thermal properties of the material, the heat extraction rate is crucial for the quality of the cast materials' structure. A low cooling rate causes a wider v angle, with more retained heat energy in the melt, this can lead to substantial breakout, which results from the inability of the crust to withstand the weight of the liquid core. However, higher cooling rates, which produce the less problematic narrow v angles, may produce residual stresses on the surface and undesirable surface defects.

4.2 Recommendations

Future experimental investigations are appropriate in the following areas;

The effect of a short term increase in the heat extraction rate from hypoeutectic solutions, at the initial onset of the overcooling phenomenon, should be investigated.

Since, stratification phenomena are so widely reported and emphasis is given to these effects in many studies, the degree to which, aspect ratio and other geometric parameters affect the formation of these strata should be investigated. In light of the flow field coupling effects reported in these experimental investigations, the geometric shape of the sump and its cross sectional profile should be systematically investigated to determine the degree to which flow field coupling effects either suppress or enhance the stratification phenomenon.

The significant extent of the changes in the flow field that were achieved by the application of bottom cooling suggest that further experimentation would yield valuable data with regard to the effects of other thermal boundary condition arrangements. Additionally, since, a proportion of cast products are manufactured with, other than rectangular, cross sections, valuable insights may be derived from experiments in sumps with varying geometric configurations.

The current data and the emphasis of this experimental program, leads to the conclusion that a sub-scale model of the dynamic continuous casting process is both, a viable and a valuable direction for continued experimental research. Apparatus for this

experimentation and modeling is presently being constructed in the Florida International University Thermal Science group, solidification laboratory.

Specific recommendations with regard to procedures and apparatus are;

Continued use of type 'E' thermocouples, .8mm diameter, probes of this size appear to be most adequate for system response and temperature profile definition. Notwithstanding, the availability of a non-intrusive method of temperature data collection. The small probe volume of these thermocouples minimizes the, previously reported, conduction in probe distortion and provides a minimal source of nucleation, although not optimal.

Acquisition of a small scale optical probe to accumulate concentration data automatically at the probe tip, with collocated thermal data collection is recommended. Current, state of the art, acquisition systems using light transmission in a fiber optic can give reliable, precise refractive index responses and from our correlation salinity gradients could be profiled.

Laser illumination and the use of Digital Particle Image Velocimetry techniques for velocity field and visualization data collection and enhancement would be a valuable addition to the current data collection equipment inventory. Laser illumination provides an, in cell, light energy density that, with appropriate seeding, aids in tracking the flow patterns in the sump and facilitates the analysis of the visual data by enhancing the clarity of the imagery.

Great value could be derived from a parallel analysis of the experimental data by a comparison to a numerical simulation. The value of a numerical simulation, achieved in concert with experimental data collection, is that the two techniques can be used to refine the numerical model by the use of repeatable experimental data as a cross checking tool. Subsequently, adjustment of the parameters affecting, microscale and macroscale, phenomena can be adjusted to produce an, industrially valuable, parametric analysis of the continuous casting process. The literature suggest that, very few of the extensive group of numerical models, especially the temporal transient continuous models, have been verified by direct experimental comparison.

Asai, S. and Muchi, I., 1978, *"Theoretical Analysis and Model Experiments on the Formation Mechanism of Channel-Type Segregation,"* Trans. ISIJ, **18**, pp. 90-98.

Backerud, L. and Chalmers, B., 1969, *"Some Aspects of Dendritic Growth in Binary Alloys: Study of the Aluminum - Copper System"*, Trans, Metall. Soc. AIME, Vol.245, pp. 309 - 318.

Banerjee, D. and Marsh, S. P., 1994," *Stereology- Based Modeling of Equiaxed Solidification*", HTD-Vol. 284 / AMD- Vol. 182, ASME.

Beckermann, C., 1987, "*Melting and Solidification and Binary Mixtures with Double-Diffusive Convection in the Melt*", Ph.D. Thesis, Purdue University.

Beckermann, C. and Viskanta, R., 1988,"*Double-Diffusive Convection During Dendritic Solidification of a Binary Mixture*", PCH PhysicoChem. Hydrodynm., Vol. 10, No. 2, pp. 195 - 213.

Beckermann, C. and Feller, R. J., 1993," *Modeling of the globulitic solidification of a binary metal alloy*", Int. Comm. Heat and Mass Transfer, Vol. 20, n.3 pp 311 - 322.

Beckermann, C. and Wang, C.Y., 1994,"*Multi-Scale/-Phase Modeling of Dendritic Alloy Solidification*", HTD- Vol. 284 / AMD- Vol. 182, ASME.

Benard, C., Gobin, D., and Thevenin, J., 1989, *"Thermosolutal Natural Convection in a Rectangular Enclosure, Numerical Results,"* in Heat Transfer in Convective Flows, edited by R. K. Shah, ASME HTD-Vol. **107**, pp. 249-254.

Brimacombe, J.K et al, 1984, " *Heat Transfer*", Continuous Casting, BookCrafters Inc., Chelsea, MI, Vol.2 pp 1 - 8

Brimacombe, J.K et al, 1984, *"Spray Cooling in the Continuous Casting of Steel"*, Continuous Casting, BookCrafters Inc., Chelsea, MI, Vol.2 pp 109 - 123.

Burton, R., Ebadian, M. A. et al, 1993,"*An Experimental Investigation of the Solidification Process in a V-Shaped Sump*", HTD- Vol.261, ASME

Burton, R., Ebadian, M. A. et al, 1994,"*On the Solidification Process in a Rectangular Enclosure with Symmetric Cooling*", HTD- Vol.280, ASME..

Burton, R., Ebadian, M. A. et al, 1994,"*Effects of Boundary Conditions on Double-Diffusive Flow During the Solidification Process in a Binary Solution*", HTD- Vol.289, ASME

Chen, C. F., Briggs, D.G. and Wirtz, R.A., 1971, " *Stability of Thermal Convection in a Salinity Gradient due to Lateral Side Heating*", Int. J. Heat and Mass Trans., Vol. 14, pp. 57 - 65.

Chen, C. F.,1974, *"Onset of Cellular Convection in a Salinity Gradient Due to a Lateral Temperature Gradient,"* J. Fluid Mech., **63**, pp. 563-576.

Chen, C. F. and Turner, J.S., 1980, *"Crystallization in a Double-Diffusive System"* J. Geophys. Res., Vol. 85, pp. 2573 - 2593.

Christenson, M. A. and Incropera, F. P., 1989, *"Solidification of an Aqueous Ammonium Chloride Solution in a Rectangular Cavity-I. Experimental Study"*, Int. J. Heat Mass Transfer, **32**, pp. 47-68.

Christenson, M. A., Bennon, W. D. and Incropera, F. P., 1989, *"Solidification of an Aqueous Ammonium Chloride Solution in a Rectangular Cavity-II. Comparison of predicted and measured results"*, Int. J. Heat Mass Transfer, 32, pp. 69 -80.

Cole, G.S. and Bolling, G.F., 1965, *" The Importance of Natural Convection in Casting"*, Trans. Metall. Soc., AIME, Vol. 233, pp. 1568 - 1572.

Fisher, K. M., 1981, *"The Effects of Fluid Flow on the Solidification of Industrial Castings and Ingots,"* Physico-Chem. Hydrodyn., 2, pp. 311-326.

Gebhart, B., Jaluria Y., Mahajan R.L, Sammakia B., 1988, *"Buoyancy-induced flows and transport,"* Hemisphere Publishing Corp., New York.

Gebhart, B., 1993, *"Heat conduction and Mass Diffusion,"* McGraw-Hill Inc., New York.

Hu, C. Y. and El-Wakil, M. M., 1974, *"Simultaneous Heat and Mass Transfer in a Rectangular Cavity,"* Proc. 5th Int. Heat Transfer conf., 5, pp. 24-28.

Huppert, H.E. and Turner, J.S., 1980, *" Ice Blocks Melting into a Salinity Gradient"*, J. Fluid Mechanics, Vol. 100, pp. 367 - 384.

Incropera, F. P. and Viskanta, R., 1992, *"Effect of Convection on the Solidification of Binary Mixtures." Heat and Mass Transfer in Materials Process* (ed. by I. Tanasawa and N. Lior), pp. 295-312, Hemisphere Publishing Corp., New York.

Incropera, F. P., Gaskell, D. R. and Prescott P.J., 1992, *"The Effects of Undercooling, Recalescence and Solid Transport on the Solidification of Binary Metal Alloys"*, HTD- Vol 196, ASME.

Incropera, F. P. and Krane, M. J., 1994, *" Analysis of the effect of Shrinkage on Macrosegregation in Alloy Solidification"*, HTD- Vol. 284 / AMD- Vol. 182, ASME.

Kamotani, Y., Wang, L. W., Ostrach, S., and Zhang, H. D., 1985, *"Experimental Study of Natural Convection in Shadow Enclosures with Horizontal Temperature and Concentration Gradients,"* Int. J. Heat Mass Transfer, 28, pp. 168-173.

Khodadi, J.M., Lan, X.K. and Shen, F.,1992, *"Turbulent Mixed Convective Steel Flow and Heat Transfer in Continuous Casting Molds"*, HTD- Vol. 196, ASME.

Lee, J., Hyun, M. T., and Kim, K. W., 1988, *"Natural Convection in Confined Fluids with Combined Horizontal Temperature and Concentration Gradients,"* Int. J. Heat Mass Transfer, 31, pp. 1969-1977.

McNulty, J. P., Garimella, S. V. and Schlitz, L. Z., 1994, *"Formation and Suppression of Channels during Unidirectional Solidification of Aqueous Ammonium Chloride"*, HTD- Vol. 284 / AMD- Vol. 182, ASME.

Mehrabian, R., Keane, M. A., and Flemings, M. C., 1970, *"Experiments on Macrosegregation and Freckle Formation"*, Met. Trans., 1, pp. 3238-3241.

Mendenhall, C.E. and Mason, M., 1923, *" The Stratified Subsidence of Fine Particles (and) Theory of Settling of Fine Particles"*, Proc. Natl. Acad. Sci. U.S.A., Vol.9, pp.199 - 207.

Ostrach, S., 1983, "*Fluid Mechanics in Crystal Growth,*" The 1982 Freeman Scholar Lecture, J. Fluid Engrg., **105**, pp. 5-20.
Patankar, S. V., 1980, "*Numerical Heat Transfer and Fluid Flow*", McGraw-Hill, New York.

Streat, and Weinberg, 1974," *Macrosegreation During Solidification Resulting from Density Difference in the liquid*", Metall. Trans., Vol. 5, pp. 2539 - 2548.

Stewart, M. J. and Weinberg, F., 1972, *"Fluid Flow Through a Solid-Liquid Dendritic Interface,"* Met. Trans. **3**, pp. 333-337.

Sundarraj, S. and Voller, V. R., 1994, "*A Dual Scale Model of Segregation Phenomena*", HTD- Vol. 284 / AMD- Vol. 182, ASME.

Szekely, J. and Jassal, A. S., 1978, *"An Experimental and Analytical Study of the Solidification of a Binary Dendritic System,"* Met. Trans. B, **9B**, pp. 389-398, 1978.

Thompson, M. E. and Szekely, J., 1988, *"Mathematical and Physical Modeling of Double-Diffusive Convection of Aqueous Solutions Crystallizing at a Vertical Wall,"* J. Fluid Mech., **187**, pp. 409-433.

Turner, J. S., 1979, *Buoyancy Effects in Fluids*, Cambridge University Press, London.

Viskanta, R., 1985, "*Natural convection in melting and solidification*", *Natural Convection* (Edited by S. Kakac, W. Aung, and R. Viskanta), p. 845, Hemisphere, New York .

VanVlack, L. H., 1989, "*Elements of Materials Science and Engineering*", Addison- Wellesley Publishing Co., Reading, Ma..

APPENDICES

HTD-Vol. 261, Heat and Mass Transfer in
Materials Processing and Manufacturing
ASME 1993

AN EXPERIMENTAL INVESTIGATION OF THE SOLIDIFICATION PROCESS IN A V-SHAPED SUMP

R. Burton, F. Desir, G. Hoo, G. Yang,
Z. F. Dong, and M. A. Ebadian
Department of Mechanical Engineering
Florida International University
Miami, Florida

ABSTRACT

An experimental study of binary mixture solidification in a V-shaped sump is conducted. NH_4Cl-H_2O is used as the phase change material. The variations of temperature, concentration, as well as the location of the interface front, are measured and reported in this investigation. The results indicate that the solidification process exhibits totally different behavior when the initial component of the solution is varied. For a hypoeutectic solution, the columnar solidification in the dendritic interface is the dominant mechanism. For the hypereutectic solution, both columnar and equiaxed solidification are important. The solidification starts as the equiaxed dendrites grow and coalesce in the entire solution. They then descend and settle at the bottom of the sump to form a loose, mushy zone. The solid region grows underneath the mushy zone.

NOMENCLATURE

C	concentration
T	temperature
t	time
x	vertical location
y	horizontal location

Subscripts

o	initial
c	cooling
e	eutectic

INTRODUCTION

Solidification is a phase transformation process that is accompanied by the release of thermal energy. The common feature of a system undergoing solid/liquid phase change is the existence of a moving boundary that separates the two phases of the solution with different thermophysical properties. The majority of commercial metal products are composed of alloys of two or more constituent elements, making them differ in many respects from the solid structure of a pure substance (Fisher, 1981) and (Viskanta, 1985). During the solidification of binary mixtures, the density of the liquid varies with both temperature and concentration. Thus, natural convection can be caused by both thermally and solutally induced density gradients. Previous researchers indicate that the major cause of structural defects and inhomogeneity (macrosegration and microsegration) during solidification is attributed to an improper convection flow pattern in the melt sump and the mushy zone (Fisher, 1981). Therefore, knowledge of the transport phenomena of double diffusive convection in the melt sump is essential for maintaining satisfactory control over the casting process.

Due to the complexity of double diffusive convection during the solidification process, theoretical study on this topic is still in the developing stage (Incropera and Viskanta, 1992) and experimental study is still the most powerful means to understand this basic phenomena. Many experimental studies on this topic have been conducted using different kinds of solutions. Liquid metals have been applied to study the solidification process by some researchers [Mehrabian et al. (Al-Cu alloy, 1970) and Stewart and Weinberg (Pb-Sn alloy, 1972)]. Since the liquid metal is opaque, it is very difficult to determine the flow pattern and the moving solid front interface during the experiment. Therefore, transparent solutions are usually applied to analogue alloy solidification. Asai and Muchi (1978) and Szekely and Jassal (1978) have used the NH_4Cl-H_2O solution to measure both velocity and temperature distributions in the solution. Thompson and Szekely (1988) and Chen (1974) conducted the solidification test by using an Na_2CO_3-H_2O solution. Recently, Beckermann (1987) and

Christenson and Incropera (1989) have also studied the solidification process in a rectangular cavity by using the NH_4Cl-H_2O system. The above mentioned survey of literature indicates that the majority of existing experimental results were obtained from the rectangular cross section test sump, which focused only on static ingot solidification. During the continuous casting process, melted material is poured into a water-cooled mold and exits the mold from the bottom. After heat is lost to the mold wall, the material nearest the cooled mold is solidified first to form a crust with the liquid material in the center. This crust is continuously withdrawn from the bottom. The material in the center usually needs additional time to solidify, which results in a V-shaped liquid sump. The angle of the V-shape is about 4 to 16 degrees, which usually depends on the crust movement velocity and the thermal properties of the casting material. What is the effect of the oblique walls of the V-shaped boundary on the solidification process of the binary solution? The surveys indicate that no such information is available in the open literature. As a first step for studying the V-shaped solidification process in continuous casting, this paper presents the primary experimental results of temperature, concentration, and the moving solid front interface during the solidification process in a fixed V-shaped sump.

TEST FACILITY AND INSTRUMENTATION

A test facility, which includes a test sump and cooling system, was constructed to model the two-dimensional solidification process in a V-shaped sump. Figure 1 is a schematic of the V-shaped test sump. The test sump consists of two aluminum side walls, front and back glass windows, and a top cover. The dimensions of the test sump are 28 cm x 3 cm x 29 cm (length x wide x height), respectively. The 8 mm wide x 12 mm deep galleries were machined into the back surfaces of the aluminum sidewalls to serve as a channel for the coolant. Five J-type thermocouples were installed inside each sidewall to measure the wall temperature. Four triangular glass plates were mounted between the two sidewalls to divide the test sump into three chambers. A rectangular glass plate cover was placed at the top of the sump to ensure that these three chambers were air-tight. In order to prevent vapor condensation on the front and rear windows, the front and rear chambers (1.5 cm length on each side) were kept in a vacuum during the test. The middle chamber of the test sump is 25 cm in length, which was filled with the NH_4Cl-H_2O solution, and was also kept in a vacuum during the test to extract the gas from the solution. The test sump was covered by a syphon box to insulate it from the ambient.

Figure 2 shows the cooling system and the instruments used in this investigation. The cooling system includes three refrigerators and the associated control valves and piping. Two 425 watts Model N01268 digital refrigerated circulator baths (Refrigerators I and II) were applied to keep the sidewalls at a desired temperature during a normal test. A 175 watts Model N01267 digital refrigerated circulator bath (Refrigerator III) was used to set the initial temperature.

Seventeen (17) thermocouples were installed to monitor the temperature distribution of the solution. These thermocouples were mounted on a plexiglas frame to ensure the stability of their locations. The thermocouples were arranged in four horizontal lines, with the top line located 1 cm below the solution. The locations of each thermocouple are listed in detail in Table 1, where the origin points (x=0 and y=0) are defined at the bottom corner of the test chamber, as seen in Fig. 2. All thermocouples were calibrated individually after they were installed. The thermocouples were connected to an HP data acquisition system (Model #3852A) and monitored by a personal computer. The uncertainty of the temperature measurement is $\pm$ 0.1°C. The uncertainty of the thermocouple location is less than $\pm$ 1 mm.

Aqueous ammonium chloride (NH_4Cl-H_2O) was chosen as the test solution due to its similar solidification behavior as the liquid metal, and for its semi-transparency. The eutectic temperature and composition of the NH_4Cl-H_2O are T_e=-15.4°C and C_e =19.7%, respectively. The concentration measurement was conducted by extracting the solution through a set of syringes or test probes. An ABBE 2WAJ refractometer was used to measure the refractive index of the extracted solution. The refractive index was then transferred to the concentration through a chart, which was created by measuring a set of known concentrations. Uncertainty in the placement of the probe is about $\pm$ 1 mm. Since only a very small amount of liquid was extracted during the test, the effect of the concentration gradient near the probe tip was minor. The estimated uncertainty of the concentration measurement was about $\pm$0.5%.

The video camera was used to capture the movement of the solid/liquid fronts during the test. The video tapes were then processed by an image processing package (DATA Translation DT 2855) to determine the location of the solid/mushy/liquid fronts and to calculate the solidification rate. Basically, the test chamber is long enough to be considered a two-dimensional chamber. Since the solid/mushy/liquid fronts produce different light reflections, the image captured by the video camera can easily distinguish these three zones. Figure 3 shows the three images at hypoeutectic, eutectic, and hypereutectic conditions. The light areas in the pictures indicate the mushy (dendritic) zones. It is worthwhile to point out that in the eutectic condition (C_e = 19.7%), the bright lines represent the liquid/solid interface.

EXPERIMENTAL PROCEDURE

During the solidification process, the gas originally absorbed in the solution was released. These air bubbles can drive the surrounding liquid to form an upward flow. In order to make the solution free from gas when a new solution was poured into the test chamber, the solution was solidified and melted at least three times. The test chamber was also kept in a vacuum to prevent the solution from reabsorbing the gas.

TABLE 1
Location of the Thermocouples

Number of Thermocouples	x cm	y cm
1	0	1.52
2	-1.02	6.60
3	0	6.60
4	1.52	6.60
5	-1.27	12.7
6	0	12.7
7	1.78	12.7
8	-1.78	17.27
9	-0.76	17.27
10	0	17.27
11	1.27	17.27
12	2.29	17.27
13	-2.54	22.35
14	-1.02	22.35
15	-0.51	22.35
16	2.03	22.35
17	63.81	22.35

The results of four test runs were selected and are presented in this paper. Each test was repeated four to five times. Table 2 provides the information regarding the initial temperature, concentration, and the cooling temperature in each test run. Test Run 1 represents the case of the eutectic solidification process. Test Runs 2 and 3 indicate the case of hypoeutectic solidification, while Test Run 4 is hypereutectic solidification.

The first step of the test was to set up a uniform initial temperature, T_o, for the test solution. Refrigerator III was connected to the cooling line to provide a desired temperature through the two sidewalls. Thermocouples were closely monitored to check the temperature of the solution. The maximum temperature difference inside the solution was less than 0.5°C before starting the experiment. During the time to set up the initial temperature, Refrigerators I and II were disconnected from the cooling line and run to establish the required cooling temperature, T_c. After thermal uniformity was reached in the solution, Refrigerators I and II were connected to the cooling line and Refrigerator III was disconnected, after which the experiment began.

TABLE 2
Summary of the Experimental Conditions

Test Run	C_o (%)	T_o (°C)	T_c(°C)
1	19.7	5	-20
2	5.0	5	-10
3	15.0	5	-15
4	25	15	-20

During the test, the temperature was continuously monitored at every one minute interval for the first hour and at five minute intervals after that. The video camera continuously recorded so that the tapes could be viewed later. The concentration measurements were conducted every half hour. Although the test rack initially included nine test probes (syringes), due to solidification, only two probes could provide the concentration information throughout the test. The test times for each run were significantly different depending on the initial concentration, which varied from two hours to eight hours.

RESULTS AND DISCUSSION

The simplest case of solidification of a binary mixture is the case of eutectic composition. In eutectic composition, the solution exhibits the phase change behavior of a pure substance, and the convective flow is driven solely by the thermal buoyancy force. Figure 4 shows the history of the solid/liquid interfaces in Test Run 1. A half-hour after starting, Fig. 4a shows that the solid interface appeared on the sidewalls. The solid/liquid interfaces appeared very smooth and were well distributed along both surfaces. Since the solution temperature in the center of the test chamber was higher than that near the interface, a thermally driven natural convection was generated. The fluid near the cooling interface flowed down and then moved up in the center region to form two recirculation loops. As time elapsed, however, the solidified region increased, and the liquid region always remained in a V-shape, as seen in Figs. 4b through 4f.

For the solution with hypoeutectic composition, solute will be ejected during the solidification process and the two-phase interface is characterized as the mushy zone. As a result, there exists a high concentration region in and near the interdendritic zone. Since the solute is denser than the solution, a downward flow was generated along the interface by the solute driven natural convection, which was in the same direction as that of the thermal driven convection. Figures 5 and 6 show the variation of the temperature contours during the solidification process in a hypoeutectic

composition solution (Test Run 2). In this test, a 5% NH_4Cl composition solution was used with initial and cooling temperatures of T_o=5°C and T_c=-10°C, respectively. Figure 5 shows the temperature variation of thermocouples, #8, #9, and #10. These three thermocouples are located about 6.3 cm below the solution surface, where thermocouple #8 is 2mm away from the sidewall, and thermocouple #10 is in the center chamber. This figure indicates that the readings of thermocouples #9 and #10 were closer to each other, and that of #8 was always far below that of the other two. It is also interesting to note that instead of continuously reducing the temperature in locations #9 and #10, the reading of #8 displayed a sudden increase in the early stage. In the first 20 minutes, the solution temperature near the sidewalls (#8) steadily dropped to -5.6°C, which is lower than the freezing temperature for this concentration. This overcooling endured a few minutes until the first dendrite appeared. Visual observation indicated that the dendritic region spread very fast to cover the entire sidewall surfaces in less than one minute, while at the same time, the thermocouple reading of #8 jumped to -2.3°C. Figure 6 shows the temperature variation along the centerline of the test chamber. The vertical locations of thermocouples #1, #3, #6, #10, and #15 are 22.5 cm, 17.4 cm, 11.3 cm, 6.3 cm, and 1.7 cm, respectively. This figure indicates that temperatures in all five locations steadily dropped as time elapsed, and the temperature in the upper point was always higher than that in the lower point. Figure 7 shows the movement of the solid-liquid interface fronts. At t=30 min (Fig. 7a), visual observation indicated that the solidified region was composed of mainly long and coarse dendrite interfaces. As time elapsed, the dendrite became shorter and finer, and the solid region appeared (Fig. 7b). Since the solute-rich fluid continuously flowed down along the interface region, the concentration in the bottom region of the test chamber steadily increased, which delayed the solidifying process in this region. Figures 7c and 7d show that the interface fronts moved close to each other, and left a long, narrow gap between them. Figure 8 shows the concentration changed with time in this case. The probes, C and F, are located on the center line, 8.39 cm below the solution surface. The figure indicates that the concentration increased as time elapsed. After 90 minutes, the concentration at point C almost reached 10%.

Figure 9 shows another case of solidification in a hypoeutectic composition of 15% (Test Run 3). The dendrites appeared 15 minutes after the test. Columnar dendrites occurred on the walls of the top half of the chamber. Some of the loose columnar dendrites fell while joined with the equiaxed dendrites to pack at the bottom corner, forming a mushy zone. Figure 9a illustrates the interfaces of the liquid/mushy/solid front at t = 30 min. It can be seen that a very thin solid built up along the wall, with a thick layer of the mushy zone between the solid and the solution. Both the mushy and solid region increased after that, as seen in Fig. 6 (t = 60 min.). After one hour, the interface between the mushy zone and solution changed slowly, unlike the solid region's rapid increase (Figs. 9c and 9d). At t = 3 hours, the mushy zone near the bottom corner became solid and at t=4.5 hours, the mushy zone almost disappeared. Figure 10 indicates that the concentration at points C and F continuously increased until reaching eutectic concentration, around t = 3 hours, then remained constant, which can explain why the mushy zone disappeared later on. Figure 11 shows the temperature history for thermocouples #8, #9, and #10. This figure indicates that the horizontal temperature in this case was much more uniform than in the case of the 5% composition (Fig. 5). Also, no overcooling phenomenon was observed in this case. Figure 12 shows the vertical temperature distributions along the centerline. This figure indicates that the temperature in the upper point was always higher than that in the lower point, which is consistent with the result for the case of the 5% composition.

In contrast to the hypoeutectic composition, the ejection of water-rich interdendritic fluid will induce an upward flow in the hypereutectic composition solution, which is opposite to the thermally driven flow. Therefore, totally different solidification behavior can be expected in these two cases. Figure 13 shows that the interface front moved with time in a hypoeutectic component solution, where the initial component is 25%, T_i=15°C, and T_c=-20°C. Visual observation indicated that a few minutes after starting the test, the equiaxed dendrites appeared at the bottom corner first, and then in the entire domain. Many tiny solid particles grew and coalesced as they descended. After about another five minutes, the dendrites settled down to form a mushy zone at the bottom, as seen in Fig. 13a. The mushy zone increased slowly after that, and the solid zone grew under the mushy zone, as seen in Figs. 13b through 13d. At t = 1 hour, no solid zone could be seen at the top of the sump. The solid zone appeared at the top of the sump at t = 2 hours, and the surface of the solid zone was almost smooth. The solid region continued to grow and the loose mushy zone was reduced. The interface of the solution and the solid at the top of the sump remained smooth. Figure 14 shows that the concentration at points, C and F, reached a eutectic value around two hours and remained that way. The results of the horizontal temperature measurements are presented in Fig. 15. This figure indicates that the temperature near the wall at thermocouple #8 was much lower than the inside solutions (#9 and #10) in the first two hours. However, the temperature difference between thermocouples #9 and #10 was very minor. It is interesting to see the difference between Fig. 15 and Fig. 5, or Fig. 11. Instead of a smooth variation of the temperature, Fig. 15 shows the fluctuation of the temperature with time. This represents the existence of equiaxed solidification. Figure 16 shows the temperature distribution along the vertical direction. Like that in Fig. 15, the temperature fluctuated with time before the solution near this point solidified. It can be seen that the temperature in thermocouple #10 was higher than that in thermocouple #15, between 10 minutes to 120 minutes. That is, the temperature near the top free

surface was lower than that in the liquid center. This temperature distribution reflects the effect of the solute-driven flow. As the water-rich fluid was ejected from the dendritic interface, it flowed upward along the interface and then recirculated through the top free surface region. It is interesting to compare the temperature change behaviors of Figs. 15 and 16 and that of Figs. 5, 6, 11, and 12. In Figs. 15 and 16, the temperatures at all points fell below 5°C in the first few minutes. The equilibrium phase diagram for NH_4Cl-H_2O (Beckermann, 1987) indicates that this temperature was below the phase change temperature in the 25% concentration solution, which is why the equiaxed dendrites appeared in the entire solution. In the 5% and 15% initial concentration solutions, a considerable temperature difference existed, which is why the dendrites and the solidification mainly occurred on the sidewalls.

SUMMARY

An experimental study of the solidification for a binary mixture in a V-shaped test chamber has been conducted. Aqueous ammonium chloride was chosen as the phase change material. The effects of the NH_4Cl concentration on solidification has been examined by changing the initial component of the solution. In the eutectic solution, the solidification characterized as a smooth discrete interface always maintains a V-shaped configuration. In the hypoeutectic solution, the solidification mainly depends on the columnar growth on the dendritic interface. However, depending on the initial concentration, the shape of the final liquid/solid interface may totally differ, which may significantly affect the quality of the final product. In the hypereutectic solution, equiaxed solidification is important. In the beginning, the equiaxed dendrites appear in the entire solution and then grow and coalesce as they descend and form a loose mushy zone. The solid region then grows under the mushy zone.

ACKNOWLEDGMENT

The results presented in this paper were obtained in the course of research sponsored by the National Science Foundation under Grant No. HRD-9250087.

REFERENCES

Asai, S. and Muchi, I., 1978, "Theoretical Analysis and Model Experiments on the Formation Mechanism of Channel-Type Segregation," *Trans. ISIJ*, 18, pp. 90-98.

Beckermann, C., 1987, *Melting and Solidification and Binary Mixtures with Double-Diffusive Convection in the Melt*, Ph.D. Thesis, Purdue University.

Chen, C. F. 1974, "Onset of Cellular Convection in a Salinity Gradient Due to a Lateral Temperature Gradient," *J. Fluid Mech.*, 63, pp. 563-576.

Christenson, M. A. and Incropera, F. P., 1989, "Solidification of an Aqueous Ammonium Chloride Solution in a Rectangular Cavity-I. Experimental Study, *Int. J. Heat Mass Transfer*, 32, pp. 47-68.

Fisher, K. M., 1981, "The Effects of Fluid Flow on the Solidification of Industrial Castings and Ingots," *Physico-Chem. Hydrodyn.*, 2, pp. 311-326.

Incropera, F. P. and Viskanta, R., 1992, "Effect of Convection on the Solidification of Binary Mixtures," in *Heat and Mass Transfer in Materials Process* (ed. by I. Tanasawa and N. Lior), pp. 295-312, Hemisphere Publishing Corp., New York.

Mehrabian, R., Keane, M. A., and Flemings, M. C., 1970, "Experiments on Macrosegregation and Freckle Formation, *Met. Trans.*, 1, pp. 3238-3241.

Stewart, M. J. and Weinberg, F., 1972, "Fluid Flow Through a Solid-Liquid Dendritic Interface," *Met. Trans.* 3, pp. 333-337.

Szekely, J. and Jassal, A. S., 1978, "An Experimental and Analytical Study of the Solidification of a Binary Dendritic System," *Met. Trans. B*, 9B, pp. 389-398, 1978.

Thompson, M. E. and Szekely, J., 1988, Mathematical and Physical Modeling of Double-Diffusive Convection of Aqueous Solutions Crystallizing at a Vertical Wall," *J. Fluid Mech.*, 187, pp. 409-433.

Viskanta, R., 1985, "Natural Convection in Melting and Solidification," in *Natural Convection* (ed. by S. Kakac, W. Aung, and R. Viskanta), pp. 845-877, Hemisphere, New York.

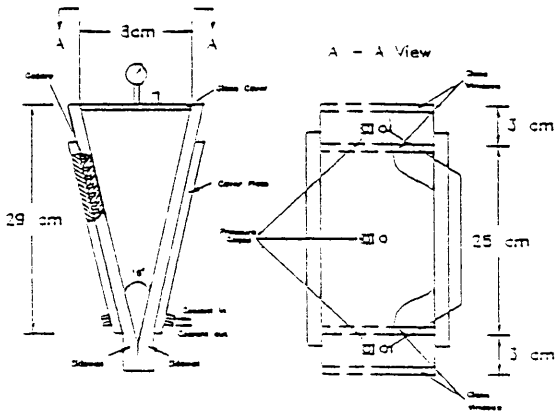

Fig. 1 Schematic representation of the test section.

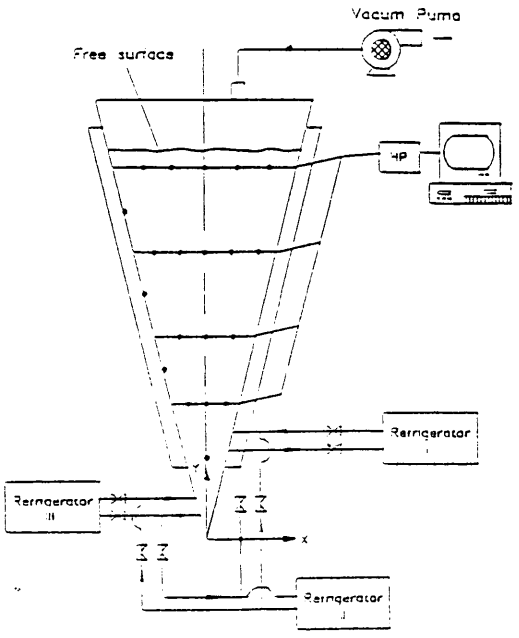

Fig. 2 Schematic representation of the cooling system.

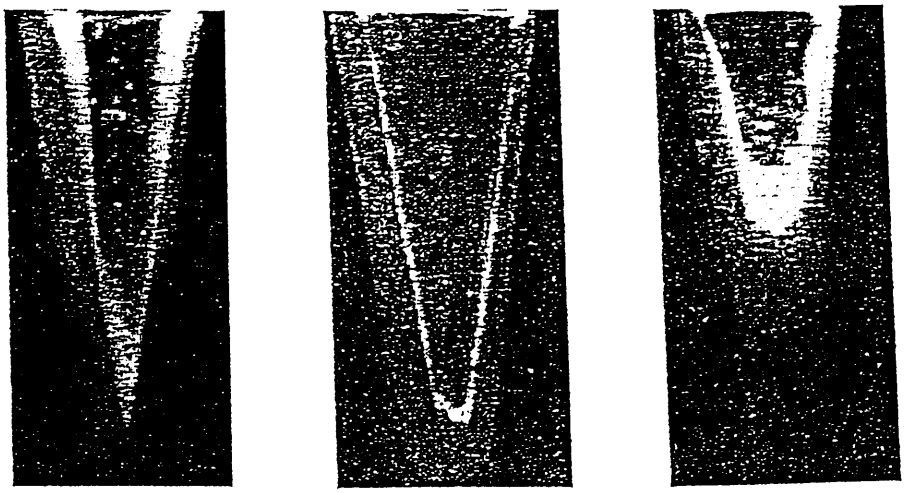

Fig. 3 Video image of the interface front.

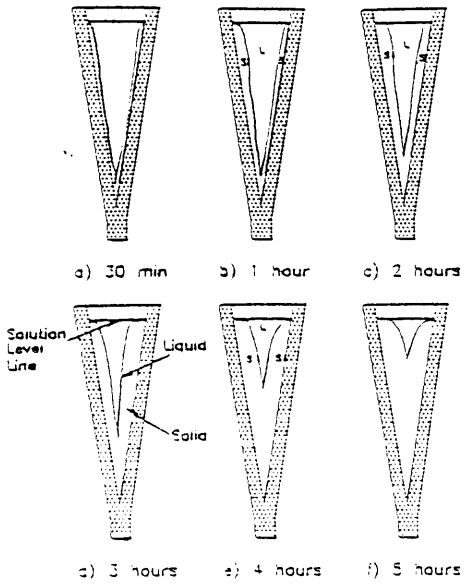

Fig. 4 Interface front in the C_o = 19.7 % solution.

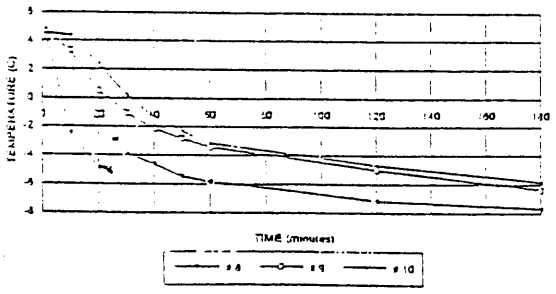

Fig. 5 Temperature history for the horizontal thermocouples (C_o =5%, t_c = -10°C, t_i =5°C).

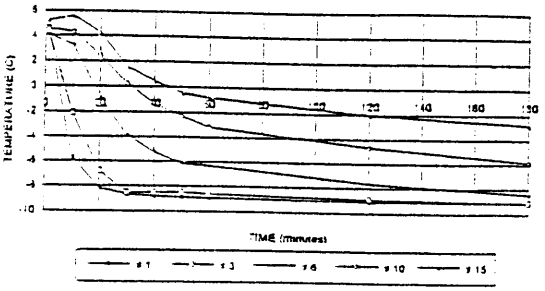

Fig. 6 Temperature history for the vertical thermocouples (C_o =5%, t_c = -10°C, t_i =5°C).

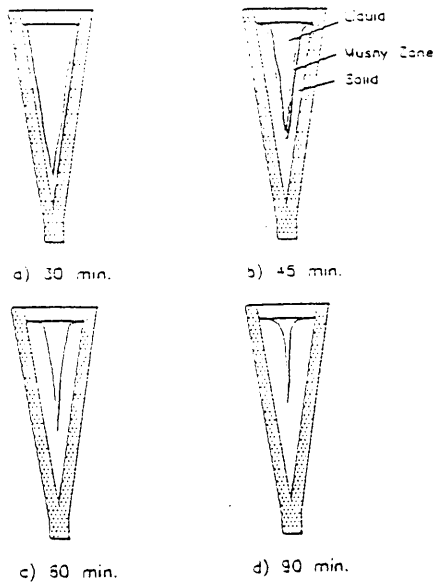

Fig. 7 Interface front in the C_o = 5 % solution.

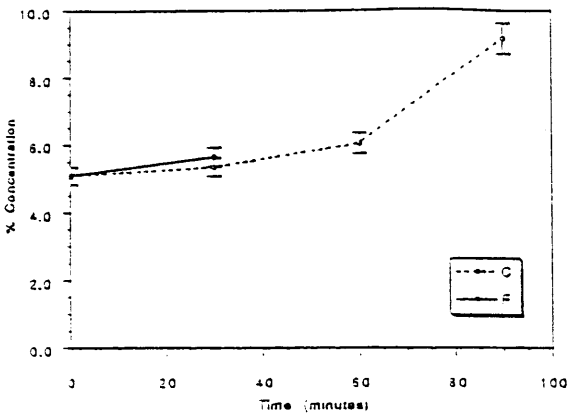

Fig. 8 Concentration variation in the C_o = 5% solution.

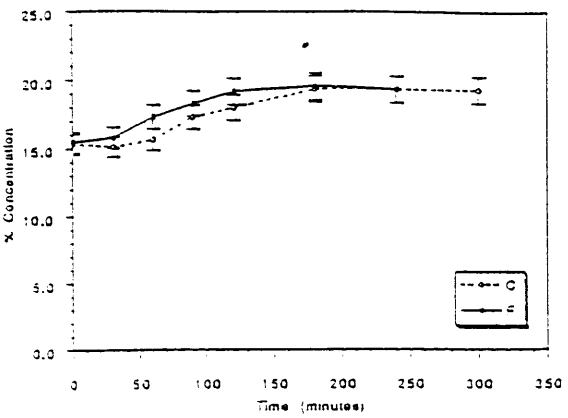

Fig. 10 Concentration variation in the C_o = 15% solution.

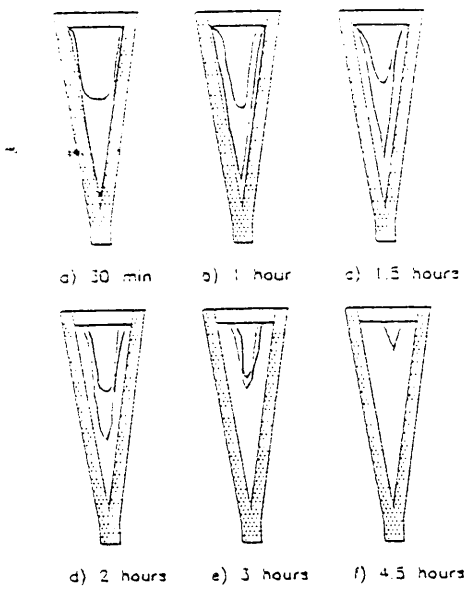

Fig. 9 Interface front in the C_o = 15 % solution.

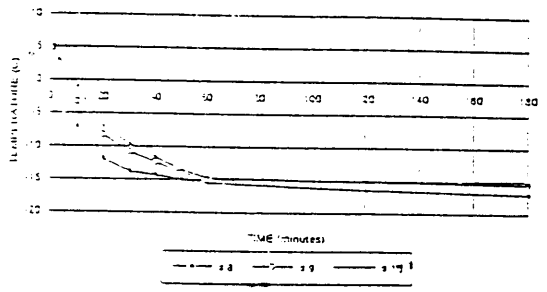

Fig. 11 Temperature history for the horizontal thermocouples (C_o =15%, t_c = -15°C, t_i =0°C).

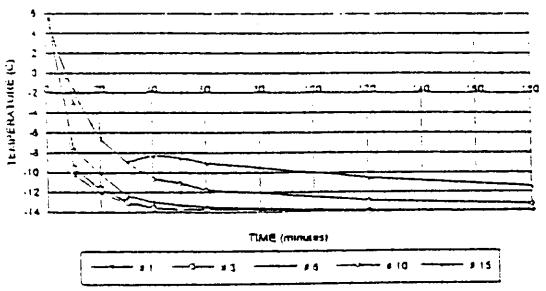

Fig. 12 Temperature history for the vertical thermocouples (C_o =15%, t_c = -15°C, t_i =0°C).

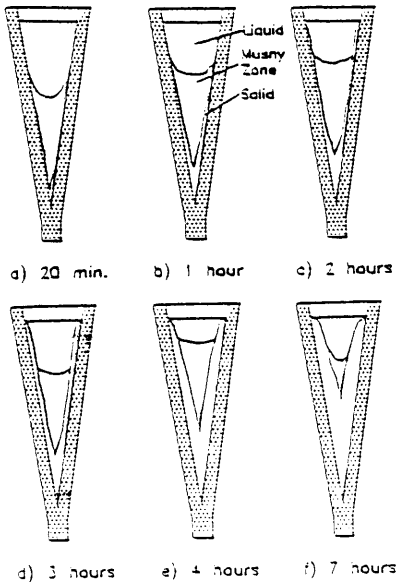

Fig. 13 Interface front in the C_o = 25% solution.

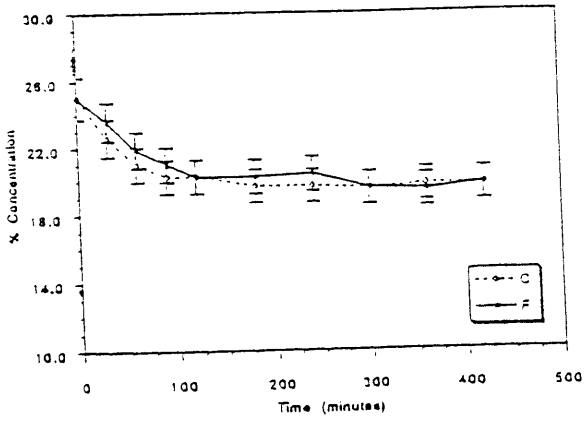

Fig. 14 Concentration variation in the C_o = 25% solution.

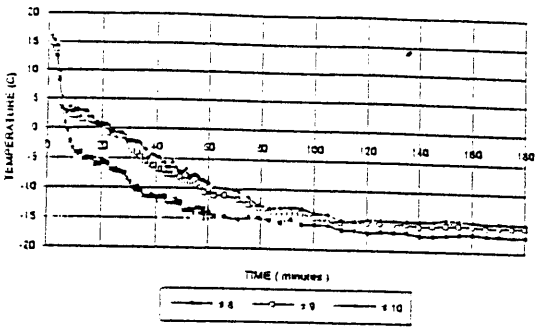

Fig. 15 Temperature history for the horizontal thermocouples (C_o =25%, t_c = -20°C, t_i =15°C).

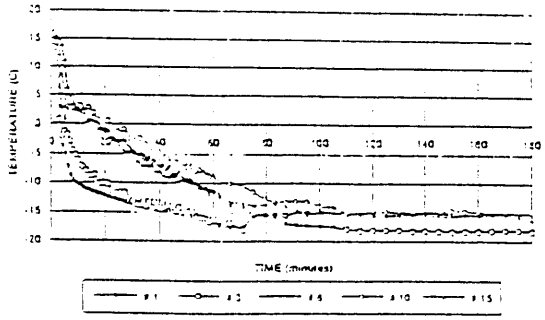

Fig. 16 Temperature history for the vertical thermocouples (C_o =25%, t_c = -20°C, t_i =15°C).

HTD-Vol. 280, Transport Phenomena
in Materials Processing and Manufacturing
ASME 1994

ON THE SOLIDIFICATION PROCESS IN A RECTANGULAR ENCLOSURE WITH SYMMETRIC COOLING WALLS

R. Burton, F. Desir, G. Hoo, G. Martin
G. Yang, Z. F. Dong, and M. A. Ebadian*
Department of Mechanical Engineering
Florida International University
Miami, Florida

ABSTRACT

An experimental study of the solidification process in a rectangular enclosure with symmetric cooling walls has been conducted. NH_4Cl-H_2O was used as a binary mixture solution, which was solidified at eutectic, hypoeutectic, and hypereutectic initial concentrations. The temperature and concentration, as well as the location of the interface front, were continuously measured and recorded during the experimentation. In the hypoeutectic solution, solidification was mainly dependent on the columnar growth of the dendritic interface. In the hypereutectic solution, equiaxed solidification was important at the beginning of the solidification process, after which solidification occurred mainly along the mushy interface. The results indicate that the evolution of the mushy zone and the temperature distribution of the symmetric line inside the liquid pool using a symmetric cooling wall is significantly different from that of the previous study using one cold wall and one insulated wall.

NOMENCLATURE

C	concentration
T	temperature
t	time
y	horizontal location

Subscripts

c	cooling
e	eutectic
o	initial

INTRODUCTION

Solidification of non-eutectic binary mixtures is widely encountered in many engineering applications, such as the growth of single crystals for the microelectronics industry, thermal energy storage devices, and the casting of alloys. Unlike that of the solidification process of a pure substance, phase change can occur in an extended temperature range, and the solid and liquid phases may have a considerable concentration difference. There is a two-phase region, or mushy zone, between the fully solid and liquid regions during the solidification of a non-eutectic binary solution. This unbalanced temperature and species concentration between the mushy zone and the liquid pool will create a natural convective flow in these two regions, which may further significantly affect the homogeneity of the crystal structure of the final product. Previous researchers have indicated that the major cause of structural defects and inhomogeneity (macrosegregation and microsegregation) during solidification is attributed to an improper convection flow pattern in the melt pool and the mushy zone (Fisher, 1981). Therefore, knowledge of the transport phenomena of thermally and solutally driven convection in a cavity is essential for maintaining satisfactory control over the solidification process.

Due to the complexity of double-diffusive convection during the solidification process, theoretical study on this topic is still in the developing stage (Incropera and Viskanta, 1992). Therefore, experimental study is still the most powerful means to understand this basic phenomena. Most of the initial studies on double-diffusive convection were performed by oceanographers, where the temperature and concentration gradients exist in a vertical direction (Turner, 1979, Ostrach, 1983). Recently, many studies have been conducted on solidification where a horizontal temperature

*Author to whom all correspondence should be addressed.

gradient is present to simulate the casting process (Hu and El-Wakil, 1974, Benard et al., 1989, Kamotani et al., 1985, Lee et al., 1988, Beckermann, 1987, Christenson and Incropera, 1989). Various kinds of binary solutions were used in these studies. Liquid metals have been applied to study the solidification process by some researchers (Mehrabian et al., 1970 and Stewart and Weinberg, 1972). Since liquid metals are opaque, it is very difficult to determine flow patterns and the movement at the solid interface during an experiment. Therefore, transparent solutions are usually applied to analogue alloy solidification. Asai and Muchi (1978) and Szekely and Jassal (1978) used an NH_4Cl-H_2O solution to measure both velocity and temperature distributions in the solution. Thompson and Szekely (1988) and Chen (1974) conducted the solidification tests by using an Na_2CO_3-H_2O solution. Recently, Beckermann (1987) and Christenson and Incropera (1989) also studied the solidification process in a rectangular cavity using the NH_4Cl-H_2O system.

The above mentioned survey of literature indicates that the majority of existing experimental results was obtained from a rectangular cavity with different wall temperature conditions. A large temperature gradient along the horizontal direction can be easily achieved in these tests, which can shorten the test process. However, in the majority of industrial applications, cooling will be applied to all vertical walls (symmetric cooling). Different cooling boundary conditions may have a profound effect on the solidification process. Some previous tests were conducted applying one cooled wall and one insulated wall to simulate symmetric cooling in a cavity. Ideally, the test chamber with one insulated wall and one cold wall is equivalent to the half-domain of a test chamber with cooling on both walls. However, the solidification is a transient process. Artificially imposing a line of symmetry to the center of the test chamber may significantly change the convective flow pattern. Therefore, the data from a test chamber with one cooling and one insulated wall may not be used to predict the behavior in the second case. The main purpose of this study is to experimentally simulate the solidification process of a binary solution with symmetric cooling walls.

TEST FACILITY AND INSTRUMENTATION

Figure 1 is a schematic of the test facilities used in this investigation. They consist of: a rectangular cavity (the test section), the cooling system, and the associated instrumentation. The cooling system includes three refrigerators and the control valves and piping. Two 425-watt digital refrigerated circulator baths (Refrigerators I and II) were applied to keep the sidewalls at a desired temperature during the test. A 175-watt digital refrigerated circulator bath (Refrigerator III) was used to set the initial temperature. The first step of the test was to set up a uniform initial temperature, T_o, in the liquid pool. Refrigerator III was connected to the cooling line to provide a desired temperature through the two sidewalls. Thermocouples were closely monitored to check the temperature of the solution. Before starting the experiment, the maximum temperature difference of the solution in the liquid pool was less than 0.5°C. Since it takes time to set up the initial temperature, Refrigerators I and II were disconnected from the cooling line and were run to establish the required cooling temperature, T_c. After thermal uniformity was reached in the liquid pool, Refrigerators I and II were connected to the cooling line and Refrigerator III was disconnected, and the experiment began.

Figure 2a shows the design of the test section. The test section consisted of two copper sidewalls, front and back plexiglass windows, and a plexiglass top cover and a plexiglass bottom wall. The dimensions of the test section were 16 cm x 6 cm x 19 cm (length x wide x height). Channels 12 mm wide x 12 mm deep were machined into the back surfaces of the copper sidewalls to serve as gutters for the coolant. Five J-type thermocouples were installed inside each sidewall to measure the wall temperature. Four rectangular plexiglass plates were mounted between the two sidewalls to divide the test section into three chambers. In order to prevent vapor condensation on the front and rear windows and prevent heat exchange through them, the front and rear chambers (1 cm in length on each side) were kept in a vacuum during the test. A layer of silica gel was also placed on the bottom of these two chambers to absorb the moisture. A plexiglass cover was placed at the top of the chambers to ensure that these three chambers remained air-tight. The middle chamber (the test chamber), 14 cm in length, was filled with the NH_4Cl-H_2O and was also kept in a vacuum during the test to extract the gas from the solution. The solution free surface was approximately 0.65 cm above the top level of the thermocouples. The test section was covered with a syphon box to insulate it from the ambient. The top front and rear parts of the syphon box could be removed. During the measurement, the front of the insulation box was usually kept open to allow the video camera to record the solidification process. The top of the syphon box was opened only when the concentration measurement was conducted. Aqueous ammonium chloride (NH_4Cl-H_2O) was chosen as the test solution due to its semi-transparency. The eutectic temperature and the composition of the NH_4Cl-H_2O solution were T_e = -15.4°C and C_e = 19.7%, respectively.

Forty thermocouples were installed inside the test section to monitor the temperature distribution during the experiment. These thermocouples were mounted on a plexiglass frame. The bead of the thermocouple was around 0.8 mm. The frame was fixed in the middle of the test chamber. The thermocouples were equally distributed in eight horizontal lines. Details of the locations for each thermocouple are given in Fig. 2b. After all thermocouples were mounted on the frame, the frame was put into a bath (chiller) to individually calibrate the thermocouples. The thermocouples were connected to an HP data acquisition system (Model #3852A) and were monitored by a personal computer. The uncertainty of the temperature measurement was ± 0.25°C. The uncertainty of the thermocouple location was less than ± 1 mm.

The concentration measurement was conducted by extracting the solution through a syringe. The test rake included five syringes, side by side, each separated by 1 cm. During

the measurement, five probes (needles) were inserted into the test chamber simultaneously through the five holes on the top cover, as indicated in Fig. 2a. The tips of the five probes were located 2cm, 6cm, 9cm, 11cm and 13cm above the bottom plate. An ABBE 2WAJ refractometer was used to measure the refractive index of the extracted solution. The refractive index was then transferred to the concentration through a chart, which was created by measuring a set of known concentrations. Uncertainty in the location of the probe tip was about ± 1 mm. Since only a very small amount of liquid was extracted during the test, the effect of the concentration gradient near the probe tip was minor. The estimated uncertainty of the concentration measurement was about ± 2.5% of the solution concentration. A video camera was used to capture the movement of the solid/liquid fronts during the test. The video tapes were then processed by an image processing package (DATA Translation DT 2855) to determine the location of the solid/mushy/liquid fronts and to calculate the solidification rate. Observation indicated that the test chamber was long enough to be considered as a two-dimensional chamber. Since the solid/mushy/liquid fronts produced different light reflections, the image captured by the video camera could easily distinguish these three regions.

During the solidification process, the gas originally absorbed in the solution was released. These air bubbles drove the surrounding liquid to form an upward flow observed in our earlier test, which can significantly affected the flow pattern in the liquid pool. In order to make the solution free from gas, the new solution was boiled in a beaker before being put into the test chamber. The test chamber was then kept in a vacuum to prevent the solution from reabsorbing the air. During the test, the temperature was continuously monitored at every one minute interval for the first hour and at five minute intervals after that. The concentration measurements were conducted every 10 minutes. The video camera recorded continuously so that the tapes could be viewed later.

EXPERIMENTAL RESULTS

The results of three test runs were selected to be presented in this paper. Each test was repeated three times. Table 1 provides the information regarding the initial solution temperature, T_o, the initial concentration, C_o, and the cooling temperature (wall temperature) in each test run. Test Run I represents the case of the eutectic solidification process. Test Run II indicates the case of hypoeutectic solidification, while Test Run III is hypereutectic solidification.

Christenson and Incropera (1989) reported their test data on solidification in a rectangular cavity with one cold and insulated wall. The geometry of their test chamber was 144 mm height, 36 mm wide, and 200 mm deep, which is more similar to the half-domain of our test chamber (our test chamber is 190 mm x 60 mm x 160 mm). Therefore, their results will be a good comparison in this study.

TABLE 1

Summary of the Experimental Conditions

Test Run	C_o (%)	T_o (°C)	T_c (°C)
I	19.7	5	-20
II	5.0	5	-10
III	25%	15	-20

Eutectic Solidification (Test Run I)

The simplest case of the solidification of a binary mixture is the case of the eutectic composition. In a eutectic composition, the solution exhibits the phase change behavior of a pure substance, and the convective flow is driven solely by the thermal buoyancy force. Figure 3 indicates the test data for the temperature distributions inside the test chamber during eutectic solidification. The locations of each thermocouple can be seen in Fig. 2. Figure 3a shows the temperature changes with time at y = 13.25 cm. Three thermocouples were located about 13.25 cm above the bottom of the test chamber. Thermocouple #31 was 0.6 cm away from the sidewall, and thermocouple #33 was in the center of chamber. It can be seen that during the first 30 minutes, these three thermocouples had almost identical readings until they reached the eutectic phase change temperature, -15.4°C. The temperature of thermocouple #31 began to drop gradually because it had been surrounded by the solidified region. The further temperature decrease of thermocouple #31 was governed by thermal conduction inside the solid. In the liquid pool, thermocouples #32 and #33, show a very uniform temperature horizontally. Figure 3b shows the horizontal temperature history at the y = 4.85 cm level. Very similar to that in Fig. 3a, the temperature was very uniform horizontally in the liquid pool. Figure 3c shows the temperature history in the vertical centerline of the test chamber. During the first 30 minutes, a considerable temperature difference existed along the vertical direction. However, since the temperature was higher at the top and lower in the bottom, the liquid was thermally stable. After thirty minutes, all readings reached the same value; that is, the temperature in the entire domain of the liquid pool was equal to the eutectic temperature.

Figure 4 shows the history of the solid/liquid interface associated with Test Run I. A half-hour after starting the test, the solid/liquid interface appeared on the sidewalls, Fig. 4a. The solid/liquid interface looked very smooth and had the same thickness along both surfaces. Due to the uniform temperature in the liquid pool, convective heat transfer vanished, which caused the solid/liquid interface to grow

parallel along the horizontal direction, Figs. 4b through 4d. A clearer view of the evolution of the solid front is presented in Fig. 4e.

Hypoeutectic Solidification (Test Run II)

For the solution with a hypoeutectic composition, the solute will be ejected during the solidification process and the two-phase interface is characterized as a mushy zone. As a result, there exists a high concentration region in and near the interdendritic zone. Since the solute is denser than the solution, a downward flow may be generated along the interface by the solute-driven natural convection. Figure 5 shows the temperature distribution in a 5% NH_4Cl-H_2O composition solution. Figure 5a indicates the measured results at the y = 13.25 cm level. This figure reveals that during the first 10 minutes, all three thermocouples had the same readings. Then the readings on thermocouples #32 and #33 got closer to each other, while that of #31 always remained far below that of the other two thermocouples, which indicated the downward solute-rich flow in this region. Figures 5b and 5c show the horizontal temperature distributions in another two levels, y = 9.05 cm and y = 4.85 cm. Unlike that in Fig. 5a, these two figures indicate that even at the beginning of the test, a temperature difference existed between the thermocouples near the cooling walls and the thermocouples in the center region. As time elapsed, the temperatures in all thermocouples in these three cross sections continued to decrease. It is interesting to note that instead of continuously reducing the temperature in thermocouple locations #12 and #13 in Fig. 5c, the reading of thermocouple #11 displayed a sudden increase in the early stage. After five minutes, the solution temperature near the sidewalls (thermocouple #11) steadily dropped to around -3°C, which is lower than the phase change temperature for this concentration. However, no dendrites formed at this stage. This overcooling endured for a few minutes until the first dendrite appeared. Visual observation indicated that the dendritic region spread very fast to cover the entire sidewall surfaces in less than one minute. At the same time, the thermocouple reading of #11 jumped to about 2°C, which corresponds to the phase change temperature at this concentration. Figure 5d illustrates the temperature history along the vertical centerline of the test chamber. The temperatures at all seven levels dropped very rapidly in the first 10 minutes; then the rate of temperature reduction slowed down, but the vertical temperature gradient increased. Overall, the temperature was lower at the bottom and was higher at the top, which is unfavorable to natural thermal convection along the centerline.

Figure 6 shows the solute concentration history along the vertical center line. The locations of the four probe tips were 2 cm, 6 cm, 9 cm, and 11 cm above the bottom of the test chamber. Initially, the concentrations in all four locations were equal to 5%. The concentrations continuously increased with time due to ejection of the solute during the solidification process, since the concentration was higher at the bottom and lower near the top, which is also unfavorable for solute driven natural convection.

Figure 7 illustrates the evolution of the mushy zone and the solid region in the 5% initial concentration solution. At t = 15 min (Fig. 7a), observation indicated that the solidified region was composed of mainly long and coarse dendrites. As time elapsed, the dendrites became shorter and finer, and the solid region appeared (Figs. 7b and 7c) beneath the dendritic region. Since the solute-rich fluid continuously flowed down along the interface region, the solidification in the region near the bottom retarded. Figure 7d shows that the interface fronts moved closer to each other near the top and left a large gap at the bottom. Figure 7e shows the evolution of the solid region during the test process. This figure shows a different solidification behavior with the test conducted by Christenson and Incropera (1989) for the rectangular cavity with one cold wall and one insulated wall (C_o = 10%), Fig. 7f.

Hypereutectic Solidification (Test Run III)

In contrast to the hypoeutectic composition, the ejection of water-rich interdendritic fluid will induce an upward flow in the hypereutectic composition solution. Figure 8 illustrates the concentration change with time in the five probes located at 2 cm, 6 cm, 9 cm, 11 cm, and 13 cm above the bottom. Concentrations in these five positions continuously diminished. The concentration near the top of the chamber diminished much faster than at the locations near the bottom, and the concentration gradient along the centerline continuously increased. In 30 minutes, the concentration difference between the top and the bottom reached 3%. After that, the concentration gradient along the center decreased, and eventually the concentrations in all positions reached a eutectic value.

Figure 9 illustrates the evolution of the mushy zone and the solid front with a 25% initial concentration solution. Observation indicated that a few minutes after starting the test, dendrites appeared on the cooling walls. At the same time, many equiaxed dendrites appeared in the liquid pool. These tiny solid particles grew and coalesced as they descended. After about 10 minutes, the dendrites covered all the cooling walls and the bottom plate, as seen in Fig. 9a. The mushy zone increased slowly after that, and the solid zone grew under the mushy zone, as seen in Fig. 9b, t=30 minutes. In this figure, the bright region indicates the mushy zone, where the dark region under the mushy zone indicates the solid ice. At t=120 minutes, the solid and the mushy zone grew mainly near the bottom, Fig. 9c. The mushy and solid zones grew continuously, but their growth was at a much slower pace compared to the beginning of the test. Figure 9d shows the mushy/solid fronts after three hours. As the solidification process continued, the solid region grew farther from the cooling wall. The thickness of the loose mushy zone was further reduced as the solidification continued, as seen in Fig. 9e. Figure 9f illustrates the solidification process in detail. For the hypereutectic concentration solution (30% initial solute concentration), Christenson and Incropera (1988) found that a set of double-diffusive interfaces (two to four, depending on the initial concentration and cooling temperature) formed just

a few minutes after the start of the solidification process. In their study, the double-diffusive recirculation region was mainly near the top of the solution surface, and a double-diffusive interface grew in the downward direction. As a result, the solidification near the top was significantly retarded, Fig. 9g. However, in our experimental test, the double-diffusive interface did not form. As seen in Fig. 9f, the solidified region along the side cooling walls grew equally in the horizontal direction in our test.

Figure 10 shows the temperature history in Test Run III. Figure 10a illustrates the temperature distribution along the vertical centerline. It is interesting to see that the temperature had a higher value near the top and a lower value near the bottom of the test chamber at the beginning of the test. As time elapsed, the temperature near the top decreased much faster than that near the bottom, and eventually the temperature distribution inversed after 6 minutes; that is, the temperature was higher at the bottom and gradually decreased as the amplitude increased. This phenomenon indicates that the temperature distributions before and after 6 minutes were controlled by different mechanisms. Before the dendrites appeared, the flow in the liquid pool was controlled by thermally driven natural convection, in which the liquid rose along the centerline and flowed downward near the solid cooling walls. After dendrites appeared, the cold water-rich liquid was ejected from the dendritic region. Since this cold liquid was lighter than the solution in the liquid pool, it flowed upward near the wall region. When the solute driven force surpassed the thermal driven force, the flow direction was inversed, which resulted in the temperature distribution inverse in Fig. 10a. The temperature gradient reached its highest value at around $t = 20$ minutes, and then slightly decreased. After $t = 90$ minutes, all temperatures in the vertical centerline achieved eutectic temperature. Figures 10b through 10d show the temperature variations in the three horizontal locations. Unlike the cases of the eutectic and hypoeutectic solutions, a temperature difference existed along the horizontal direction. From the very beginning, the temperatures of the thermocouples near the cooling wall were far below the temperatures in the center region. This can easily be explained since thick dendrites covered these thermocouple locations during the earlier time of the solidification process. It is interesting to compare the temperature along the symmetric centerline in our test and the temperature along the insulated wall in the case of Christenson and Incropera (1989). Christenson and Incropera (1989) showed that the wall temperatures at three different levels (45 mm, 65 mm, and 90 mm above the bottom) were almost the same at the same instant. Figure 10a indicates the temperature was significantly varied along the vertical centerline, and the temperature gradient even changed direction during the solidification process. The difference in the temperature distribution will significantly change the flow pattern as well as the solidification behavior. Therefore, the test results from a test with one cold wall and one insulated wall cannot simulate the situation of solidification with a symmetric cooling wall.

SUMMARY

An experimental study of the solidification for a binary mixture in a rectangular cavity with symmetric cooling walls has been conducted. Aqueous ammonium chloride was chosen as the phase change material. By changing the initial component of the solution, the results indicate that the solidification behavior of the binary solution was entirely different. In the eutectic solution, solidification was characterized as smooth discrete interfaces, which were almost parallel to the cooling surfaces and uniformly grew horizontally. In the hypoeutectic solution (5% initial concentration), solidification mainly depends on the columnar growth of the dendritic interface. In the hypereutectic solution, equiaxed solidification was important at the beginning of the solidification process. In the first five minutes of the solidification process, equiaxed dendrites appeared in the entire solution and then grew and coalesced as they descended and formed a loose mushy zone. After that, solidification progress mainly along the mushy interface, and the solid region then grew under the mushy zone. The results of this study also indicate that the evolution of the mushy zone front and the temperature distribution along the symmetric centerline of the liquid pool is significantly different from the previous study. This can be attributed to the difference in the cooling boundary condition. That is, the test chamber using one cold and one insulated wall cannot simulate the solidification process with symmetric wall cooling.

ACKNOWLEDGMENT

The results presented in this paper were obtained in the course of research sponsored by the National Science Foundation (NSF).

REFERENCES

Asai, S. and Muchi, I., 1978, "Theoretical Analysis and Model Experiments on the Formation Mechanism of Channel-Type Segregation," Trans. *ISIJ*, 18, pp. 90-98.

Beckermann, C., 1987, *Melting and Solidification and Binary Mixtures with Double-Diffusive Convection in the Melt*, Ph.D. Thesis, Purdue University.

Benard, C., Gobin, D., and Thevenin, J., 1989, "Thermosolutal Natural Convection in a Rectangular Enclosure—Numerical Results," in *Heat Transfer in Convective Flows*, edited by R. K. Shah, ASME HTD-107, pp. 249-254.

Chen, C. F. 1974, "Onset of Cellular Convection in a Salinity Gradient Due to a Lateral Temperature Gradient," *J. Fluid Mech.*, 63, pp. 563-576.

Christenson, M. A. and Incropera, F. P., 1989, "Solidification of an Aqueous Ammonium Chloride Solution in a Rectangular Cavity-I. Experimental Study, *Int. J. Heat Mass Transfer*, 32, pp. 47-68.

Fisher, K. M., 1981, "The Effects of Fluid Flow on the Solidification of Industrial Castings and Ingots," *Physico-Chem. Hydrodyn.*, 2, pp. 311-326.

HTD-Vol. 289, Thermal Processing of Materials:
Thermo-Mechanics, Controls and Composites
ASME 1994

EFFECTS OF BOUNDARY CONDITIONS ON DOUBLE-DIFFUSIVE FLOW DURING THE SOLIDIFICATION PROCESS IN A BINARY SOLUTION

R. Burton, F. Desir, G. Hoo, G. Martin, G. Yang,
Z. F. Dong, and M. A. Ebadian
Department of Mechanical Engineering
Florida International University
Miami, Florida

ABSTRACT

The effects of boundary conditions on the double-diffusive flow inside a liquid pool during the solidification process of a binary solution are experimentally studied. Four test sumps are built in this study. Two rectangular sumps are built to investigate the effects of bottom cooling in addition to sidewall cooling on the flow inside a rectangular cavity, which is used to simulate the solidification process during a ingot static casting. The other two V-shaped sumps are designed and built to simulate the effects of bottom angles on convective flow during continuous casting. The temperature distribution in the liquid pool is used to analyze the flow patterns driven by both thermal and concentration buoyancy forces. The results indicate that in a rectangular cavity, adding bottom cooling will reduce the thermally driven convective flow before the solidification starts. After dendrites appear, the cavity with the bottom cooling will approach a uniform temperature inside the liquid pool much faster than that in a cavity without bottom cooling. The results also indicate that the bottom angle of a V-shaped sump can significantly change the heat transfer mechanism and flow conditions inside the liquid pool. At an angle of 16 degrees, the thermally driven convective heat transfer controls the fluid flow and heat transfer before solidification starts. After the dendrites appear, a major portion of the domain is controlled by conduction heat transfer. At a small angle, 4 degrees, conduction is the dominant heat transfer mechanism before and after dendrites appear.

NOMENCLATURE

C	concentration
T	temperature
t	time
y	vertical location

Greek Symbols

α	angle

Subscripts

c	cooling
e	eutectic
0	initial

INTRODUCTION

Solidification of non-eutectic binary mixtures is widely encountered in many engineering applications, such as the growth of single crystals for the microelectronics industry, thermal energy storage devices, and the casting of alloys. Unlike that of the solidification process of a pure substance, the solidification of a binary solution can generate both the temperature and concentration gradients in a liquid pool. These two buoyancy forces can either enhance or suppress the fluid flow and heat transfer patterns in the liquid pool, and further affect the growth of dendrites in the two-phase region, or mushy zone. Previous researchers have indicated that the major cause of structural defects and inhomogeneity (macrosegregation and microsegregation) during solidification is attributed to an improper convection flow pattern in the

*Corresponding author.

major cause of structural defects and inhomogeneity (macrosegregation and microsegregation) during solidification is attributed to an improper convection flow pattern in the liquid pool and the mushy zone (Flemings, 1974, and Fisher, 1981). Therefore, knowledge of the transport phenomena of thermally and solutally driven convection in a cavity is essential for maintaining satisfactory control over the solidification process.

Due to the complexity of double-diffusive convection during the solidification process, theoretical study on this topic is still in the developing stage (Incropera and Viskanta, 1992). Therefore, experimental study is still the most powerful means to understand this basic phenomena. Most of the initial studies on double-diffusive convection were performed by oceanographers, where the temperature and concentration gradients exist in a vertical direction (Turner, 1979, Ostrach, 1983). Recently, many studies have been conducted on solidification where a horizontal temperature gradient is present to simulate the casting process (Hu and El-Wakil, 1974, Benard et al., 1989, Kamotani et al., 1985, Lee et al., 1988, Beckermann, 1987, Christenson and Incropera, 1989). An extensive survey indicates that the double-diffusive flow and heat transfer in a cavity is very sensitive to changes in the boundary conditions—that is, the condition of the boundary geometry and cooling conditions. The main purpose of this study is to experimentally study the effect of boundary conditions on the double-diffusive flow inside the liquid pool. Two cases will be studied: 1) the effects of additional bottom cooling in a rectangular cavity, which is used to simulate the solidification process in static ingot casting; and 2) the effect of the bottom angle of a V-shaped sump, which is used to simulate the solidification process during continuous casting.

The double-diffusive flow in a cavity during solidification of a binary solution is very weak, the velocity of which is on the order of less than 1 mm/sec. The technique for accurately measuring this low velocity is still not available for engineering applications. On the other hand, flow visualization requires an injection of dye or luminous material with close density into the tested solution. However, during the solidification process, the solution concentration, as well as the density, continuously change, while the dye particles may still maintain their initial density. Following the loci of the dye particles may present an erroneous flow pattern due to the fact that the fluid flow is too slow. Furthermore, dye injection may significantly change the flow pattern in the liquid pool since the velocity of the dye injection is much greater than that of the convective velocity. In this study, many thermocouples were installed in the test cavity and the temperature changes inside the test sump were continuously monitored. Due to the low operation temperature, $T_{solution} <$ 300K, the radiative heat transfer can be neglected. The temperature distribution in the test sump is controlled by both thermal conduction and thermal/solutal convection. Since the sump is cooled through sidewalls, pure conductive heat transfer will generate a smooth change temperature field, with a positive temperature gradient from the wall to the center region. Any sudden discontinuity of temperature or temperature gradients in the liquid pool can be attributed to the convective flow. In this study, the changes in the temperature distribution will be used to qualitatively analyze the convective flow patterns inside the sump.

TEST FACILITY AND INSTRUMENTATION

Figure 1 is a schematic view of the test facilities used in this investigation. They consist of the test sump, the cooling system, and the associated instrumentation. Four test sumps were built for this study, and share the same cooling system. The cooling system includes three refrigerators, control valves, and piping. Two 425-watt digital refrigerated circulator baths (Refrigerators I and II) were applied to maintain the cooling walls at a desired temperature during the test. A 175-watt digital refrigerated circulator bath (Refrigerator III) was used to set the initial temperature of the test solution in the sump. The first step of the test was to set up a uniform initial temperature, T_0, in the liquid pool. Refrigerator III was connected to the cooling line to provide a desired temperature through the two sidewalls. Thermocouples were closely monitored to check the temperature of the solution. Before starting the experiment, the maximum temperature difference of the solution in the liquid pool was less than 0.5°C. Since it takes time to set up the initial temperature, Refrigerators I and II were disconnected from the cooling line and were run to establish the required cooling temperature, T_c. After thermal uniformity was reached in the liquid pool, Refrigerators I and II were connected to the cooling line and Refrigerator III was disconnected, after which the experiment began.

Aqueous sodium carbonate, Na_2CO_3, was chosen as the test solution in this study due to its semi-transparency. As seen in Fig. 2, the eutectic temperature and the concentration of the Na_2CO_3 solution are T_e = -2.1°C and C_e =5.9%, respectively. To simulate the metal casting process, a hypereutectic concentration of 10% is chosen as the initial concentration. The initial solution temperature, T_0, and the cooling wall temperature, T_c, are chosen as 15°C and -15°C, respectively. During the solidification process, the gas originally absorbed in the solution was released. These air bubbles drove the surrounding liquid to form an upward flow observed in our earlier test, which can significantly affect the flow pattern in the liquid pool. In order to ensure that the solution was free from gas, the new solution was boiled in a beaker before being placed into the test chamber. The test chamber was then kept in a vacuum to prevent the solution from reabsorbing the air.

Thermocouples were installed inside the test sumps to monitor the temperature distribution during the experiment. The bead of the thermocouple is around 0.8 mm. These thermocouples are mounted on a plexiglas frame. Three of which were made to fit the geometry of each test sump. The frame was then attached to the middle of the test sump. Details of the locations of the thermocouples for each test sump are given in the Results and Discussion section. After all the thermocouples were mounted on the frame, the frame was then placed into a bath (chiller) to individually calibrate the thermocouples. The thermocouples are connected to an HP data acquisition system (Model #3852A) and are monitored by a personal computer. During the test, the temperature was continuously recorded at every one minute interval for the first hour and at five minute intervals after that. The uncertainty of the temperature measurement is ± 0.25°C, and the uncertainty of the thermocouple location is less than ± 1 mm.

RESULTS AND DISCUSSION

Effect of Bottom Cooling

Experimental tests were conducted on two rectangular test sumps, both having the same geometry and dimensions (Fig. 3), 19cm X 6cm X 16cm (height X width X depth). Both sumps have two copper sidewalls, front and back plexiglas windows, and a plexiglas top cover. The bottom wall of sump A (Fig. 3a) is constructed of a plexiglas plate to simulate an adiabatic boundary condition. The bottom wall of sump B (Fig. 3b), is made of a copper plate. Channels 12mm wide by 12mm deep were machined into the back surfaces of the copper sidewalls and bottom wall to serve as gutters for the coolant. Five thermocouples were installed inside each cooling wall to measure the wall temperature. The cooling wall was assumed to have a uniform temperature since the temperature difference between these thermocouples is less than 1°C for the cooling walls. The test sump was then covered with a syphon box to insulate it from the ambient. The front and rear chambers were kept in a vacuum during the test, and the front of the syphon box was kept open for recording by the video camera. Due to its length, the test section was assumed to be a two-dimensional chamber. Figure 4 shows that forty thermocouples were equally distributed in eight horizontal lines, where y indicates the vertical location in relation to the bottom surface of the test sump. The distance between the two thermocouples is 1.2 cm in a horizontal direction and 2.1 cm in the vertical direction. The thermocouples near the wall are 0.6cm away from the solid wall.

Figure 5a shows the temperature distribution along the centerline of test sump A. Thermocouple #3 (only numbers will be used to present thermocouple locations in this paper) is 0.65 cm from the bottom wall, and #38 is 15.35 cm from the bottom. For the first four minutes, the temperatures of all thermocouples continuously decreased. Between 4 to 10 minutes, the majority of the thermocouples increased in temperature and then decreased again. The large amounts of equiaxed dendrites that appeared were associated with this rise in temperature. Since different mechanisms for controlling the flow patterns in the liquid pool before and after solidification are involved, separate discussions are given for the period before and after the 4 minutes. In the first four minutes, the temperature of #13 (4.85 cm above the bottom) reduced by almost 16°C. At higher levels, the temperature reduction was lessened; for example, the temperature of #33 reduced only 4°C during this time period.

Figure 5b shows the horizontal temperature distributions at two heights. This figure indicates that at y=4.85 cm, the three thermocouples (#11 through #13) had the same temperature in the first four minutes, which indicates a strong horizontal direction flow around this area. At y=9.05 cm, the horizontal temperature distribution was much different from that of y=4.85 cm. The temperature of a thermocouple near the cooling wall, #21, was far below the temperatures of the thermocouples in the center region (#22 and #23) during the same time period. Since the solution was well mixed before the test, the cooling walls were parallel to the centerline, and no phase change occurred, the only possibility for obtaining the temperature distribution like in Fig. 5 was from the thermally driven convective flow as shown in Fig. 6a. Figure 6a shows that the fluid flowed down along the cooling wall, then flowed from the wall region to the center of the sump around 5cm from the bottom. After that, it flowed upward as it warmed. A small flow loop also existed in the bottom region below this large flow loop, as seen in Fig. 6a.

After 4 minutes, Fig. 5a shows that the temperatures of all the thermocouples along the centerline increased, except for #38. Figure 5b shows that at y=9.05cm, the temperatures of thermocouples #22 and #23 increased around 3°C and then dropped after that, while the thermocouples near the wall continuously decreased with time. At y=4.85 cm, the temperature increased even the thermocouple near the wall, #11. The temperature changes in Figs. 5a and 5b indicate that the fluid flow changed its direction during this period of time—that is, the fluid flowed downward along the centerline and upward near the solid wall region. This downward flow brought the warm fluid from the top region to warm the thermocouples below it. This inverse flow loop was driven by the concentration gradients generated by solidification. During solidification of a hypereutectic solution, the solute will be solidified first, while the water will be ejected from the dendritic region. Since the water was lighter than the solution, it generated an upward buoyancy force near the wall region. This buoyancy force was eventually overcome by the thermal buoyancy force, and changed the direction of the flow. It is interesting to see that the temperature of #13 reduced much slower than that at other locations. It had a negative temperature gradient in all directions after 10 minutes, as seen in Figs. 5a and 5b. This suggests that the fluid heat transfer around thermocouple #13 was mainly controlled by conduction. The fluid flow inside the liquid

pool can be illustrated as in Fig. 6b, which shows that the bottom region is covered by loose equiaxed dendrites, only one flow loop is formed during this period of time.

Figure 7 illustrates the temperature distributions along the centerline in test sump B. Before the dendrites appeared, a negative temperature gradient existed from the top to the bottom along the centerline, which indicates only one thermally driven flow loop in each half-domain. The thermal convective flow in sump B was not as strong as in sump A due to the small temperature gradient between the center and wall region. After dendrites appeared at around the fourth minute, the bottom region was rapidly covered with dendrites, which is evidenced by the fact that the temperature of thermocouple #3 dropped rapidly below the eutectic temperature. The concentration driven convective flow overcame the thermally driven flow after 10 minuets. Unlike what occurred in sump A, no significant temperature increase was observed in sump B. Comparatively, the temperatures of the liquid pool in sump B reached uniformity much faster than that in sump A. During static ingot solidification, this hot spot in sump A may result in local structural defects and inhomogeneity, while bottom cooling can effectively improve this drawback.

Effect of the Angle of the Sump

During the continuous casting process, the melted material is poured into a water-cooled mold and exits the mold from the bottom. The material near the cooled mold is solidified first and forms a V-shaped liquid crust. The angle of the V-shape is about 4 to 16 degrees, which depends on the crust movement speed, the temperature difference between the liquid and the cooling wall, and the thermal properties of the casting material. The purpose of this study is to determine the effect of the sump (crust) angle on the double-diffusive flow pattern.

Two test sumps were built to study the effect of the angle on the flow patterns. Both sumps have a dimension of 29 cm in height and 25 cm in height. Figure 8 is a schematic view of the V-shaped test sump. The test sump consists of two cooling sidewalls, front and back vacuum chambers and a plexiglas cover. The angle, α, of sumps C and D was 16 degrees and 4 degrees, respectively. Five E-type thermocouples were installed inside each sidewall to measure the wall temperature. The front and rear vacuum chambers were made with plexiglas so that the solidification process could be observed and recorded by a video camera. The two cooling walls were attached on the front and rear vacuum chambers to form a V-shaped sump. The sidewalls were insulated by a syphon plate. Forty-one and thirty thermocouples were installed inside the liquid pool of sumps C and D to monitor the temperature change during the test. Details of the locations of each thermocouple are given in Figs. 9a and 9b.

Figure 10a depicts the temperature distribution in sump C along the centerline. This figure indicates that before the dendrites appeared, which happened around 5 minutes after the test started, the heat transfer in the liquid pool was controlled by thermal convective flow. According to the temperature distribution along the centerline, two flow loops existed in the liquid pool. One was between thermocouples #24 to #39, and another one was in the region between thermocouples #4 to #19. In the region below thermocouple #2, the dominant heat transfer mechanism was conduction. Figure 10b shows the temperature distribution along two horizontal lines. At y=12 cm, Fig. 10b shows that the fluid temperature increased from the wall to the centerline (thermocouples #12, #13, and #14) in the first four minutes. However, at y=17 cm, the temperature of thermocouple #24 (at the centerline) was lower then the temperature of #22 and #23 at the same height, which indicates a strong upward convective flow near the center region. After solidification occurred, the concentration driven buoyancy force balanced the thermal convection, and the temperature changed smoothly in all directions—that is, the heat transfer during this period was dominated by thermal conduction.

Figure 11a shows the vertical temperature distribution along the centerline in sump D. This test sump has a very large height/width ratio, which is around 13 based on the maximum width of the sump, the maximum distance between the two cooling walls is less than 2 cm). Solidification started around 8 minutes. Unlike what occurred in sump with 16°, this figure indicates that the temperature increased smoothly as the height increased before the dendrites appeared. It should be emphasized that the distance between the cooling wall and the centerline increased as the height increased. Figure 11b illustrates the temperature distributions along two horizontal locations, y=21.5 cm and y=25.5 cm. This figure indicates that the temperature increased smoothly from the cooling wall to the centerline. The temperature distribution presented in Figs. 11a and 11b reflects that conductive heat transfer was the dominate heat transfer mechanism during this period. After solidification occurred, Figs. 11a and 11b illustrate that the temperatures at different thermocouples were close to each other, but the temperature still increased smoothly from the cooling wall to the centerline and from the bottom to top—that is, conduction was still the dominant mechanism for heat transfer inside the liquid pool.

SUMMARY

The effects of boundary conditions on the double-diffusive flow inside a liquid pool during the solidification process in a binary solution has been experimentally studied. Many thermocouples were installed in the cross section to measure temperature change during the experimental test. The temperature distribution was then used to analyze the flow patterns inside the liquid pool. The major results indicate that

1) in a rectangular cavity, the addition of bottom addition of bottom cooling will reduce the thermally driven convective flow before solidification starts. After the dendrites appear, the cavity with bottom cooling will reach a uniform temperature much faster than a cavity without bottom cooling. During static ingot solidification, the cavity with bottom cooling can help to reduce local structural defects and inhomogeneity.

2) the bottom angle of a V-shaped sump can significantly change the heat transfer mechanism and the flow conditions inside the liquid pool. At a large angle, 16 degrees, the thermally driven convective heat transfer controls the fluid flow and heat transfer before solidification starts. After the dendrites appear, conduction becomes the major mechanism for heat transfer. At a small angle, 4 degrees, conduction is the dominant heat transfer mechanism before and after the dendrites appear.

ACKNOWLEDGMENT

The results presented in this paper were obtained in the Course of Research Sponsored by the National Science Foundation (NSF).

REFERENCES

Beckermann, C., 1987, *Melting and Solidification and Binary Mixtures with Double-Diffusive Convection in the Melt*, Ph.D. Thesis, Purdue University.

Benard, C., Gobin, D., and Thevenin, J., 1989, "Thermosolutal Natural Convection in a Rectangular Enclosure—Numerical Results," *Heat Transfer in Convective Flows*, edited by R. K. Shah, ASME HTD-Vol. 107, pp. 249-254.

Christenson, M. A. and Incropera, F. P., 1989, "Solidification of an Aqueous Ammonium Chloride Solution in a Rectangular Cavity - II. Experimental Study," *Int. J. Heat Mass Transfer*, 32, pp. 47-68.

Fisher, K. M., 1981, "The Effects of Fluid Flow on the Solidification of Industrial Castings and Ingots," *Physico-Chem. Hydrodyn.*, 2, pp. 311-326.

Flemings, M. C., 1974, *Solidification Processing*, Chapter 6, McGraw-Hill, New York, New York.

Hu, C. Y. and El-Wakil, M. M., 1974, "Simultaneous Heat and Mass Transfer in a Rectangular Cavity," *Proc. 5th Int. Heat Transfer Conf.*, 5, pp. 24-28.

Incropera, F. P. and Viskanta, R., 1992, "Effect of Convection on the Solidification of Binary Mixtures," in *Heat and Mass Transfer in Materials Process* (ed. by I. Tanasawa and N. Lior), pp. 295-312, Hemisphere Publishing Corp., New York.

Kamotani, Y., Wang, L. W., Ostrach, S., and Zhang, H. D., 1985, "Experimental Study of Natural Convection in Shadow Enclosures with Horizontal Temperature and Concentration Gradients," *Int. J. Heat Mass Transfer*, 28, pp. 168-173.

Lee, J., Hyun, M. T., and Kim, K. W., 1988, "Natural Convection in Confined Fluids with Combined Horizontal Temperature and Concentration Gradients," *Int. J. Heat Mass Transfer*, 31, pp. 1969-1977.

Ostrach, S., 1983, "Fluid Mechanics in Crystal Growth," The 1982 Freeman Scholar Lecture, *J. Fluid Engrg.*, 105, pp. 5-20.

Turner, J. S., 1979, *Buoyancy Effects in Fluids*, Cambridge University Press, London.

FIGURE CAPTIONS

Fig. 1 Schematic of the test facilities.
Fig. 2 Phase diagram of Na_2CO_3.
Fig. 3 Rectangular sumps.
Fig. 4 Thermocouple distribution.
Fig. 5 Vertical and horizontal temperature history, 10% Na_2CO_3.
Fig. 6 The flow patterns in the rectangular test sump.
Fig. 7 Vertical and horizontal temperature history, 10% $NaCO_3$.
Fig. 8 V-shaped sump.
Fig. 9 Thermocouple location for 16° and 4° V-shaped sump.
Fig. 10 Vertical and horizontal temperature history, 16° V-shaped sump.
Fig. 11 Vertical and horizontal temperature history, 4° V-shaped sump.

An experimental investigation of the solidification process in a V-shaped sump

R. BURTON, G. YANG, Z. F. DONG and M. A. EBADIAN†

Department of Mechanical Engineering, Florida International University, Miami, FL 33199, U.S.A.

(*Received* 11 *April* 1994 *and in final form* 28 *November* 1994)

Abstract—An experimental study of binary mixture solidification in a V-shaped sump is conducted. NH_4Cl–H_2O is used as the phase change material. The variations of temperature, concentration, as well as the location of the interface front, are measured and reported in this investigation. The results indicate that the solidification process exhibits totally different behavior when the initial component of the solution is varied. For a hypoeutectic solution, the columnar solidification in the dendritic interface is the dominant mechanism. For the hypereutectic solution, both columnar and equiaxed solidification are important. The solidification starts as the equiaxed dendrites grow and coalesce in the entire solution. They then descend and settle at the bottom of the sump to form a loose, mushy zone. The solid region grows underneath the mushy zone.

1. INTRODUCTION

Solidification is a phase transformation process that is accompanied by the release of thermal energy. The common feature of a system undergoing solid–liquid phase change is the existence of a moving boundary that separates the two phases of the solution with different thermophysical properties. The majority of commercial metal products are composed of alloys of two or more constituent elements, making them differ in many respects from the solid structure of a pure substance [1, 2]. During the solidification of binary mixtures, the density of the liquid varies with both temperature and concentration. Thus, natural convection can be caused by both thermally and solutally induced density gradients. Previous researchers indicate that the major cause of structural defects and inhomogeneity (macrosegration and microsegration) during solidification is attributed to an improper convection flow pattern in the melt sump and the mushy zone [1]. Therefore, knowledge of the transport phenomena of double diffusive convection in the melt sump is essential for maintaining satisfactory control over the casting process. Due to the complexity of double diffusive convection during the solidification process, theoretical study on this topic is still in the developing stage [3] and experimental study is still the most powerful means for understanding this basic phenomenon. Many experimental studies on this topic have been conducted using different kinds of solutions. Liquid metals have been applied to study the solidification process by some researchers (Al–Cu alloy) [4] and (Pb–Sn alloy) [5]. Since the liquid metal is opaque, it is very difficult to determine the flow pattern and the moving solid front interface during the experiment. Therefore, transparent solutions are usually applied to analogue alloy solidification. The NH_4Cl–H_2O solution was used to measure both velocity and temperature distributions in the solution [6, 7], and a solidification test was conducted by using an Na_2CO_3–H_2O solution [8, 9]. Recently, the solidification process in a rectangular cavity was also studied by using the NH_4Cl–H_2O system [10, 11]. The above mentioned survey of the literature indicates that the majority of existing experimental results were obtained from the rectangular cross section test sump, which focused only on static ingot solidification. During the continuous casting process, melted material is poured into a water-cooled mold and exits the mold from the bottom. After heat is lost to the mold wall, the material nearest the cooled mold is solidified first to form a crust with the liquid material in the center. This crust is continuously withdrawn from the bottom. The material in the center usually needs additional time to solidify, which results in a V-shaped liquid sump. The angle of the V-shape is about 4–16°, which usually depends on the crust movement velocity and the thermal properties of the casting material. What is the effect of the oblique walls of the V-shaped boundary on the solidification process of the binary solution? The surveys indicate that no such information is available in the open literature. As a first step for studying the V-shaped solidification process in continuous casting, this paper presents the primary experimental results of temperature, concentration, and the moving solid front interface during the solidification process in a fixed V-shaped sump.

2. TEST FACILITY AND INSTRUMENTATION

A test facility, which includes a test sump and cooling system, was constructed to model the two-dimen-

† Author to whom correspondence should be addressed.

NOMENCLATURE

C	concentration	Subscripts	
T	temperature	c	cooling
t	time	e	eutectic
x	vertical location	o	initial.
y	horizontal location.		

sional solidification process in a V-shaped sump. Figure 1 is a schematic of the V-shaped test sump. The test sump consists of two aluminum side walls, front and back glass windows, and a top cover. The dimensions of the test sump are 28 cm × 3 cm × 29 cm (length × width × height), respectively. The galleries, which were 8 mm wide × 12 mm deep, were machined into the back surfaces of the aluminum side walls to serve as a channel for the coolant. Five J-type thermocouples were installed inside each side wall to measure the wall temperature. Four triangular glass plates were mounted between the two side walls to divide the test sump into three chambers. A rectangular glass plate cover was placed at the top of the sump to ensure that these three chambers were airtight. In order to prevent vapor condensation on the front and rear windows, the front and rear chambers (1.5 cm length on each side) were kept in a vacuum during the test. The middle chamber of the test sump is 25 cm in length, which was filled with the NH_4Cl–H_2O solution, and was also kept in a vacuum during the test to extract the gas from the solution. The test sump was covered by a syphon box to insulate it from the ambient.

Figure 2 shows the cooling system and the instruments used in this investigation. The cooling system includes three refrigerators and the associated control valves and piping. Two 425 watt Model N01268 digital refrigerated circulator baths (Refrigerators I and II) were applied to keep the side walls at a desired temperature during a normal test. A 175 W Model N01267 digital refrigerated circulator bath (Refrigerator III) was used to set the initial temperature.

Seventeen thermocouples were installed to monitor the temperature distribution of the solution. These thermocouples were mounted on a plexiglas frame to ensure that they remained in place during the solidification process. The thermocouples were arranged in four horizontal lines, with the top line located 1 cm below the solution. The locations of each thermocouple are listed in detail in Table 1, where the origin points ($x = 0$ and $y = 0$) are defined at the bottom corner of the test chamber, as seen in Fig. 2. All thermocouples were calibrated individually after they were installed. The thermocouples were connected to an HP data acquisition system (Model No. 3852A) and monitored by a personal computer. The uncertainty of the temperature measurement is ± 0.3°C. The uncertainty of the thermocouple location is less than ± 1 mm.

Aqueous ammonium chloride (NH_4Cl–H_2O) was chosen as the test solution due to its similar solidification behavior as the liquid metal, and for its semi-

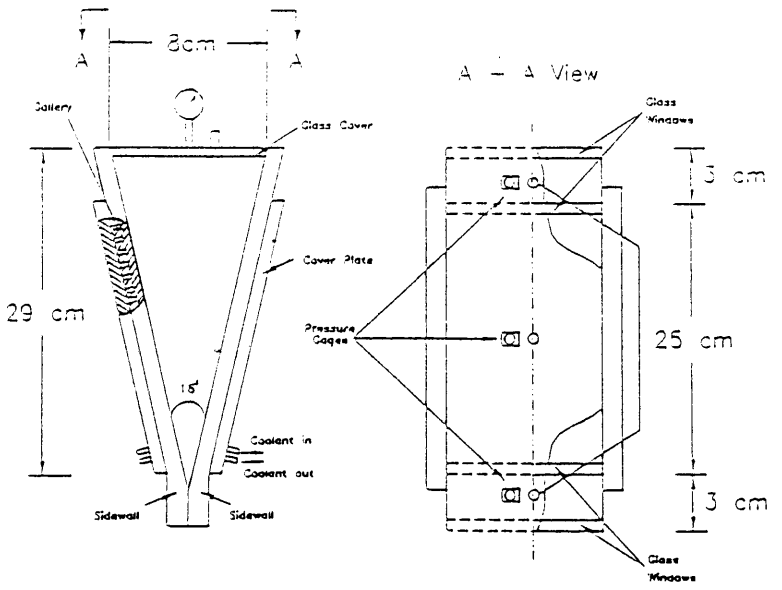

Fig. 1. Schematic representation of the test section.

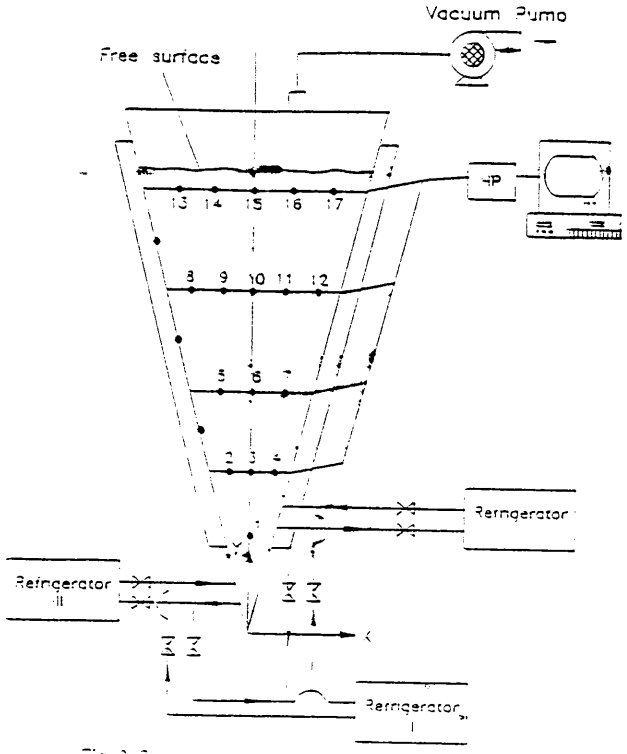

Fig. 2. Schematic representation of the cooling system.

Table 1. Location of the thermocouples

Number of thermocouples	x (cm)	y (cm)
1	0	1.52
2	−1.02	6.60
3	0	6.60
4	1.52	6.60
5	−1.27	12.7
6	0	12.7
7	1.73	12.7
8	−1.78	17.27
9	−0.76	17.27
10	0	17.27
11	1.27	17.27
12	2.29	17.27
13	−2.54	22.35
14	−1.02	22.35
15	−0.51	22.35
16	1.03	22.35
17	2.31	22.35

transparency. The eutectic temperature and composition of the NH_4Cl–H_2O are $T_e = -15.4°C$ and $C_e = 19.7\%$, respectively. The concentration measurement was conducted by extracting the solution through a set of syringes (test probes). Nine syringes were used to measure the liquid concentration. During solidification, the tips of these syringes were located in different x and y positions. However, 30 min after the start of the test the majority of the locations of the tips of the syringes were either occupied by ice or were mushy. Only two syringes (probes C and F) could provide us with information during the entire process. Both probes C and F were located along the centerline of the sump, with the tips located at 4 cm and 6.39 cm below the surface of the liquid (or 23 cm and 20.11 cm from the bottom corner). An ABBE 2WAJ refractometer was used to measure the refractive index of the extracted solution. The refractive index was then transferred to the concentration through a chart, which was created by measuring a set of known concentrations. Uncertainty in the placement of the probe was about ± 1 mm. Since only a very small amount of liquid was extracted during the test, the effect of the concentration gradient near the probe tip was minor. The estimated uncertainty of the concentration measurement was about $\pm 0.5\%$.

A video camera was used to capture the movement of the solid–liquid fronts during the test. The video tapes were then processed by an image processing package (DATA Translation DT 2855) to determine the location of the solid–mushy–liquid fronts and to calculate the solidification rate. Basically, the test chamber is long enough to be considered a two-dimensional chamber (2D). Since the solid–mushy–liquid fronts produced different light reflections, the image captured by the video camera could easily distinguish these three zones. Figure 3 shows the three images at hypoeutectic, eutectic and hypereutectic conditions. The light areas in the pictures indicate the mushy

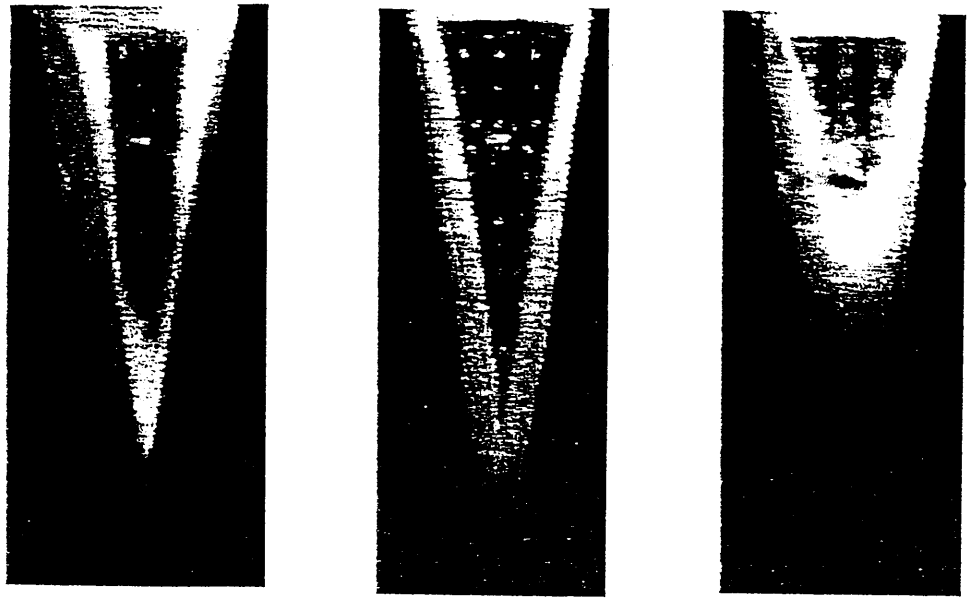

Fig. 3. Video image of the interface front.

Table 2. Summary of the experimental conditions

Test run	C_o [%]	T_o [°C]	T_c [°C]
1	19.7	5	−20
2	5.0	5	−10
3	15.0	5	−15
4	25	15	−20

(dendritic) zones. It is worthwhile to point out that in the eutectic condition (C_o = 19.7%), the bright lines represent the liquid–solid interface.

3. EXPERIMENTAL PROCEDURE

During the solidification process, the gas originally absorbed in the solution was released. These air bubbles can drive the surrounding liquid to form an upward flow. In order to make the solution free from gas when a new solution was poured into the test chamber, the solution was solidified and melted at least three times. The test chamber was also kept in a vacuum to prevent the solution from reabsorbing the gas. The results of four test runs were selected and are presented in this paper. Each test was repeated four to five times. Table 2 provides the information regarding the initial temperature, concentration, and the cooling temperature in each test run. Test Run 1 represents the case of the eutectic solidification process. Test Runs 2 and 3 indicate the case of hypoeutectic solidification, while Test Run 4 is hypereutectic solidification.

The first step of the test was to set up a uniform initial temperature, T_o, for the test solution. Refrigerator III was connected to the cooling line to provide a desired temperature through the two side walls. Thermocouples were closely monitored to check the temperature of the solution. The maximum temperature difference inside the solution was less than 0.5°C before starting the experiment. During the time to set up the initial temperature, Refrigerators I and II were disconnected from the cooling line and run to establish the required cooling temperature, T_c. After thermal uniformity was reached in the solution, Refrigerators I and II were connected to the cooling line and Refrigerator III was disconnected, after which the experiment began.

During the test, the temperature was continuously monitored at every 1 min interval for the first hour and at 5 min intervals after that. The video camera continuously recorded so that the tapes could be viewed later. The concentration measurements were conducted every 30 min. Although the test rack initially included nine test probes (syringes), due to solidification, only two probes could provide the concentration information throughout the test. The test times for each run were significantly different depending on the initial concentration, which varied from 2 to 8 h.

4. RESULTS AND DISCUSSION

The simplest case of solidification of a binary mixture is the case of eutectic composition. In eutectic composition, the solution exhibits the phase change behavior of a pure substance, and the convective flow is driven solely by the thermal buoyancy force. Figure 4 shows the history of the solid–liquid interfaces in Test Run 1. A half-hour after starting, Fig. 4(a) shows that the solid interface appeared on the side walls. The

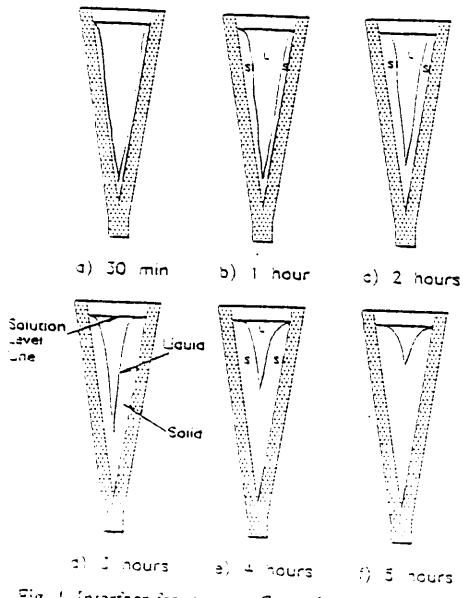

Fig. 4. Interface front in the $C_0 = 19.7\%$ solution.

solid–liquid interfaces appeared very smooth and were well distributed along both surfaces. Since the solution temperature in the center of the test chamber was higher than that near the interface, a thermally driven natural convection was generated. The fluid near the cooling interface flowed down and then moved up in the center region to form two recirculation loops. As time elapsed, however, the solidified region increased, and the liquid region always remained in a V-shape, as seen in Fig. 4(b)–(f).

For the solution with a hypoeutectic composition, the solute will be ejected during the solidification process and the two-phase interface is characterized as the mushy zone. As a result, there exists a high concentration region in and near the interdendritic zone. Since the solute was denser than the solution, a downward flow was generated along the interface by the solute driven natural convection, which was in the same direction as that of the thermal by driven convection. Figures 5 and 6 show the variation of the temperature contours during the solidification process in a hypoeutectic composition solution (Test Run 2). In this test, a 5% NH_4Cl composition solution was used with initial and cooling temperatures of $T_0 = 5°C$ and $T_c = -10°C$, respectively. Figure 5 shows the temperature variation of thermocouples, Nos 8, 9 and 10. These three thermocouples are located about 6.8 cm below the solution surface, where thermocouple No. 8 is 2 mm away from the side wall, and thermocouple No. 10 is in the center chamber. This figure indicates that the readings of thermocouples Nos 9 and 10 were closer to each other, and that of No. 8 was always far below that of the other two. It is also interesting to note that instead of continuously reducing the temperature in locations Nos 9 and 10, the reading of No. 8 displayed a sudden increase in the early stage. In the first 20 min, the solution temperature near the side walls (No. 8) steadily dropped to $-5.6°C$, which is lower than the freezing temperature for this concentration. This overcooling endured a few minutes until the first dendrites appeared. Visual observation indicated that the dendritic region spread very fast to cover the entire side wall surfaces in less than 1 min, while at the same time, the thermocouple reading of No. 8 jumped to $-2.3°C$. Figure 6 shows the temperature variation

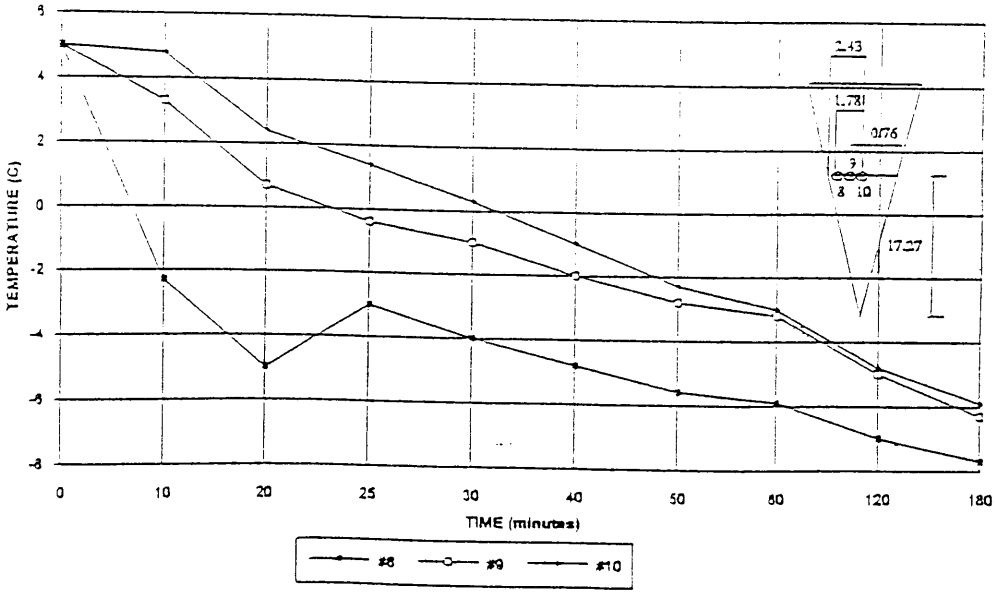

Fig. 5. Temperature history for the horizontal thermocouples ($C_0 = 5\%$, $T_c = -10°C$, $T_i = 5°C$).

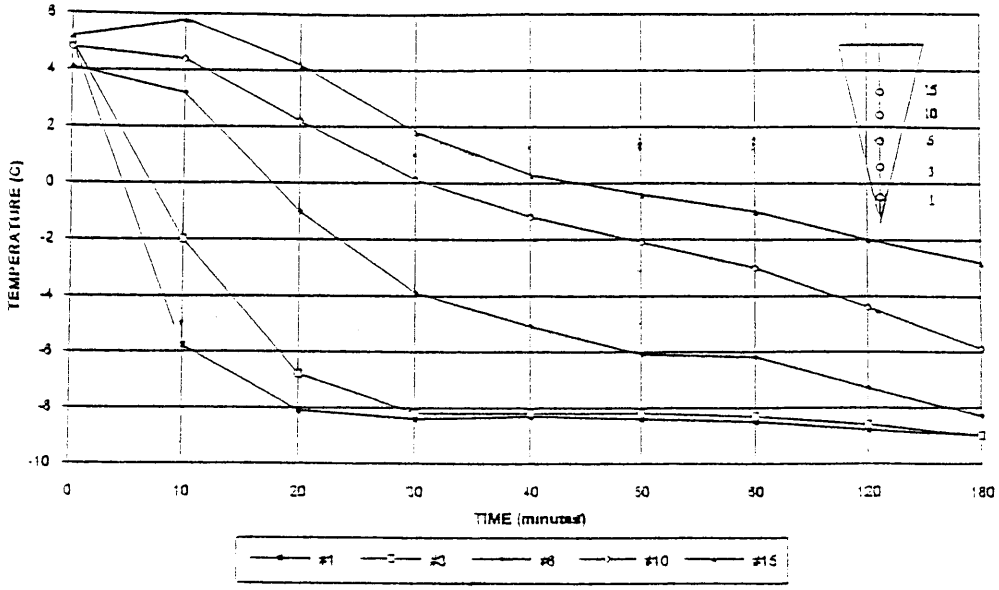

Fig. 6. Temperature history for the vertical thermocouples (C_o = 5%, T_c = −10°C, T_i = 5°C).

along the centerline of the test chamber. The vertical locations of thermocouples, Nos 1, 3, 6, 10 and 15, are 22.5, 17.4, 11.3, 6.3 and 1.7 cm, respectively. This figure indicates that temperatures in all five locations steadily dropped as time elapsed, and the temperature in the upper point was always higher than that in the lower point. Figure 7 shows the movement of the solid–liquid interface fronts. At t = 30 min, Fig. 7(a), visual observation indicated that the solidified region was composed of mainly long and coarse dendrite interfaces. As time elapsed, the dendrite became shorter and finer, and the solid region appeared, Fig. 7(b). Since the solute-rich fluid continuously flowed down along the interface region, the concentration in the bottom region of the test chamber steadily increased, which delayed the solidifying process in this region. Figures 7(c) and (d) show that the interface fronts moved close to each other, and left a long narrow gap between them. Figure 8 shows that the concentration changed with time in this case. The probes, C and F, are located below the solution surface. The figure indicates that the concentration increased as time elapsed. After 90 min, the concentration at point C almost reached 10%.

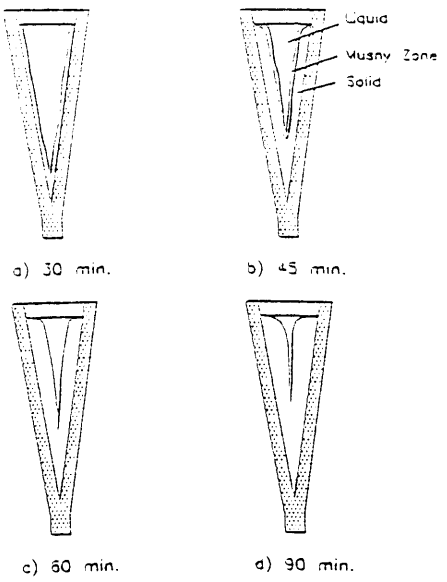

Fig. 7. Interface front in the C_o = 5% solution.

Figure 9 shows another case of solidification in a hypoeutectic composition of 15% (Test Run 3). The dendrites appeared 15 min after the test. Columnar dendrites occurred on the walls of the top half of the chamber. Some of the loose columnar dendrites fell while joined with the equiaxed dendrites to pack at the bottom corner, forming a mushy zone. Figure 9(a) illustrates the interfaces of the liquid–mushy–solid front at t = 30 min. It can be seen that a very thin solid built up along the wall, with a thick layer of the mushy zone between the solid and the solution. Both the mushy and solid regions increased after that, as seen in Fig. 6 (t = 60 min.). After one hour, the interface between the mushy zone and the solution changed slowly, unlike the solid region's rapid increase (Fig. 9(c) and (d)). At t = 3 h, the mushy zone near the bottom corner became solid and at t = 4.5 h, the mushy zone almost disappeared. Figure 10 indicates that the concentration at points C and F continuously increased until reaching eutectic concentration, around t = 3 h, then remained constant, which can explain why the mushy zone disappeared later on.

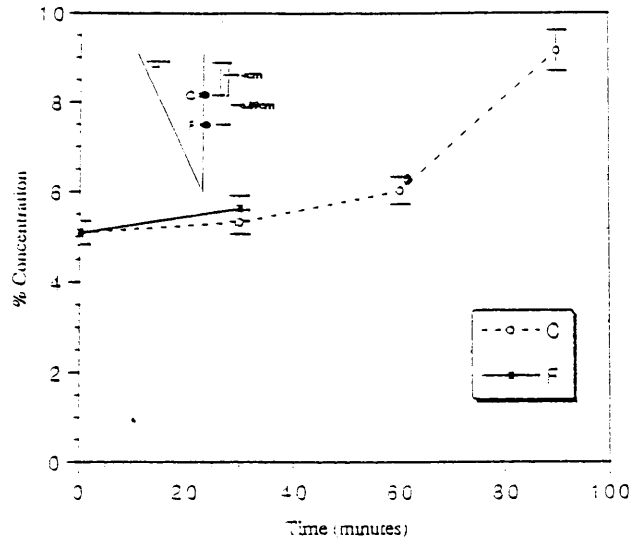

Fig. 8. Concentration variation in the C_0 = 5% solution.

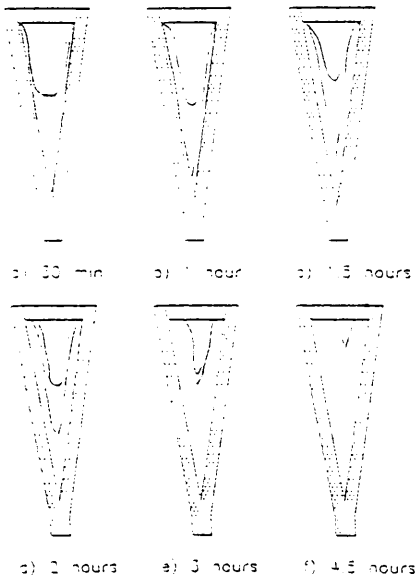

Fig. 9. Interface front in the C_0 = 15% solution.

Figure 11 shows the temperature history for thermocouples Nos 8, 9 and 10. This figure indicates that the horizontal temperature in this case was much more uniform than in the case of the 5% composition (Fig. 5). Also, no overcooling phenomenon was observed in this case. Figure 12 shows the vertical temperature distributions along the centerline. This figure indicates that the temperature in the upper point was always higher than that in the lower point, which is consistent with the result for the case of the 5% composition.

In contrast to the hypoeutectic composition, the ejection of water-rich interdendritic fluid will induce an upward flow in the hypereutectic composition solution, which is opposite to the thermally driven flow. Therefore, totally different solidification behavior can be expected in these two cases. Figure 13 shows that the interface front moved with time in a hypoeutectic component solution, where the initial component is 25%, T_i = 15°C, and T_c = −20°C. Visual observation indicated that a few minutes after starting the test, the equiaxed dendrites appeared at the bottom corner first, and then in the entire domain. Many tiny solid particles grew and coalesced as they descended. After about another 5 min, the dendrites settled down to form a mushy zone at the bottom, as seen in Fig. 13(a). The mushy zone increased slowly after that, and the solid zone grew under the mushy zone, as seen in Fig. 13(b)–(d). At t = 1 h, no solid zone could be seen at the top of the sump. The solid zone appeared at the top of the sump at t = 2 h, and the surface of the solid zone was almost smooth. The solid region continued to grow and the loose mushy zone was reduced. The interface of the solution and the solid at the top of the sump remained smooth. Figure 14 shows that the concentration at points C and F reached a eutectic value after around 2 h and remained that way. The results of the horizontal temperature measurements are presented in Fig. 15. This figure indicates that the temperature near the wall at thermocouple No. 8 was much lower than the inside solutions (Nos 9 and 10) in the first 2 h. However, the temperature difference between thermocouples Nos 9 and 10 was very minor. It is interesting to see the difference between Figs. 15 and 5, or 11. Instead of a smooth variation of the temperature, Fig. 15 shows the fluctuation of the temperature with time. This represents the existence of equiaxed solidification. Figure 16 shows the temperature distribution along the vertical direction. Like that in Fig. 15, the temperature fluctuated with time before the solution near this point

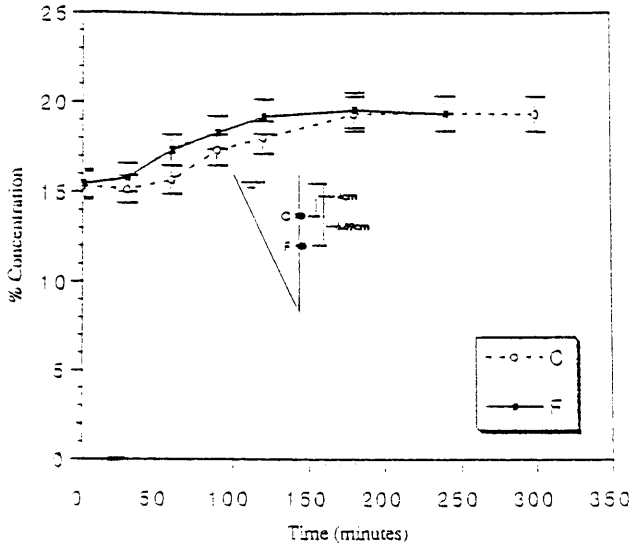

Fig. 10. Concentration variation in the $C_0 = 15\%$ solution.

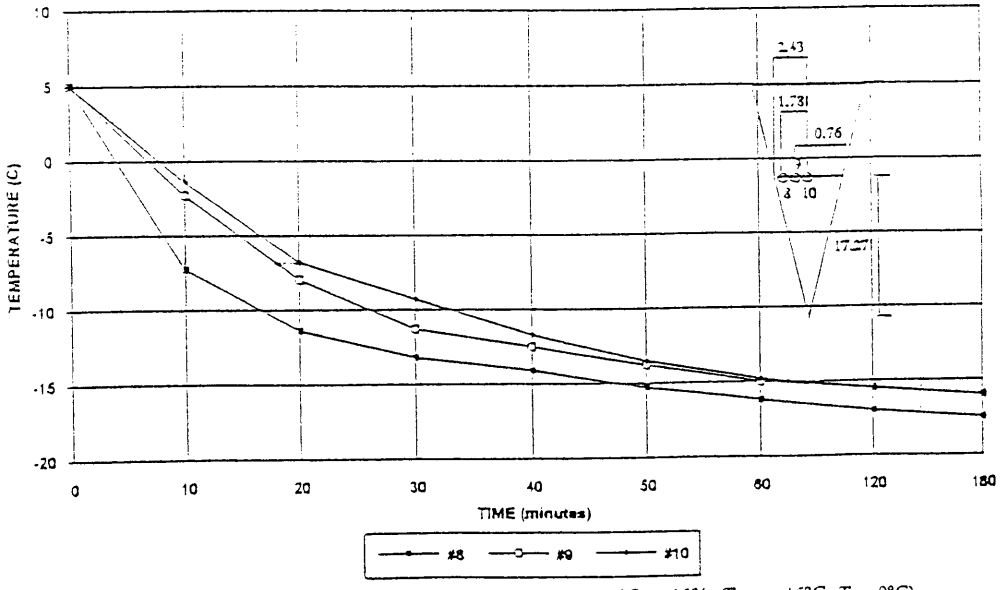

Fig. 11. Temperature history for the horizontal thermocouples ($C_0 = 15\%$, $T_c = -15°C$, $T_i = 0°C$).

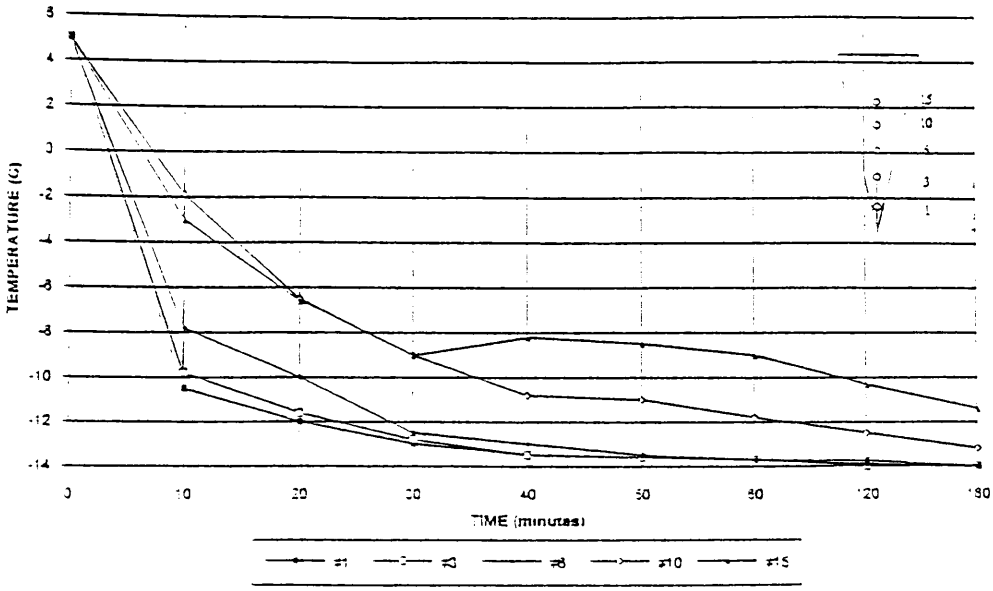

Fig. 12. Temperature history for the vertical thermocouples (C_0 = 15%, T_i = −5°C, T = 0°C).

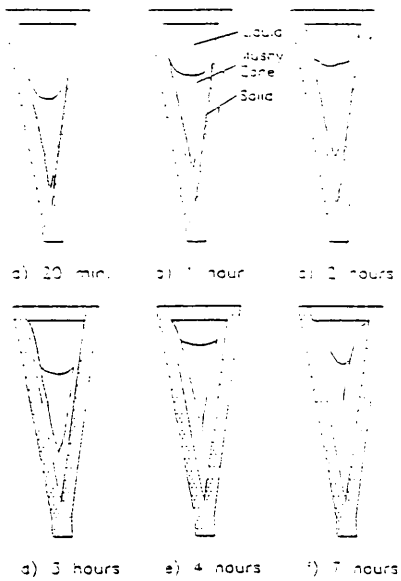

Fig. 13. Interface front in the C_0 = 25% solution.

solidified. It can be seen that the temperature in thermocouple No. 10 was higher than that in thermocouple No. 15, between 10 and 120 min. That is, the temperature near the top free surface was lower than that in the liquid center. This temperature distribution reflects the effect of the solute-driven flow. As the water-rich fluid was ejected from the dendritic interface, it flowed upward along the interface and then recirculated through the top free surface region. It is interesting to compare the temperature change behaviors of Figs. 15 and 16 and that of Figs. 5, 6, 11 and 12. In Figs. 15 and 16, the temperatures at all points fell below 5°C in the first few minutes. The equilibrium phase diagram for NH_4Cl–H_2O [10] indicates that this temperature was below the phase change temperature in the 25% concentration solution, which is why the equiaxed dendrites appeared in the entire solution. In the 5% and 15% initial concentration solutions, a considerable temperature difference existed, which is why the dendrites and the solidification mainly occurred on the side walls.

5. SUMMARY

An experimental study of the solidification for a binary mixture in a V-shaped test chamber has been conducted. Aqueous ammonium chloride was chosen as the phase change material. The effects of the NH_4Cl concentration on solidification have been examined by changing the initial component of the solution. In the eutectic solution, the solidification characterized as a smooth discrete interface always maintained a V-shaped configuration. In the hypoeutectic solution, the solidification mainly depended on the columnar growth on the dendritic interface. However, depending on the initial concentration, the shape of the final

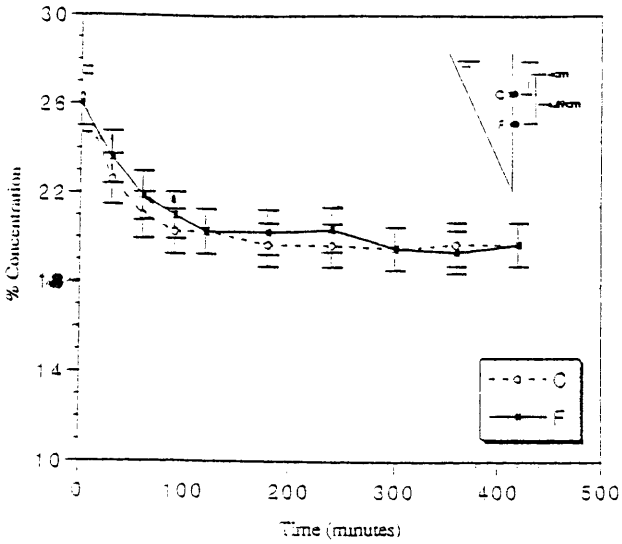

Fig. 14. Concentration variation in the $C_o = 25\%$ solution.

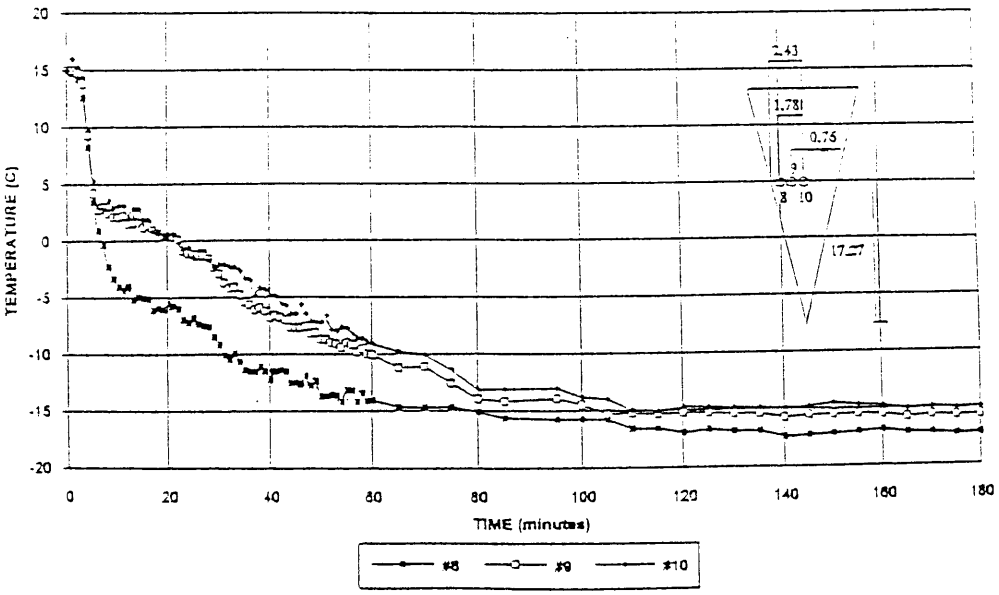

Fig. 15. Temperature history for the horizontal thermocouples ($C_o = 25\%$, $T_c = -20°C$, $T_i = 15°C$).

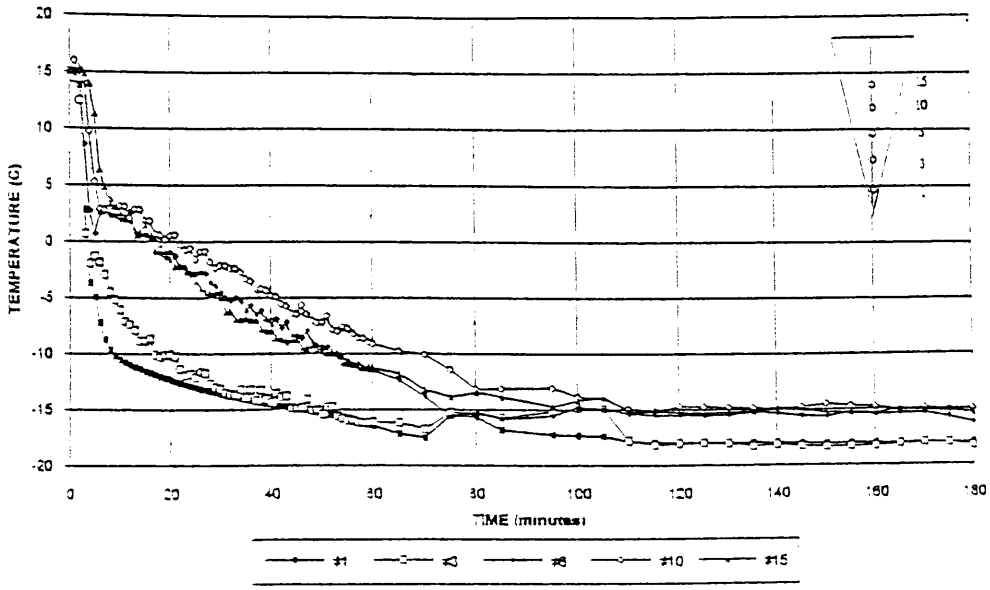

Fig. 16. Temperature history for the vertical thermocouples ($C_0 = 25\%$, $T_1 = -20°C$, $T = 15°C$).

liquid–solid interface may differ totally, which may significantly affect the quality of the final product. In the hypereutectic solution, equiaxed solidification is important. In the beginning, the equiaxed dendrites appeared in the entire solution and then grew and coalesced as they descended and formed a loose mushy zone. The solid region then grew under the mushy zone.

Acknowledgements—The results presented in this paper were obtained in the course of research sponsored by the National Science Foundation. The authors would also like to thank Mr G. Martin, F. Desir and G. Hoo for their assistance throughout this study.

REFERENCES

1. K. M. Fisher. The effects of fluid flow on the solidification of industrial castings and ingots. *Physico-Chem. Hydrodyn.* 2, 311–325 (1981).
2. R. Viskanta. Natural convection in melting and solidification. In *Natural Convection* (Edited by S. Kakac, W. Aung and R. Viskanta), p. 845. Hemisphere, New York (1985).
3. F. P. Incropera and R. Viskanta. Effect of convection on the solidification of binary mixtures. In *Heat and Mass Transfer in Materials Process* (Edited by I. Tanasawa and N. Lior), p. 295. Hemisphere, New York (1992).
4. R. Mehrabian, M. A. Keane and M. C. Flemings. Experiments on macrosegregation and freckle formation. *Met. Trans.* 1, 3223–3241 (1970).
5. M. J. Stewart and F. Weinberg. Fluid flow through a solid–liquid dendritic interface. *Met. Trans.* 3, 333–337 (1972).
6. S. Asai and I. Muchi. 1978. Theoretical analysis and model experiments on the formation mechanism of channel-type segregation. *Trans. ISIJ* 18, 90–98 (1978).
7. J. Szekely and A. S. Jassal. An experimental and analytical study of the solidification of a binary dendritic system. *Met. Trans. B* 9, 389–398 (1978).
8. M. E. Thompson and J. Szekely. Mathematical and physical modeling of double-diffusive convection of aqueous solutions crystallizing at a vertical wall. *J. Fluid Mech.* 187, 409–433 (1988).
9. C. F. Chen. Onset of cellular convection in a salinity gradient due to a lateral temperature gradient. *J. Fluid Mech.* 63, 563–576 (1974).
10. C. Beckermann. Melting and solidification and binary mixtures with double-diffusive convection in the melt. Ph.D. Thesis, Purdue University (1987).
11. M. A. Christenson and F. P. Incropera. Solidification of an aqueous ammonium chloride solution in a rectangular cavity—I. Experimental study. *Int. J. Heat Mass Transfer* 32, 47–68 (1989).